Spring 2014

Investigation of Porphyrins as Potential G-Quadruplex Stabilizing Ligands and Fluorescent Probes

Navin C. Sabharwal , '14

Investigation of Porphyrins as Potential G-Quadruplex Stabilizing Ligands and Fluorescent Probes

Presented as a Senior Honors Thesis

in Chemistry

Navin C. Sabharwal

Advisor: Dr. Liliya A. Yatsunyk

Department of Chemistry and Biochemistry, Swarthmore College

Swarthmore, Pennsylvania

April 28, 2014

Table of Contents

Acknowledgements

First and foremost, I wish to thank Professor Liliya Yatsunyk for accepting me into her laboratory and serving as a dedicated research advisor to me during my time at Swarthmore. Her exceptional guidance has taught me a tremendous amount and is helping me become a better and more mature scientist. I would also like to thank Steven Barrett, Vienna Tran, Jack Nicoludis, Michelle Ferreira, Joshua Turek-Herman, Supriya Davis, Mary Kuchenbrod, KJ Bredder, and all other members of Yatsunyk lab for their support and camaraderie; our lab bonding activities are some of my fondest memories from the summer of 2012. I am especially grateful for the help Vienna Tran and Steven Barrett provided me during my first days in the lab.

I also wish to thank Dr. Jean-Louis Mergny for generously allowing us to work in his laboratory at the Institute Europeén de Chimie et Biologie (IECB) in Bordeaux, France, during the summer of 2013 and for his sage advice on all things quadruplex. Living and working in France was an eye-opening experience that I will always cherish. I also wish to thank all my colleagues at the IECB for their friendship and assistance during my time there, including Jun Zhou, Nassima Gueddouda, Amandine Renaud de la Faverie, Amina Bedrat, Aurore Guedin-Beaurepaire, Samir Amrane, Abdelaziz Kerkour, Souheila Amour, Oscar Mendoza, Gilmar Salgado, Anne Bourdoncle, Mathilde Bourguet, and Aurore de Rache. I wish to extend a special thank you to Aurore Guedin-Beaurepaire (Aurore "Un") for her extensive support and assistance in the lab and Oscar Mendoza for helping me with my platinum porphyrin project. I am also thankful for the friendships I formed with Michael Challenor, Monica Birrento, and Kimberly Davis, who were visiting the Mergny lab from Australia.

I am grateful for collaborations with researchers both at Swarthmore and elsewhere. I thank Nick Kaplinsky of the Swarthmore Biology department for allowing us to make extensive use of his RT-PCR machine. I would also like to thank Dr. Veronika Szalai of the National Institute of Standards and Technology (NIST) for her assistance with the NMM project and for allowing me to visit her lab at NIST to perform fluorescence lifetime experiments. Thank you to Dr. Alessandro D'Urso of the University of Catania in Sicily, Italy for providing us with the TCPPSpm4 porphyrin and instigating a fruitful collaboration between our labs.

I thank all of my friends, and especially Raul, Jasmeet, and Howard, for providing me with support and keeping me sane throughout the thesis-writing process. Lastly, and most importantly, I wish to thank my parents for always supporting me in any endeavor I choose to pursue and for first teaching me the joys and beauty of science.

Abstract

G-quadruplex (GQ) DNA is a non-canonical DNA structure thought to form throughout the human genome. Because the stabilization of quadruplexes formed in the telomeres and in the promoters of oncogenes may prevent the spread of cancer cells, there is great interest in developing and studying molecules that may bind to and stabilize these unique DNA structures. This thesis investigates the interactions between porphyrins and GQ DNA with the goal of determining how strongly and selectively porphyrins can stabilize the quadruplex structure. There is also great interest in developing luminescent probes for GQ structures to allow for their detection *in vivo*. Because porphyrins are also known to fluoresce intensely in the presence of quadruplex DNA, this thesis also investigates the extent to which porphyrins may be used as fluorescent probes for quadruplexes in the cell.

The first chapter focuses on N-methylmesoporphyrin IX (NMM), a porphyrin that has been shown to bind selectively to quadruplex DNA over other DNA structures. NMM is especially unique because it binds selectively to parallel quadruplexes over other quadruplex topologies. Given that NMM has also been shown to display a selective increase in fluorescence in the presence of quadruplexes over duplex structures, we wished to systematically investigate the effect of secondary DNA structure on NMM fluorescence. Results indicate that NMM displays a selective fluorescence increase in the presence of parallel GQs over single-stranded DNA, double-stranded DNA, i-motif structures, anti-parallel GQs, and mixed hybrid GQs. NMM is also found to probe parallel quadruplexes even in the presence of excess duplex DNA, and thus has promise a selective fluorescent probe for parallel GQs. Fluorescence lifetime studies indicate solvent exclusion as the mechanism for NMM's fluorescence enhancement.

The second chapter investigates the interactions between the Pt(II) and Pd(II) derivatives of 5,10,15,20-tetrakis(N-methyl-4-pyridyl)porphyrin (TMPyP4), a well-examined GQ ligand. These porphyrins are of interest because of their square planar geometry; the lack of axial-ligands on the metal center could potentially facilitate stronger binding and intercalation between the quartets. Moreover, Pt(II) complexes are known to have powerful luminescent properties, so Pt(II)-TMPyP4, like NMM, may have promise a fluorescent probe. Results indicate that the two porphyrins bind tightly to the human telomeric GQ in a high ratio and stabilize the GQ extremely well at low ligand concentrations. Pt(II)-TMPyP4 is found to display selective fluorescence enhancement in the presence of GQs over duplex structures, but is not as selective as NMM.

Finally, the third chapter presents preliminary work examining the interactions between 5,10,15,20-tetrakis((N-spermido)benzamide)porphyrin (TCPPSpm4), a tentacle porphyrin with long side chains, and the human telomeric GQ. The results of this project, which is currently ongoing, suggest that the porphyrin stabilizes the GQ well and with good affinity. The results also seem to suggest a high ligand:GQ binding ratio and potentially cooperative binding to the GQ, although further work is needed to confirm these hypotheses.

“A scientist is not a person who gives the right answers, he’s one who asks the right questions.”

– Claude Lévi-Strauss

Chapter I: Introduction to G-quadruplexes

Structure and function of guanine quadruplex DNA

Deoxyribonucleic acid (DNA) is the biomolecule that encodes the genetic information necessary for the functioning and development of organisms. James Watson and Francis Crick revolutionized the world of molecular biology in 1953 when they demonstrated that DNA consists of two helical chains, each of which contains nucleotides composed of a nucleobase (either guanine, cytosine, adenine, or thymine) attached to a phosphate-sugar backbone with each helical turn consisting of approximately 10 base pairs.[1] The double helix is held together by hydrogen bonds between complementary guanine-cytosine and adenine-thymine base pairs.

Although this Watson-Crick duplex, also known as B-DNA, is the primary form of DNA found in the cell, other secondary DNA structures may also exist. A-DNA, for instance, has a shorter and more compact double helix than B-DNA and is formed in alcohol-water solutions.[2] Z-DNA contains a left-handed double helical structure that zig-zags to the left.[2] Structures with 9.3 base pairs per turn (C-DNA) and 8.5 base pairs per turn (D-DNA) are also known to form.[2] Secondary DNA structures containing more than two strands are also possible. Triplex DNA, for example, consists of three nucleic acid polymers wound around each other, with one oligonucleotide binding to a double-helix through Hoogsteen hydrogen bonds.[3] Guanine quadruplex (GQ), the focus of this thesis, is a non-canonical secondary DNA structure found in guanine rich DNA and RNA sequences.[4] Four guanine residues (Figure 1.1A) associate together through Hoogsteen hydrogen bonding between the N_1-O_6 and N_2-N_7 positions to form G-quartets (Figure

1.1B). These quartets have large π surfaces due to the presence of four nucleotide bases and thus stack on top of one another through π-π stacking. A phosphate-sugar backbone links the quartets together to form the final right-handed helical quadruplex structure (Figure 1.1C). GQ's are stabilized by a variety of monovalent cations, including K^+, Na^+, and NH_4^+, which coordinate to the lone pair electrons on the O_6 and therefore stabilize the GQ arrangement.[4]

GQ's exhibit structural diversity and adopt various topologies depending on the number of strands that comprise the quadruplex and the orientation and type of loop that connects these strands in the GQ structure (Figure 1.2A).[5] Quadruplexes may consist of one, two, or four strands, forming structures referred to as uni, bi, and tetramolecular, respectively. Moreover, the 5' to 3' directionality of DNA strands leads to three possible orientations of the strands relative to one another in the quadruplex structure. In a simplified view, parallel GQs have four strands in the same direction; mixed hybrid GQs have three strands in one direction and the fourth in the opposite direction; anti-parallel GQs have two strands in one direction and the other two in the opposite direction.[5] These strand orientations are defined by the conformation of the glycosidic bond between the guanine and the ribose sugar, which may be either anti or syn as depicted in Figure 1.3. Specifically, parallel GQs contain tetrads with guanines whose glycosidic conformations are all anti; mixed hybrid structures contain three anti and one syn or one anti and three syn guanines; and anti-parallel GQs contain two syn and two anti guanines.[5]

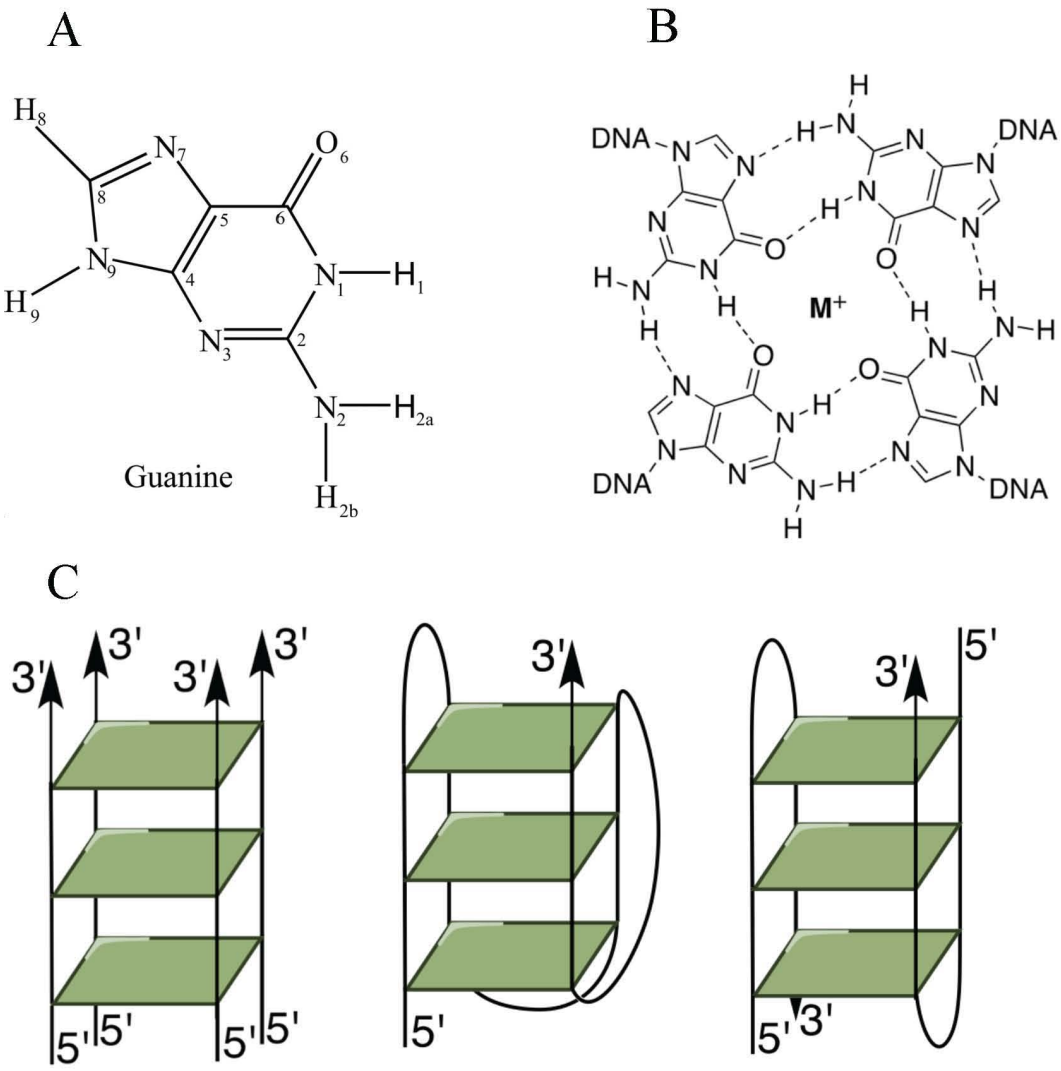

Figure 1.1. (A) Guanine molecule with atoms numbered.[6] (B) Four guanines come together through Hoogsteen H-bonding to form a G-quartet. M^+ is the stabilizing metal cation, such as K^+, Na^+, or NH_4^+. (C) Schematic representations of quadruplex structures. From left to right: tetramolecular parallel quadruplex, mixed hybrid monomolecular quadruplex, and antiparallel biomolecular quadruplex. (A) was taken from Bera et al. 2005; (B) and (C) were prepared by John M. Nicoludis '12.

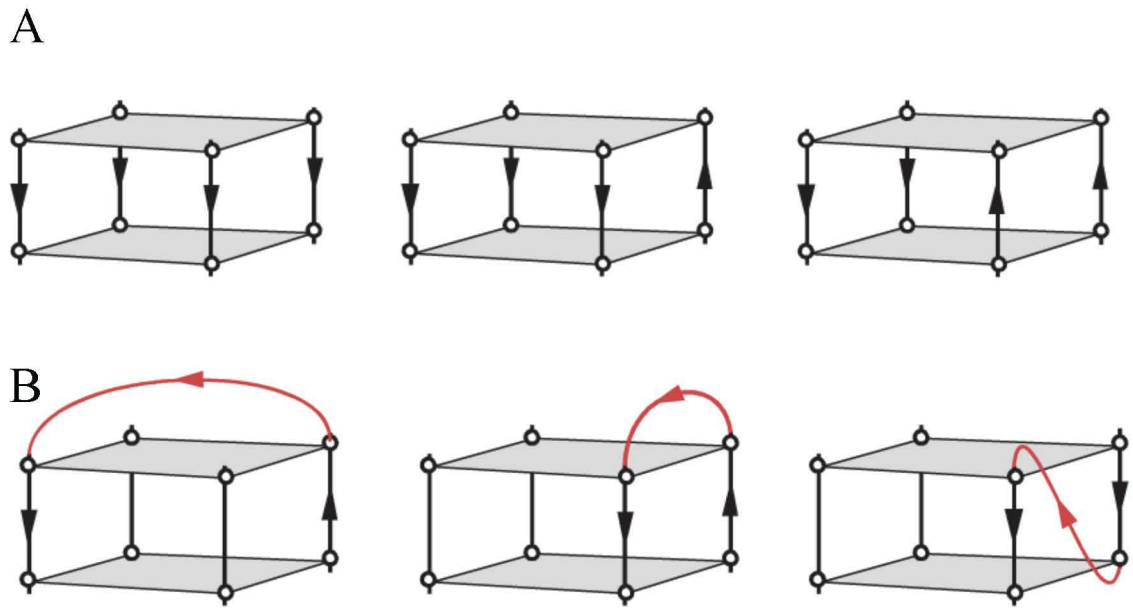

Figure 1.2. (A) Schematic of potential GQ strand orientations. From left to right: parallel, mixed hybrid, and anti-parallel. (B) Schematic of loops that connect GQ strands. From left to right: diagonal, edgewise, or double-chain reversal. Arrows point from the 5' to 3' direction.[5] Figure taken from Phan 2010.

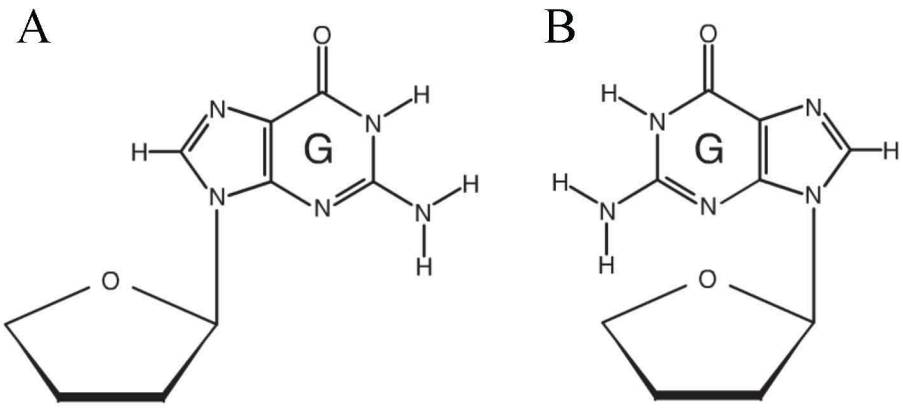

Figure 1.3. (A) Anti and (B) syn glycosidic conformations of guanine.[5] Figure taken from Phan 2010.

Three loop types connect the strands together (Figure 1.2B). Diagonal loops connect two anti-parallel strands diagonally across the tetrad; edgewise loops attach adjacent anti-parallel stands; and double-chain reversal loops, also known as propeller loops, connect adjoining parallel strands.[5]

I-Motif DNA

It has also been proposed that the C-rich strand complementary to quadruplex-forming G-rich one forms a secondary structure called an i-motif (Figure 1.4). This four-stranded structure, which is sometimes referred to as a cytosine quadruplex, is composed of two interweaving ladders held together with $C{\equiv}C^+$ bonds. Because i-motifs require the protonation of the cytosine's N_3 ($pK_a = 4.2$), they are stable in slightly acidic conditions ($pH \leq 6$).[4, 7]This acidic criterion for stability has created controversy as to whether i-motifs can form under physiological conditions. Studies have revealed, however, that the presence of the crowding agent polyethylene glycol (PEG) raises the pK_a of the hemi-protonated $C{\equiv}C^+$ pairs, leading to the formation of stable i-motif structures at neutral pH.[8] It is thus possible that i-motifs may form *in vivo* due to molecular crowding. I-motifs have also been shown to form under physiological conditions under negative supercoiling,[9] and interactions between cytosine residues in the loop of the i-motif formed in the oncogene Bcl-2 are thought to stabilize the structure.[10]

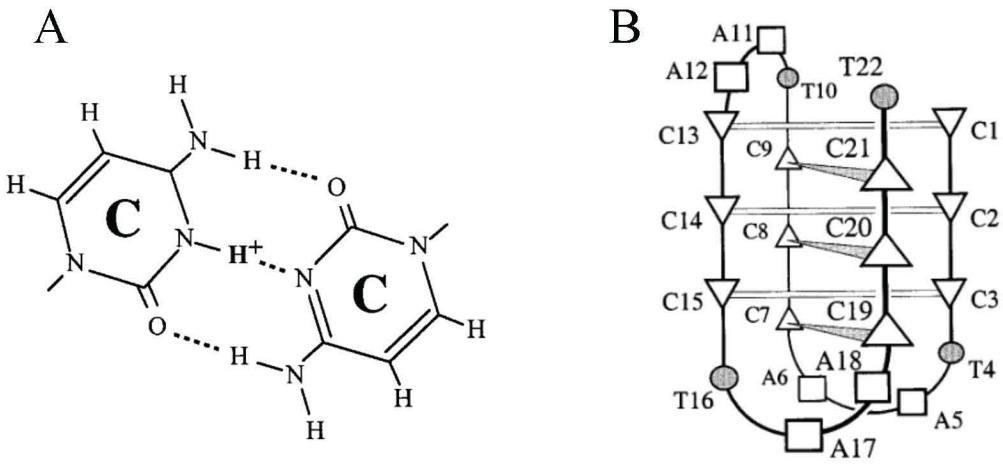

Figure 1.4. (A) Cytosine base pair involved in i-motif formation.[11] (B) Diagram of the intermolecular i-motif formed in the sequence d[$(CCCTAA)_3CCCT$].[11] Figure taken from Phan et al. 2002.

Biologial significance of quadruplex DNA

The presence of GQs in the telomeres

A telomere is a repeating nucleotide sequence that protects the end of chromosomes of most eukaryotic organisms from degradation by exonucleases and fusion with other chromosomes (Figure 1.5).[12] In all vertebrates, the telomeric sequence is $(TTAGGG)_n$. This essential function of telomeres was first elucidated by cytogenic studies performed by Muller[13,14] and McClintock[15,16] in the 1930s and 40s, who noted the unusual stability of breaks at the ends of chromosomes of maize and drosophila and proposed a capping mechanism for telomeres that protects the chromosomal ends.

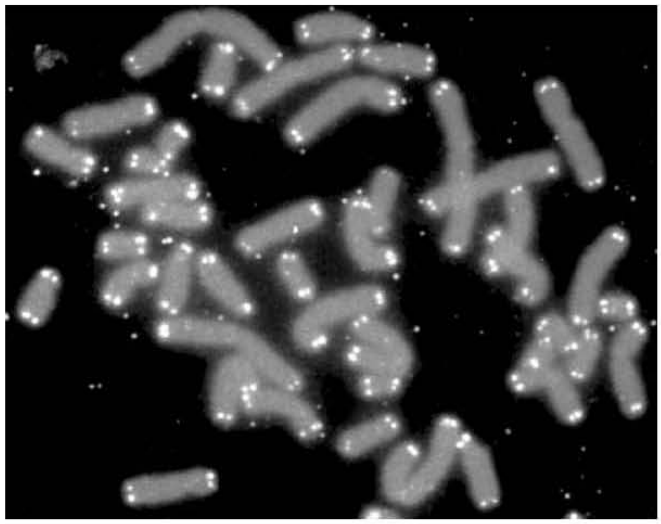

Figure 1.5. Immunofluorescence showing telomeres (white) capping chromosomes (grey). Image obtained from U.S. Department of Energy Human Genome Program.

Telomeres also serve as buffers at the ends of chromosomes, which are shortened during cell division; this phenomenon may be understood by considering the mechanism of DNA replication. DNA polymerase, the enzyme responsible for the DNA replication that occurs during cell division, needs RNA primers to begin replication. Because DNA is composed of antiparallel strands and the enzyme only synthesizes DNA in the 5' to 3' direction, one daughter strand (the leading strand) is synthesized continuously whereas the second (the lagging strand) is produced in small pieces called Okazaki fragments, which are stitched together by DNA ligase. The RNA primer is eventually degraded but the lagging strand cannot be filled by DNA repair because of the lack of a 3' OH available onto which a nucleotide may be added, leading to the presence of gap and a 3' single-stranded overhang. Without the last end of the lagging strand replicated, the new DNA molecule will become shorter each time it is replicated, a phenomenon known as the end-replication problem (Figure 1.6). After reaching a critical loss of DNA, telomeres are identified as double-break strands, resulting in the overexpression of the

tumor suppressor protein p53 that initiates cell death.[17] Thus, without a means to replicate the ends of the chromosomes, a cell will eventually its telomeric DNA and undergo apoptosis or senescence, leading to a limit on the number of times it may divide known as the Hayflick limit.[18]

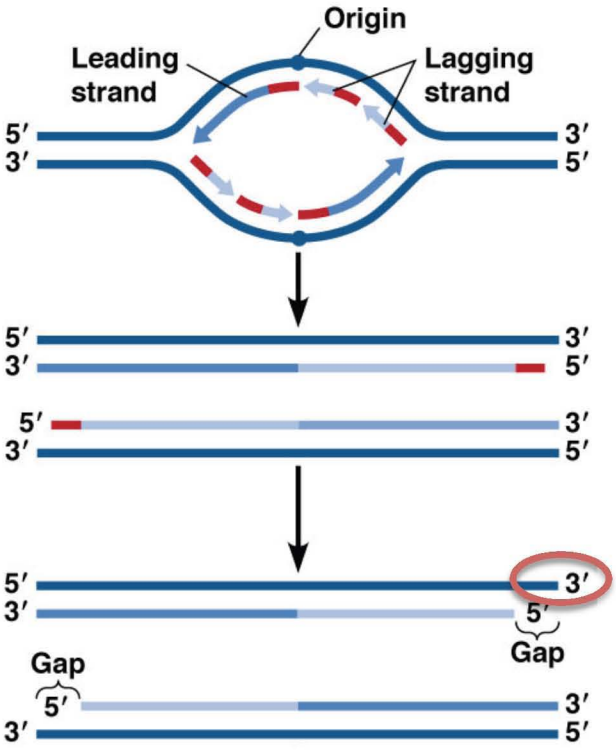

Figure 1.6. Diagram illustrating the end replication problem. DNA replication begins at the origin and requires an RNA primer (shown in red). The RNA primer is ultimately degraded and not replaced, leading to the presence of a gap and a shortening of the telomere. The 3' overhang is circled in red.

Image obtained from Pearson Education Inc.

The enzyme telomerase allows certain cells to solve this end-replication problem and become immortal. Human telomerase consists of human telomerase reverse transcriptase (TERT), an RNA subunit (TERC), and the protein dyskerin (DSKC1).[19] The enzyme binds to the 3' overhang strand of the telomere complementary to the telomerase RNA and uses the TERC subunit to add TTAGGG repeats to the 3' ends of chromosome through reverse transcriptase activity, thereby elongating the telomere and making the cell immortal.[20] Embryonic stem cells, which by function need to replicate numerous

times, activate telomerase to avoid cell death.[21] Because 80 to 90% of cancer cells are also thought to express telomerase to avoid limits on cell division and thus proliferate indefinitely[22,23] efforts are being made to find ways to inhibit telomerase activity and thus prevent the spread of cancer.[4]

Given that the human telomeric repeat sequence d[$(TTAGGG)_n$] is rich in guanines and single-stranded in the 3' overhang, it is unsurprising that it has been shown to fold into a quadruplex *in vitro* (Figure 1.7). The 22 nucleotide sequence d[$AG_3(T_2AG_3)_3$], henceforth abbreviated as Tel22, has been particularly well studied and forms various GQ topologies depending on the conditions used. Early NMR studies revealed that Tel22 forms an antiparallel basket structure Na^+ solution.[24] In molecular crowding and crystalline conditions with K^+, however, a parallel lateral-loop propeller structure was found using X-ray crystallography.[25] Recent studies indicate Tel22 forms various mixed hybrid structures which exist in equilibrium with each other in pseudo-physiological conditions with K^+.[26,27]

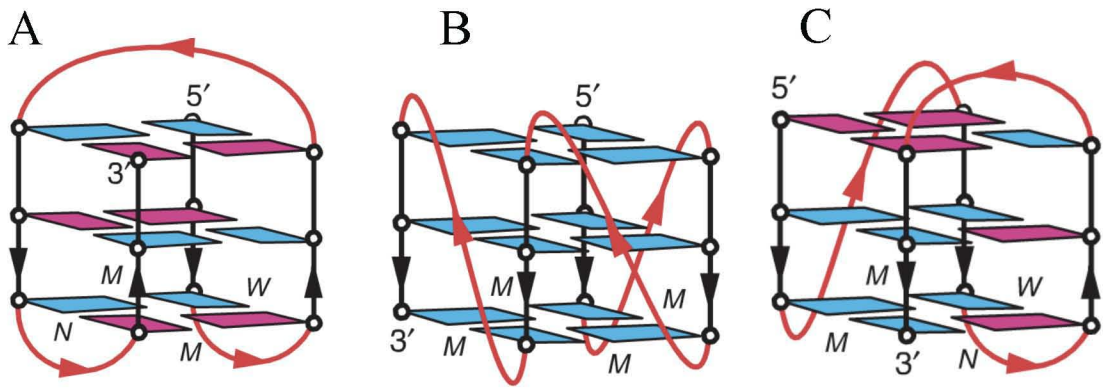

Figure 1.7. Schematic representations of the various GQ topologies the human telomeric repeat sequence can form. (A) Unimolecular anti-parallel basket formed in Na^+ conditions. (B) Bimolecular parallel form observed in high K^+ conditions. (C) Mixed hybrid form seen in pseudo-physiological K^+ conditions.[5] Figure taken from Phan 2010.

The potential presence of GQs in the telomeres may have important implications for preventing the growth and spread of cancer cells. It has been proposed that formation of ligand-induced stabilization of GQ structures in the 3' overhang of the telomere may inhibit the activity of telomerase by blocking the single-stranded substrate the enzyme must bind to, leading to shortening of the telomeres and eventual apoptosis and senescence.[28]

Quadruplex formation in oncogene promoters

An oncogene is a gene that can cause cancer when mutated or expressed at abnormally high levels. Oncogenes can cause cancer in a variety of ways, including the induction of uncontrolled mitosis and the inhibition of apoptosis, the process of programmed cell death.[29,30] Cells require growth factors to initiate division. These growth factors bind to receptors on the cell, resulting in a signal transduction pathway inside the cell. Kinases, enzymes that add phosphate groups to a protein, are integral to the pathway. Ultimately, phosphorylation by kinases activates transcription factors that bind to the promoters of genes and induces their transcription. Mutations in genes involved in these processes can results in their overexpression, causing them to create an overabundance of their product and ultimately uncontrolled cell division and cancer.[31] The oncogene *c-Myc*, for instance, codes for a crucial transcription factor that regulates genes involved in cell proliferation, and thus its overexpression is involved in a variety of cancers.[32] Oncogenes may also create cancerous cells by inhibiting apoptosis. Apoptosis destroys damaged cells that could potentially cause cancer, so mechanisms that keep these cells alive and dividing are implicated in the development of the disease. *Bcl-2* (B-cell lymphoma 2), for example, encodes for an important regulator protein involved in

this process, and its overexpression is associated with melanoma, breast, lung, and prostate cancers.[33]

Because oncogene overexpression helps create cancerous cells as described above, modulating their transcription is being explored as form of anti-cancer therapy.[4] It has been suggested that the G-rich kilobase upstream of the transcription start site in the promoters of various oncogenes, including *c-Myc, VEF, Bcl-2, c-kit*, and *HIF-1α*, form G-Quadruplexes.[34,35] Moreover, experiments have demonstrated that the porphyrin and GQ ligand 5,10,15,20-tetrakis(N-methyl-4-pyridyl)porphyrin (TMPyP4) binds to the GQ formed in the promoter of certain oncogenes including *c-Myc*[36] and *KRAS*[37] and leads to their downregulation. Based on this evidence, a simple model has been proposed and observed in which an equilibrium exists between the double helix and quadruplex forms of DNA in the oncogene promoter (Figure 1.8).[38] On the double helix side, transcription occurs normally resulting the production of the protein product. The formation of the quadruplex, however, serves as a steric block to transcription by preventing the binding of RNA polymerase. Although the duplex form is more thermodynamically stable than the quadruplex form, adding a small molecule such as a GQ-binding ligand or a protein may favor the GQ energetically and therefore shift the equilibrium from the duplex to the quadruplex, thereby reducing the transcription of the oncogene.[4]

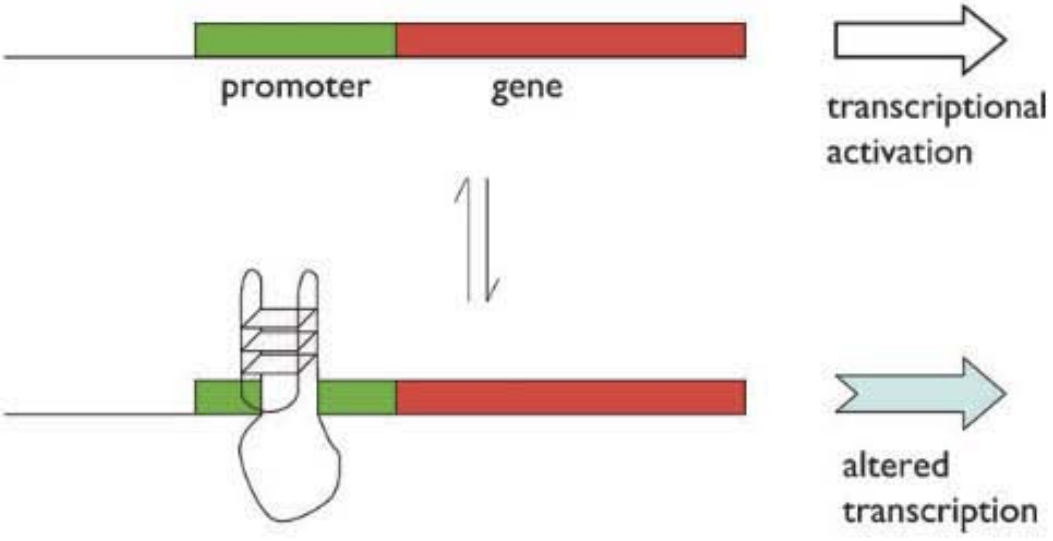

Figure 1.8. Schematic of the equilibrium model for GQ transcriptional regulation. Addition of a GQ-binding ligand or protein can shift the equilibrium to the GQ side, thus inhibiting transcription and mitigating cancer cell growth.[4] Figure taken from Huppert 2008.

Detecting quadruplexes in the cell

While extensive spectroscopic and crystallographic experiments indicate the structure and formation of quadruplexes *in vitro*, acquiring *in vivo* evidence of quadruplexes has proven to be a more challenging but essential task in the field.[39] There is great interest in developing and identifying fluorescent probes that are capable of directly detecting the formation and location of GQs in the cell;[40] this would allow for more definitive correlation of quadruplexes with biological processes discussed earlier. As highlighted in a recent review by Vummidi and coworkers,[39] a good fluorescent probe should have good water solubility, bind to GQs with high affinity, exhibit a large fluorescence emission enhancement upon binding, and exhibit high selectivity for

quadruplex over other DNA structures. It is also desirable that a fluorescent GQ probe be specific for and able to detect one quadruplex topology over the others, given that the specific GQ topology may dictate its biological function[41,42] and is thus crucial to know in the cell.

A variety of small molecule fluorescent probes have been reported in the literature,[39,40] but most display low selectivity for either GQ structures over duplex DNA or for one specific GQ topology. The Balasubraniam group, for instance, employed an antibody-based probe to successfully visualize GQs in the cell using immunofluorescence, but this probe is unable to discriminate between GQ topologies.[43] It is also uncertain if the probe induces GQ formation, putting into question whether GQs were actually present in the cell before the probe addition. An acetylene-bridged purine dimer (APD) fluorescent probe selective for quadruplex over duplex DNA and sensitive to quadruplex topology was recently reported, but this molecule requires a lengthy synthesis.[44] Consequently, there is a still a need for a readily available and simple probe that discriminates against DNA structures and is also selective for one specific GQ topology.

Small molecules as G-Quadruplex binding ligands

Because of the potentially therapeutic effects of GQ stabilization, there is great interest in developing ligands that bind to and stabilize these structures. In addition to having a high affinity for quadruplex structures, desirable ligands should be selective for GQ DNA over other forms of DNA in the cell, particularly the predominant duplex form. An anti-tumor drug that binds readily to duplex DNA may cause cytotoxicity and will

require a greater concentration to achieve its therapeutic effect. Because quadruplex formation in certain regions may have negative physiological effects, ideal ligands should also be selective for one GQ topology over another. Studies demonstrate that GQ presence at the RNA sections of human telomerase enhances telomere maintenance *in vivo,*[45] so ligands not specific for a particular GQ topology intended to halt telomerase can actually increase telomerase activity and lead to undesired tumor growth.[46]

Molecules with large π surfaces are promising candidates for such anti-cancer drugs as they may interact with the guanine quartets through π-π stacking.[4] Moreover, positively charged molecules can interact electrostatically with the negative phosphate groups of the GQ backbone. To date, a variety of ligands have been discovered or synthesized that bind tightly to GQs. A series of acridine compounds, such as BRACO-19 (Figure 1.9A),[47] have been shown to stabilize GQ DNA well. The tightest known GQ binder is telomestatin (Figure 1.9B),[48] a large macrocycle synthesized by the bacterium *Streptomyces analutus*.

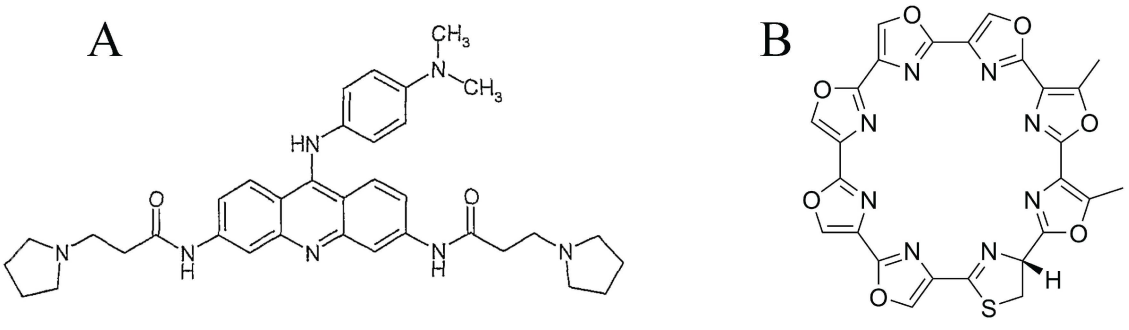

Figure 1.9. Structure of (A) BRACO-19 and (B) telomestatin, two well known GQ binders.

Porphyrins, organic compounds that contain a heterocylic macrocycle with four pyrrole subunits connected together with methane bridges, are particularly important GQ binders. The length of their macrocycle (~10Å) is close to that of a G-quartet (11 Å), and studies have shown that they are readily uptaken by the cell through pinocytosis.[49] Moreover, additional functional groups can be easily added to the porphyrin core, allowing for modification to optimize stability and selectivity for GQ structures. Numerous porphyrins have been synthesized and reported as GQ binders in literature. 5,10,15,20-tetrakis(N-methyl-4-pyridyl) porphyrin (TMPyP4, Figure 1.10), for instance, has been thoroughly examined as a GQ stabilizer; studies in literature suggest that TmPyP4 binds tightly to GQ DNA and is a potent inhibitor of telomerase, although it is not selective for quadruplex DNA.[50,51] Porphyrins can bind to quadruplexes through a variety of ways. Spectroscopic studies have suggested the intercalation of the porphyrin between the guanine quartets, although no crystal structures showing this have been reported.[52] Stacking of the porphyrin onto the ends of the quadruplex through π- π stacking has also been observed.[53] Finally, the porphyrin may also interact with the loops or grooves of the GQ structure.

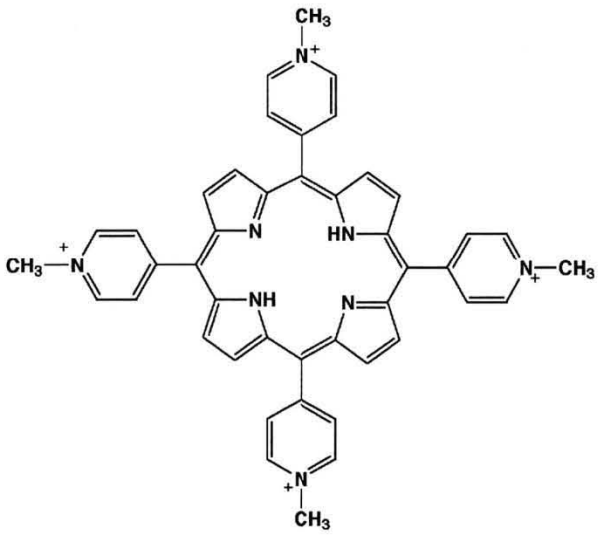

Figure 1.10. Structure of TMPyP4, a strong but non-selective stabilizer of GQ DNA.

Porphyrins are also being investigated as fluorescent probes for the detection of GQ structures *in vivo*. The fluorescence of certain porphyrins increases dramatically when bound to DNA most likely because of the exclusion of solvent molecules that quench the fluorescence. If these fluorescent porphyrins bind tightly and selective to quadruplex DNA, then inserting them into the cell and measuring the fluorescence would provide a means of demonstrating the existence and location of GQ structures in the cell. N-methyl mesoporphyrin IX (NMM, Figure 1.11), for instance, is considered a promising candidate for such a probe. First identified as a potent inhibitor of heme synthesis by preventing Fe^{2+} insertion into protoporphyrin IX,[54] NMM has been thoroughly investigated as a GQ ligand. Competitive dialysis experiments reveal NMM's selectivity for GQ over single-stranded (ss), duplex, triplex, and i-motif DNA and single-stranded RNA and DNA-RNA hybrid.[55] Moreover, studies have shown that NMM interacts selectively with parallel GQ structures.[56] If NMM binds to and fluoresces selectively in the presence of parallel GQs, it might be used a strand selective probe of GQ DNA.

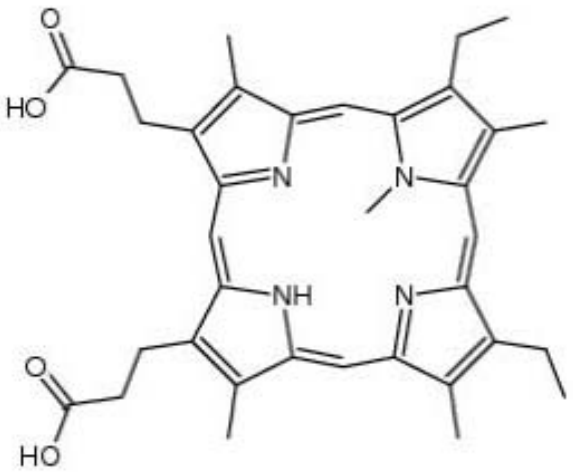

Figure 1.11. Structure of NMM, a moderate but extremely selective GQ binder.

Biophysical tools for studying quadruplexes

A variety of methods, including X-ray crystallography, NMR spectroscopy, UV-Vis spectroscopy, and fluorescence spectroscopy are used to study quadruplex structure, formation, stability, and interactions with ligands.[57] Here, circular dichroism spectroscopy and fluorescence resonance energy transfer, two physical methods used extensively in this work, are introduced.

Circular Dichroism (CD) spectroscopy

Circular dichroism (CD) refers to the differential absorption of right and left circularly polarized light by optically active chiral molecules and is useful in distinguishing secondary DNA structure and especially quadruplex strand orientation.[58,59] Quadruplexes are chiral as a result of the stacking of adjacent G-quartets in a right-handed way and display either homopolar stacking (guanines dipoles in adjacent quartets oriented in the same direction) or heterpolar stacking (guanine dipoles in adjacent quartets oriented in the opposite direction) as shown in Figure 1.12.[60] Although there are

no methods available to calculate the CD spectrum from a quadruplex,[59] the type of stacking (homopolar or heteropolar) has been found to be empirically correlated with quadruplex topology, allowing one to determine the GQ topology from the spectrum. For instance, homopolar stacking, which leads to a peak at ~260 nm and trough at ~250 nm in the CD spectrum, is correlated with parallel quadruplexes, and heteropolar stacking, which produces a peak at ~295 nm and trough at ~260 nm, is associated with antiparallel quadruplexes (Figure 1.13). The mixed hybrid form, which can be considered to have both parallel and anti-parallel components, exhibits an intermediate CD spectrum, with a small peak at 260 nm and a larger peak at 295 nm. It is important to note, however, that CD cannot be used to unambiguously assign a CD spectrum to a GQ structure,[59] as there are some cases where the CD data are inconsistent with the structure determined by other methods. Despite this limitation, CD spectroscopy is extremely useful in qualitatively assessing the effect of cation or ligand on quadruplex structure.[59]

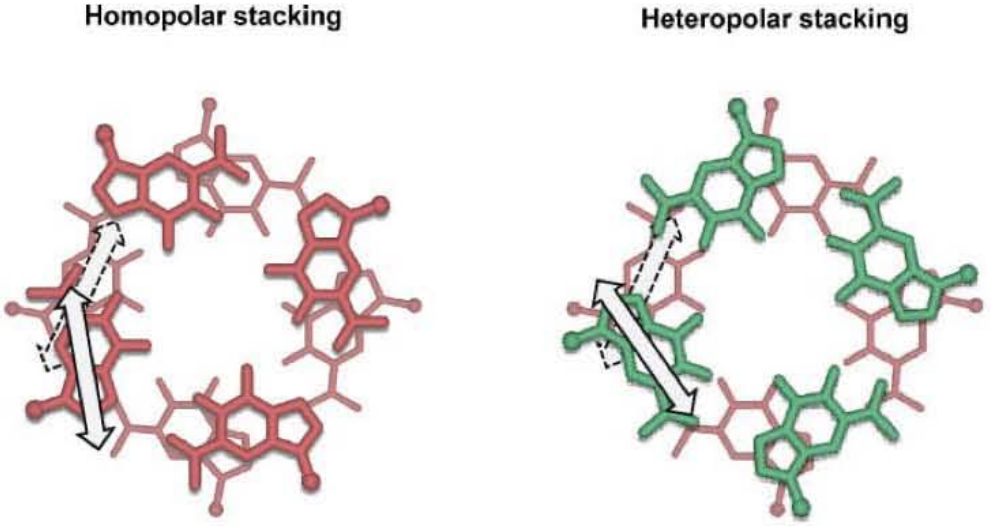

Figure 1.12. Schematic illustrating homopolar and heteropolar stacking of guanine quartets. White arrows indicate transition moments from the absorption band.[60] Figure taken from Masiero et al 2010.

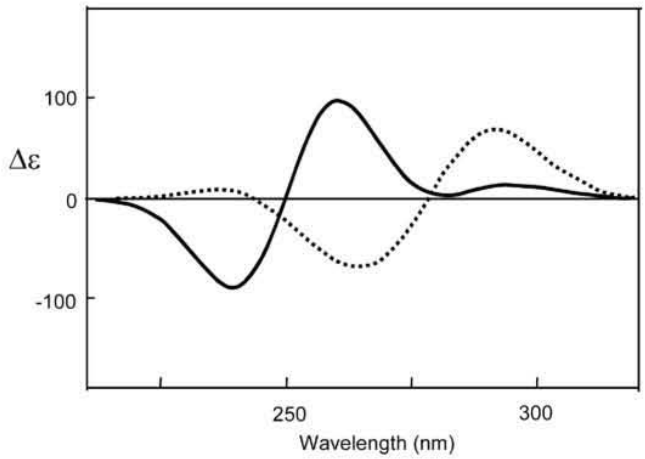

Figure 1.13. Representative CD spectra of a parallel quadruplex exhibiting homopolar stacking (solid line) and antiparallel quadruplex with heteropolar stacking (dotted line).[60] Figure obtained from Masiero et al 2010.

Fluorescence resonance energy transfer (FRET) assays

Fluorescent energy resonance transfer (FRET) refers to the nonradiative transfer of energy between a donor and acceptor chromophore and may be used to study quadruplex folding and stability.[61,62] In these experiments, a fluorescent dye (donor chromophore) and quencher molecule (acceptor chromophore) are placed on the 5' and 3' ends of a GQ-forming sequence. When the quadruplex is fully folded, the dye and quencher are in close proximity, leading to the quenching of the fluorescent signal by the quencher and a low measured fluorescence. If the temperature is increased, however, the quadruplex will begin to unfold, leading to increased distance between the dye and quencher. As the dye and quencher move further apart, the quencher will not be able to quench the fluorescence as effectively, leading to an increased measured fluorescence signal (Figure 1.14A). A graph of the fluorescence as a function of temperature may then be constructed (Figure 1.14B), and the maximum of the first derivative of this curve (Figure 1.14C) yields the melting temperature and thus stability of the quadruplex.[63] The

stabilizing effects of ligands may be readily assessed using FRET by measuring the melting temperature of the quadruplex in the presence of varying concentrations and comparing these values with the melting temperature of the quadruplex alone.

Because the efficiency of the energy transfer between chromophores is inversely proportional to the sixth power of the distance between the quencher and dye.[64,65] FRET is an extremely sensitive technique and hence requires small amounts DNA. Moreover, because the fluorescence can be monitored using a real time PCR machine with up to 96 samples at a time, large libraries of potential-GQ binding ligands may be easily screened for their stabilizing capabilities using this technique.[63]

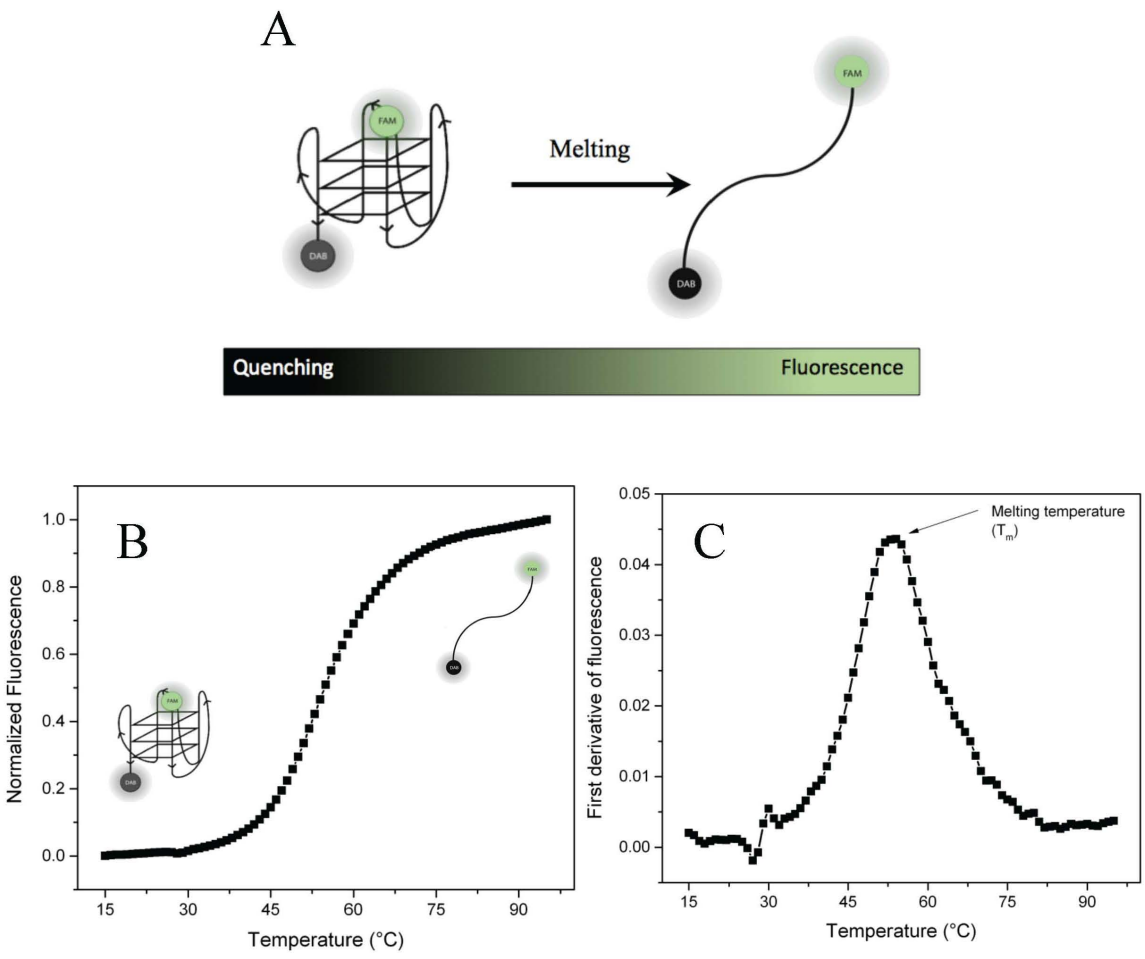

Figure 1.14. Illustration of the principle behind FRET. Part (A) of the figure was prepared by John M. Nicoludis '12.

Chapter II: Materials and Methods

Materials and Reagents

Porphyrins

Pd(II)- 5,10,15,20-tetrakis(N-methyl-4-pyridyl)porphyrin (PdTMPyP4) and N-methyl mesoporphyrin IX (NMM) were purchased from Frontier Scientific (Logan, UT, USA). Pt(II)- 5,10,15,20-tetrakis(N-methyl-4-pyridyl)porphyrin (PtTMPyP4) was a generous gift from Dr. Robert F. Pasternack, Swarthmore College. 5,10,15,20-tetrakis((N-spermido)benzamide)porphyrin (TCPPSpm4) was provided by Dr. Alessandro d'Urso, University of Catania (Sicily, Italy). Porphyrins were diluted in double-distilled (dd) H_2O to 0.3 to 1.3 mM concentrations and stored at 4°C in the dark. Porphyrin concentrations were determined via UV-vis spectroscopy using extinction coefficients found in Table 1.

Table 1. Names and extinction coefficients of porphyrins used in this work.

Abbreviated name	**Full compound name**	**Extinction Coefficient (ε) at λ_{max} ($M^{-1}cm^{-1}$) (ref)**	**λ_{max} (nm)**
NMM	N-methylmesoporphyrin IX	1.45×10^5 (66)	379
PtTMPyP4	Pt(II)- 5,10,15,20-tetrakis(N-methyl-4-pyridyl)porphyrin	1.72×10^5 (67)	401
PdTMPyP4	Pd(II)- 5,10,15,20-tetrakis(N-methyl-4-pyridyl)porphyrin	1.68×10^5 (68)	418
TCPPSpm4	5,10,15,20-tetrakis((N-spermido)benzamide)porphyrin	2.24×10^5 *	415

*determined experimentally in this work; see **Porphyrin aggregation and extinction coefficient determination** section for details.

Oligonucleotides

Oligonucleotides were purchased from either Midland Certified Reagent Company (Midland, TX, USA) or Eurogentech (Liège, Belgium). Fluorescently-labeled oligonucleotide 5′-6-FAM-$G_3(TTAG_3)_3$-Dabcyl-3′ (F21D) and unlabeled calf thymus (CT) DNA were purchased from IDT (Coralville, IA, USA). F21D was diluted to ~100 μM and stored at -80 °C. CT DNA was dissolved in 10 mM lithium cacodylate, 1 mM Na_2EDTA, and placed on a nutator for 1 week at 4 °C before use. All other DNA stocks were dissolved in dd H_2O to ~1 mM and kept at 4 °C for no longer than one month. To induce the formation of the most thermodynamically stable species, oligonucleotides were melted at 90 °C for ten minutes in the appropriate buffer, cooled to room temperature over 3 to 4 hours, and incubated for at least 12 hours at 4 °C. I-motif structures were prepared by dissolving C-rich sequences in acidic conditions (pH = 5.8) and annealing as described above. All oligonucleotide concentrations were determined via UV-vis spectroscopy using the extinction coefficients found in Table 2 and calculated using the nearest neighbor approximation method.

Table 2. Extinction coefficients of oligonucleotides used in this work. All values reported per GQ strand unless otherwise stated.

Abbrev.	Sequence (5′→ 3′)	ε_{260} ($M^{-1}cm^{-1}$)
G4	TTTTGGGGTTTT	1.064×10^5
G8	TTTTGGGGGGGGTTTT	1.468×10^5
CT	Genomic calf thymus DNA	1.22×10^4 (per base pair)
ds12-A	GGCTTGAGTGCG	1.127×10^5
ds12-B	CCGAACTCACGC	1.083×10^5
ds26	CAATCGGATCGAATTCGATCCGATTG	2.532×10^5
Tel22	AGGGTTAGGGTTAGGGTTAGGG	2.285×10^5

VEGF	GGGAGGGTTGGGGTGGG	1.714×10^5
cMyc	TGAGGGTGGGTAGGGTGGGTAA	2.287×10^5
C8	AAAACCCCCCCCAAAA	1.574×10^5
i-cMyc	TTACCCACCCTACCCACCCTCA	2.287×10^5
TC_4T	TCCCCT	4.56×10^5
$C_4T_4C_4$	CCCCTTTTCCCC	9.02×10^5
26TelG4	AGGGGTTAGGGGTTAGGGGTTAGGGG	2.689×10^5
Bcl-2	GGGCGCGGGAGGGAATTGGGCGGG	2.374×10^5
cKit1	GGGAGGGCGCTGGGAGGAGGG	2.132×10^5
cKit2	GGGCGGGCGCGAGGGAGGGG	1.991×10^5
G4TERT	AGGGGAGGGGCTGGGAGGGC	2.029×10^5
TBA	GGTTGGTGTGGTTGG	1.433×10^5
$G_4T_4G_4$	GGGGTTTTGGGG	1.152×10^5

Buffers

Cacodylate buffers containing K^+ or Na^+ were used for most studies presented in this thesis. These buffers were preferred over Tris or phosphate buffers because they do not absorb light in the far UV region and their pK_a is temperature independent.[63] The ionic strength of most buffers used was kept at 110 mM salt so as to best match the ionic strength present in the cell. All buffers used in this study are summarized in Table 3:

Table 3. Names and compositions of buffers used in this work.

Buffer name	**Composition**
5K	10 mM lithium cacodylate, pH = 7.2, 5 mM KCl, 95 mM LiCl
5K 5.8	10 mM lithium cacodylate, pH = 5.8, 5 mM KCl, 95 mM LiCl
150K	10 mM lithium cacodylate, pH = 7.2, 150 mM KCl
KPi	10 mM potassium phosphate, pH = 7.0, 50 mM KCl
50Na	10 mM lithium cacodylate, pH = 7.2, 50 mM NaCl, 50 mM LiCl
100Li	10 mM lithium cacodylate, pH = 7.2, 100 mM LiCl

Uv-Vis Spectroscopy

Instrument and data collection

UV studies were performed on Cary 300 Varian or Bioserv Uvikon XL/XS spectrometers with Peltier temperature control units (error of ± 0.3 °C). Scans were collected from 350 to 650 nm for porphyrin samples and 220 to 330 nm for DNA samples. All spectra were baselined with a cuvette containing a solution of buffer. All experiments were performed at least three times unless stated otherwise.

Porphyrin aggregation studies and extinction coefficient determination

The conjugated system in the porphyrin tetrapyrrole core leads to strong absorption bands in its UV-Vis spectrum corresponding to $\pi \rightarrow \pi^*$ transitions.[69] Beer's law states the this absorbance (A) is related to its extinction coefficient (ε), concentration (C) of porphyrin, and the pathlength of the cuvette used (l) as follows:

$$A = \varepsilon \times l \times c \quad \textbf{eq.1}$$

Adherence to the Beer-Lambert law for a certain concentration range indicates a lack of porphyrin aggregation. In order to test for porphyrin aggregation, UV-Vis spectra were taken on PtTMPyP4, PdTMPyP4, TCPPSpm4, and ZnTCPPSpm4 samples with concentrations ranging from 0.5 to 50 μM diluted in either dd H_2O or 5K prepared in 1 cm methylacrylate cuvettes and 1 mm quartz cuvettes. The value of the extinction coefficient of TCPPSpm4 were determined from the slope of a best-fit line of absorbance vs. porphyrin concentration. Solutions of varying porphyrin concentrations were prepared from a solution with a known concentration of 361.4 μM.

Porphyrin UV-Vis titrations

The electronic structure of a porphyrin is altered when it is bound to DNA, resulting in a change in the intensity and location of the Soret peak. In UV-Vis titration experiments, these changes in the spectrum upon the addition of increasing amounts of DNA are used to determine the binding constant, binding mode, and binding stoichiometry of the GQ-porphyrin interaction.

Titrations were performed by stepwise addition of a small volume of Tel22 annealed in buffer to a solution of 1 mL ~1-9 μM porphyrin in buffer. In some titrations, Tel22 samples contained the same amount of porphyrin used to eliminate dilution effects upon Tel22 addition; in others, Tel22 did not contain porphyrin and the effect of dilution was factored out mathematically before data analysis. 1 cm path length methacrylate cuvettes were used to avoid porphyrin adsorption to the walls of quartz cuvettes. Spectra were collected after adding Tel22 to ligand, mixing thoroughly, and waiting up to two minutes for equilibration. Tel22 was added until no significant change in the UV-Vis spectrum was observed. The red shift, $\Delta\lambda$, was obtained from titration data by determining the difference in the position of the Soret band maximum between free and bound porphyrin, and the % hypochromicity, **%**H, was calculated as follows:

$$\%H = \frac{\varepsilon_f - \varepsilon_b}{\varepsilon_f} \times 100\% \qquad \textbf{eq. 2}$$

Here, ε_f and ε_b are the extinction coefficients of free and bound porphyrin, respectively, at Soret maxima.

Fluorescence Spectroscopy

Instrument and data collection

Fluorescence experiments were performed at 25 °C on a Photon Technology International QuantaMaster 40 or a Horiba Fluoramax-4 spectrofluorimeters equipped with temperature control units. For experiments with NMM, samples were excited at 399 nm and the emission was measured from 550 to 750 nm; the excitation wavelength and emission range were selected based on previous NMM fluorescence studies reported by the Bolton laboratory.[70,71] For PtTMPyP4 samples, the excitation wavelength was 412 nm and the emission was measured from 600 to 800 nm. The optimal excitation wavelength was taken as the value that produced the maximum fluorescence intensity value of 3D plot of excitation wavelength vs. emission wavelength vs. fluorescence intensity (Supplementary Figure S1) constructed by taking fluorescence spectra on a sample of PtTMPyP4 in dd H_2O for a variety of excitation wavelengths. The precise scan parameters used varied depending on the experiment and porphyrin and are thus discussed at the end of each experiment described below.

Porphyrin fluorescence titrations

Porphyrins exhibit strong fluorescence emission most likely due to a $\pi^* \rightarrow \pi$ transition.[72] Some porphyrins exhibit an increase in fluorescence emission in the presence of GQs, allowing for the determination of the binding constant from fluorescence titrations. For all experiments, the solutions were inverted at least ten times after addition of DNA and left to equilibrate for at least thirty seconds before scans were taken.

1. PtTMPyP4 + Tel22 titrations

A 2mL solution of 1-2 μM PtTMPyP4 in 5K buffer was titrated with either 0.1 mM Tel22 or 0.1 mM CT DNA in a 3mL methacrylate fluorescence cuvette with a 1 cm path length. DNA was added until there was no observed increase in fluorescence. Scan parameters were as follows: increment = 1 nm; integration time = 0.5 sec; slit length = 5 nm for excitation and emission.

2. NMM + GQ titrations

0.1 - 1 μM solutions of NMM were titrated with VEGF in 5K buffer, $G_4T_4G_4$ in 5K and 50Na buffer, or 26TelG4 in 50Na buffer in 2 mL quartz cuvettes until the fluorescence signal was saturated, or the final concentration of DNA was at least ten times greater than the concentration of porphyrin. Competition titration experiments were performed to assess NMM's selectivity for GQ structures in the presence of excess duplex DNA. In the first experiment of experiments, 1μM NMM with 10 μM VEGF in 5K was titrated with increasing amounts of CT DNA. In the second set of experiments, 1μM NMM containing either 10 or 100 μM CT DNA in 5K was titrated with increasing amounts of VEGF. Scan parameters were as follows: increment = 1 nm; integration time = 0.5 sec; slit length = 2 nm for excitation and emission.

Fluorescence enhancement studies

A 1 μM solution of NMM or PtTMPyP4 was prepared in buffer in either a 400 μL or 2 mL quartz fluorescent cuvette and its spectrum was taken. To ensure that all the porpyrin was bound, a 10 fold excess of DNA (NMM) or 5 fold excess of DNA (PtTMPyP4) was added and the fluorescence spectrum was retaken after up to 1 hour of equilibration. The increase in fluorescence was quantified by calculating the fluorescence enhancement (F.E.), which is defined as follows:

$$F.E. = \frac{FL(P + DNA) - FL(P)}{FL(P)} \times 100\% \quad \textbf{eq. 3}$$

where FL(P) is the maximum value of fluorescence of porphyrin alone in buffer and FL(P + DNA) is the maximum fluorescence of porphyrin with DNA.

Scan parameters for fluorescence enhancement studies with NMM were as follows: increment = 1 nm; integration time = 0.5 sec; slit length = 2 nm for excitation and emission. Scan parameters for fluorescence enhancement studies with PtTMPyP4 were as follows: increment = 1 nm; integration time = 0.5 sec; slit length = 5 nm for excitation and emission.

Measuring the effect of pH on NMM fluorescence

These pH studies were performed to determine if NMM's fluorescence signal change is affected by pH. 1 -2 μM NMM was titrated with 0.1 M NaOH, LiOH, or HCl to achieve the desired pH, and fluorescent scans were taken. Experiments were performed using both the titration method and batch method. Reversibility experiments were also performed to see if the change in NMM's fluorescent signal at various pH values was reversible. The pH was reduced to ~3 with 0.1 HCl and the fluorescent spectrum was recorded. The pH was then brought back up to ~7 with 0.1 NaOH or LiOH and the spectrum was remeasured. The pH of a second sample of NMM was brought up to ~11 with NaOH or LiOH, and a fluorescent scan was taken. The pH was then reduced to ~7 with HCl and fluorescence was re-measured.

Scan parameters for NMM pH studies were as follows: increment = 1 nm; integration time = 0.5 sec; slit length = 3.5 - 5 nm for excitation and emission.

Fluorescence lifetime measurements

Experiments were performed with NMM in various buffers on a multi-frequency cross-correlation phase and modulation fluorimeter at room temperature. Samples were prepared such that the NMM:GQ ratio ranged from 1:4 to 1:30 and the concentration of NMM ranged from 0.7 to 2.3 μM, depending on the sample. After the sample was excited at 399 nm, its emission was filtered and referenced to a scatterer which produced counts to match the sample. Data was collected in the frequency range of 1 – 250 MHz. 10-50 frequencies were collected depending on the sample. The value of the fluorescence lifetimes were calculated as described in Jameson et al. 1984.[73]

Circular Dichroism

All experiments were performed on an AVIV 410 spectropolarimeter containing a Peltier heating unit (error of ± 0.3 °C) or a Jasco J-18 spectropolarimeter using a 1 cm quartz cuvette. Scans of 1 to 5 μM DNA were collected three to five times from 330 to 220 nm with a 1 nm bandwidth and an average time of 1 sec at 20 °C and averaged. Data were baseline-corrected by subtracting the CD spectra of buffer alone in the cuvettes used for sample scans and zeroed by subtracting the average absorbance for the last 15-20 nm. These values were converted into molar ellipticity using the equation:

$$\Delta\varepsilon = \frac{\theta}{C \times l \times 3.3 \times 10^4} \qquad \textbf{eq. 4}$$

where Δε is molar ellipticity, θ represents CD signal in mdeg, C is the concentration of DNA in mol L^{-1}, and l is the path length of the cuvette in cm. Data were then smoothed with a Savitzky-Golay smoothing filter using a 13-point quadratic function. In certain experiments, CD spectra of DNA sequences were taken in the presence of up to 2 fold

excess ligand so as to determine the effect of ligand on the DNA structure. In these experiments, samples were annealed with or without ligand at 90 °C for ten minutes, cooled slowly to room temperature, and incubated from 0 to 12 hours at 30 °C depending on the ligand before scans were taken. All CD experiments were repeated three times unless stated otherwise.

Binding Constant Determination

Direct fitting

Direct fitting was performed to determine the value for the association constant K_a from UV-Vis and fluorescence titrations of porphyrin with DNA. Signal (either absorbance or fluorescence) at the wavelength maxima of the titration were simultaneously fit to the equation:

$$Y = Y_0 - \frac{x}{C_t}\left(Y_0 - Y_f\right) \quad \textbf{eq. 5}$$

where Y_0 and Y_f are the initial and final signal at each peak, C_t is the total porphyrin concentration, and x is concentration of ligand-GQ complex. The value for x is derived from the simple equilibrium equation for the reaction Porphyin + GQ → Porphyrin-GQ complex:

$$K_a = \frac{x}{(C_s - x)\times(C_t - x)} \quad \textbf{eq. 6}$$

Here, C_s is the concentration of DNA. It is important to note that the direct fitting method assumes a 1:1 binding stoichiometry between ligand and GQ. In order to fit data with a different binding stoichiometry, the concentration of DNA used in the equation must be

multiplied by the ligand:GQ ratio to obtain the concentration of ligand binding sites Fitting was done with GraphPad Prism Software 4.0.

Scatchard analysis

A scatchard plot is a method used to determine the affinity constant and binding stoichiometry for a ligand/receptor binding interaction[74] and can confirm value of these parameters obtained from other methods. Scatchard plots were used to ascertain binding information from UV-Vis and fluorescence titration data by plotting the binding ratio r vs r/C_f, where r is the ratio C_b / [DNA]. The concentration of bound porphyrin, C_b, and the concentration of free porphyrin, C_f, are determined from the total porphyrin concentration, C_t, as follows: $C_b = C_t \times \alpha$ and $C_f = C_t - C_b$. The fraction of bound porphyrin, α, is determined from the equation:

$$\alpha = \frac{I_{free} - I}{I_{free} - I_{bound}} \quad \textbf{eq. 7}$$

where I_{free} and I_{bound} are the values of absorbance or fluorescence of free and bound porphyri, respectively, at the Soret maximum for free porphyrin.[75] Data points are then fit using a best fit line with linear equation

$$\frac{r}{C_f} = K_a(n - r) \quad \textbf{eq. 8}$$

where K_a is the binding constant at equilibrium and n is the number of ligand molecules bound to each GQ.[75]

FRET melting studies

In this work, fluorescently-labeled human telomeric DNA (F21D) was used to ascertain the stability of quadruplexes in the presence of various ligands using FRET. F21D forms a hybrid intramolecular GQ in 5K and anti-parallel GQ in 50Na like it's unlabeled counterpart, Tel22, as confirmed by CD and thermal denaturation studies (TDS) reported in literature; TDS produces quadruplex-specific signatures and CD spectra of F21D are similar to those of Tel22.[56] Stability is indicated by ΔT_m, the difference between the melting temperature of the GQ in the presence of porphyrin and the melting temperature of the GQ alone.

FRET experiments can be used to determine ligand's selectivity for GQ DNA vs any unlabeled competitor. Because duplex DNA is present in excess in the cell, CT DNA, which represents a generic duplex DNA, was selected as the primary competitor. Selectivity of a ligand for GQ DNA is determined by finding the melting temperature of F21D in the presence of increasing concentrations of CT DNA at a fixed concentration of ligand. Ligands selective for GQ DNA should bind to the GQ in the presence of the competitor as strongly as they bind to GQ alone, so unchanging melting temperatures observed with increasing CT DNA concentration are consistent with excellent selectivity. The selectivity was then quantified by calculating the selectivity ratio, the concentration of competitor (in μM) necessary to reduce ΔT_m in half.

Experiments were performed on a MJ Research DNA Engine (RT-PCR machine). For both stability and competition studies, a solution of 0.25 μM F21D was prepared in 5K buffer. 40 μL of this solution was placed in white BioRad RT-PCR tube strips and diluted with porphyrin and/or buffer to obtain a final concentration of 0.2 μM DNA and

with a total well volume of 50 μL; see **FRET sample setup for stabilization and competition studies** section of the Appendix for precise information on how each FRET sample was prepared. Samples were then incubated for one hour at 4 °C and melted on the RT-PCR machine. The 6-FAM dye was excited at 496 nm and measured at 519 nm. The following melting protocol was implemented for both stability and competition studies: First, the sample was incubated at 15 °C for 5 minutes. Second, the sample was melted from 15.0° to 95.0° C at a rate of1 °C min^{-1} and fluorescence was read every 1.0 °C. Finally, the sample was cooled from 95.0° to 15.0° C at a rate of 1 °C min^{-1} and the fluorescence was read every 1.0 °C

Each experiment contained duplicate samples. Data from duplicate experiments were averaged and normalized from 0 to 1 using the formula:

$$Y' = \frac{Y - Y_{min}}{Y_{max} - Y_{min}} \quad \textbf{eq. 9}$$

where Y represents the fluorescent signal. Normalized data were smoothed with a Savitzky-Golay smoothing filter using a 5-point quadratic function, and the visually-determined maximum of the first derivative of fluorescence vs. temperature (error of ± 0.5 °C) yielded the melting temperature. Each experiment was repeated three times and the mean and standard deviation were obtained. Origin Software was used for data analysis.

Chapter III: N-methylmesoporphyrin IX fluorescence as a reporter of quadruplex strand orientation

This chapter represents a summary of the important findings of my work investigating NMM's potential role as a selective GQ reporter, which lead to a publication entitled "N-methylmesoporphyrin IX fluorescence as a reporter of strand orientation in guanine quadruplexes" in the *FEBS Journal* earlier this year;[76] a copy of the paper can be found in Appendix. As detailed in the introduction, NMM is known be high selectivity for quadruplex DNA over a variety of other DNA structures[55,66] and binds selectively to parallel quadruplexes over anti-parallel or mixed hybrid ones.[56] Moreover, studies by the Bolton group have shown that NMM fluorescence increases in the presence of quadruplex but not double-stranded (ds) DNA,[70,71] leading us to hypothesize that NMM may be an attractive candidate for fluorescent GQ probe. In this work, we systematically investigate NMM's ability to discriminate between quadruplex DNA and other secondary DNA structures through fluorescence. We also test NMM's ability to probe GQ DNA in an excess of duplex DNA and elucidate the mechanism of NMM fluorescence enhancement.

Selection of examined sequences.

The goal of this work was to evaluate NMM's candidacy as a highly selective fluorescent reporter of quadruplexes. To this end, we examined the fluorescence of NMM in the presence of variety of DNA sequences including parallel, anti-parallel, and mixed hybrid GQs, i-motifs, single-stranded DNA, and duplex DNA. GQ-forming sequences assessed were chosen based the diversity of GQ topologies expected to form and their presence in the promoters of several important oncogenes. As discussed previously, it has been postulated that the strand complementary G-rich strands in human genome is C-rich and can form four-stranded i-motif structures consisting of two interleaved ladders with pairs of strands associated together through diagonal $C{\equiv}C^+$ bond at acidic pH (Figure 1.4).[4] In an effort to examine the interaction between these potentially biologically significant molecules and NMM, we also analyzed i-cMyc, the complement of the promoter of the oncogene cMyc, and C8, TC_4T, and $C_4T_4C_4$, C-rich sequences thought to form an i-motif structure.[11] Information on all sequences used may be found in Table 2.

NMM displays selective fluorescence enhancement in the presence of DNA

The key experiment in this work was to test fluorescence of NMM in the presence of the variety of DNA secondary structures. Specifically, the fluorescence of NMM was measured before and immediately after the addition of DNA. DNA was present in a ten-fold excess to ensure complete binding of NMM. Alone, NMM fluoresces weakly because the interactions with solvent relax absorbed energy non-radiatively.[70] When NMM is bound to DNA, however, water is excluded from the porphyrin environment,

increasing its measurable fluorescence. The data collected are represented as the enhancement of the NMM fluorescent signal in Figure 3.1. The fluorescent intensity of NMM increases dramatically in the presence of parallel-stranded GQ-forming sequences, with the fluorescence enhancement ratio of 40 to 70. The fluorescence of NMM in the presence of antiparallel GQs and mixed hybrid GQs also increases, though less so, in the range of 2 to 18 and 35 to 60, respectively. The negligible increase in fluorescence of NMM in the presence of single-stranded and duplex DNA and i-motifs structures suggests little interaction between NMM and these sequences. The data were analyzed for statistical significance using an unpaired two-tailed t-test, and the difference in fluorescence enhancement for parallel vs other DNA structures was found to be significant at the 95% confidence interval. Overall, data suggest that NMM is capable of discriminating between GQ topology and may thus have potential as a quadruplex probe.

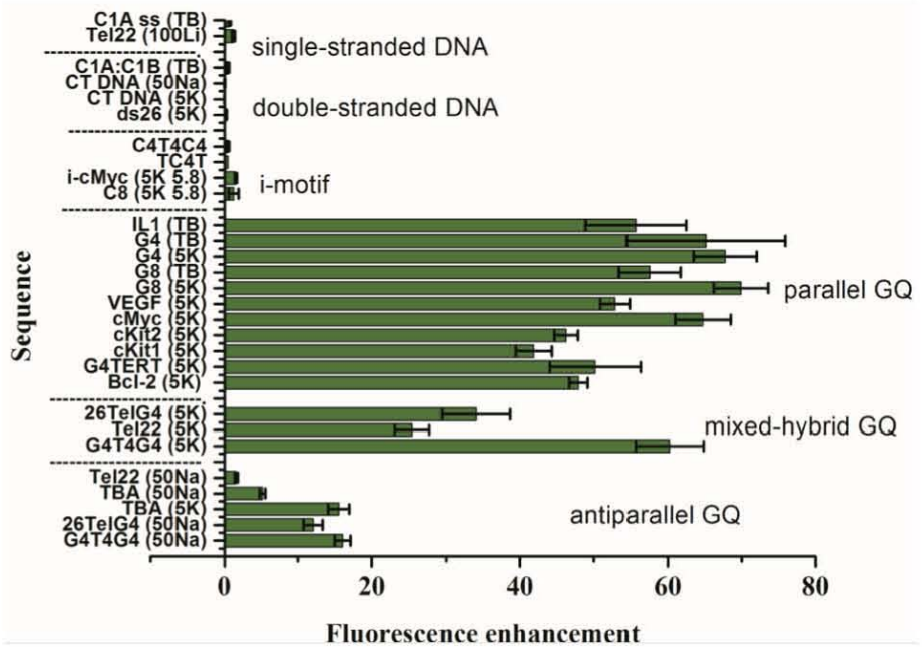

Figure 3.1. Values of the fluorescence enhancement of NMM in the presence of a 10-fold excess of DNA. Error bars indicate one standard deviation.

CD spectroscopy demonstrates the effect of NMM on GQ structure

Figure 3.1 shows one curious detail: the addition of anti-parallel or mixed hybrid GQ-forming sequences leads to a smaller fluorescence enhancement relative to parallel sequences, with the exception of $G_4T_4G_4$ in 5K buffer, addition of which lead to fluorescence enhancement of 60 ± 5. Indeed, both solution NMR and crystallographic studies indicate that $G_4T_4G_4$ has an anti-parallel structure, yet the sequence behaves like a parallel GQ. In order to determine the cause of this anomaly, CD scans of $G_4T_4G_4$ in 5K and 50Na were taken both with and without a 2-fold excess of NMM (Figure 3.2). An increased signal of the peak at 264 nm and a decrease in signal for the peak at 295 nm for $G_4T_4G_4$ in 5K and 50Na is consistent with the induction of more parallel character and may help explain the unusually high fluorescence enhancement value obtained in the fluorescence studies. To determine if NMM affects the topology of other mixed hybrid and anti-parallel GQs, we performed similar CD studies with DNA alone and DNA in the presence of 2-fold excess of NMM for TBA in 50Na and 26TelG4 in 50Na both with and (Figure 3.2). Spectra of TBA in 50Na and 26TelG4 in 50Na are identical with or without NMM, indicating that the presence of the porphyrin does not significantly alter their structure.

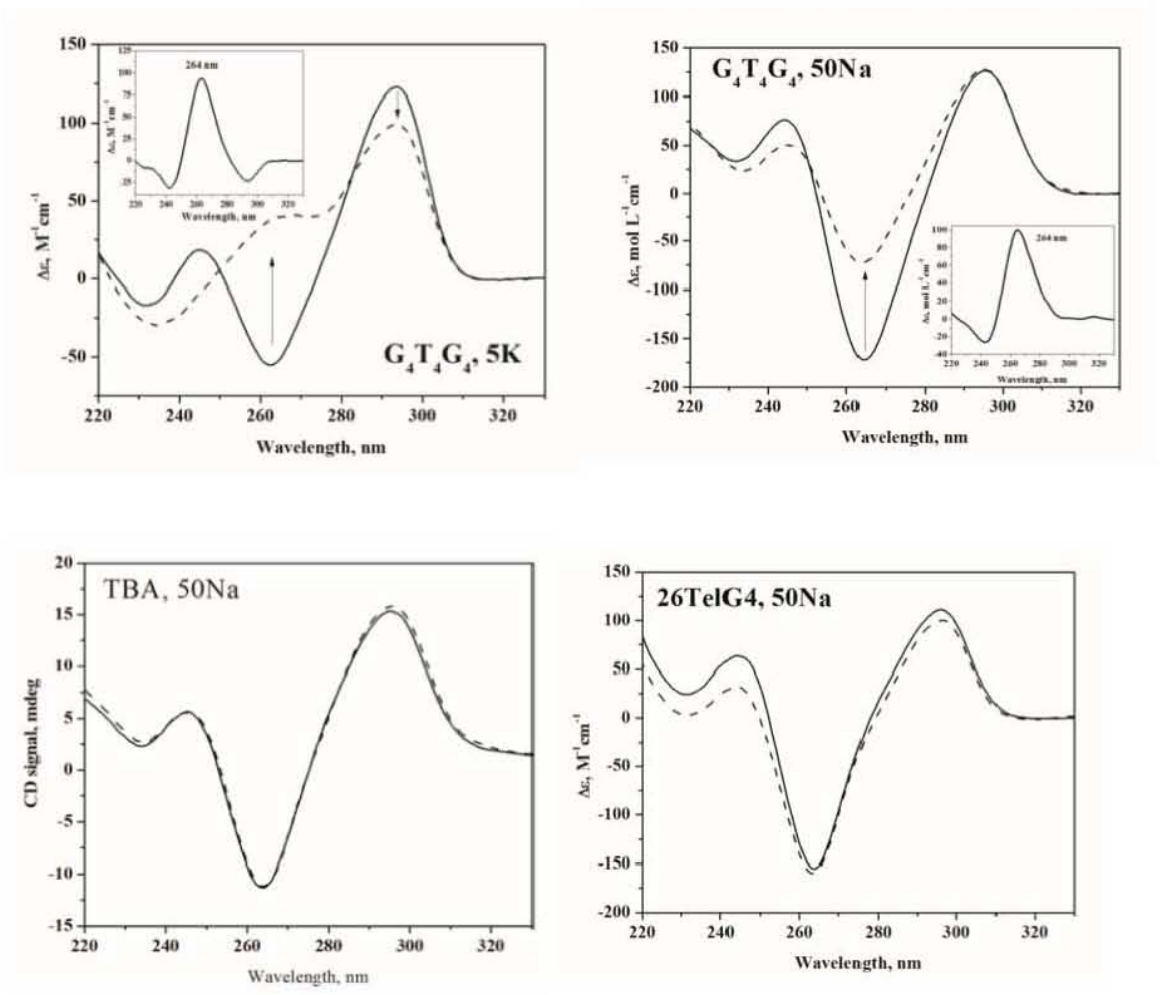

Figure 3.2. CD spectra of $G_4T_4G_4$ in 5K and 50Na and TBA and 26TelG4 in 50Na buffers alone (solid line) or in the presence of a 2-fold excess of NMM (dashed line). Samples were annealed at 90 °C, cooled to 30 °C slowly, and incubated at 30 °C for > 12 hours to ensure equilibration with NMM. NMM induces a more parallel character in the structure in G4T4G4 in both 5K and 50Na buffer, demonstrated by the increase of the peak at 264 nm. The inset depicts the difference spectra between $G_4T_4G_4$ alone and in the presence of NMM. In both cases the difference spectra indicate formation of parallel structure upon NMM addition.

NMM fluorescence probes parallel GQs even in the presence of excess duplex DNA

Duplex DNA is the primary form found in the cell and is thus likely present in higher concentrations than quadruplex DNA, so a successful GQ probe must be capable of binding to a quadruplex even in the presence of excess duplex structures. In order to test NMM's ability to bind selectively to parallel GQs in the presence of excess duplex DNA as well as quantify this binding interaction, competition fluorescent titrations were designed. In these experiments, increasing amounts of a representative parallel-GQ (VEGF) were added to a solution of 1 μM NMM alone or NMM containing 100-fold excess of CT DNA relative to the final concentration of VEGF. Both these titrations were run in 5K and in parallel to ensure that lamp fluctuation or other experimental error were factored out. Results of these studies yielded a nearly identical binding curves (Figure 3.3) indicating that binding of NMM to VEGF and NMM fluorescent enhancement is unaffected by the excess of dsDNA. In order to obtain a value for the binding constant, the data were fit to two different models; one first assumes the formation of 1:1 DNA:NMM complex and the second a 2:1 complex. The latter model produced the best fitting results judging by the value of R^2 (0.9728 for 1:1 and 0.9900 for 1:2); obtained K_a are (6.9± 0.5) × 10^6 L mol^{-1} and (7.0 ± 0.8) × 10^6 L mol^{-1} for NMM binding to VEGF alone or in the presence of duplex DNA, respectively, values which are within error of each other. Job plot experiments were carried out to confirm the binding stoichiometry; the results (Figure 3.4) indicate that the VEGF GQ binds to NMM in a 1:1 ratio when the concentrations of DNA and porphyrin are approximately the same but binds in a 2:1 ratio when VEGF is present in excess (as in our fluorescence studies).

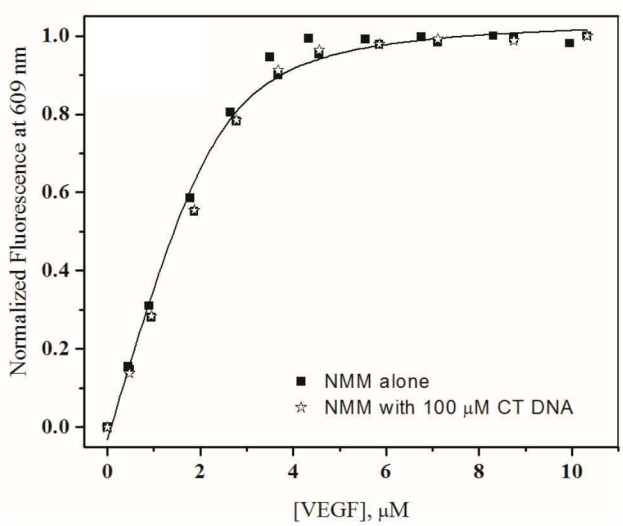

Figure 3.3. Representative titration of VEGF into a solution of NMM in 5K either alone (solid square) or in the presence of 100 μM CT DNA (open star) at 25 °C. The line is the best fit to the experimental data assuming 1:2 DNA:NMM model.

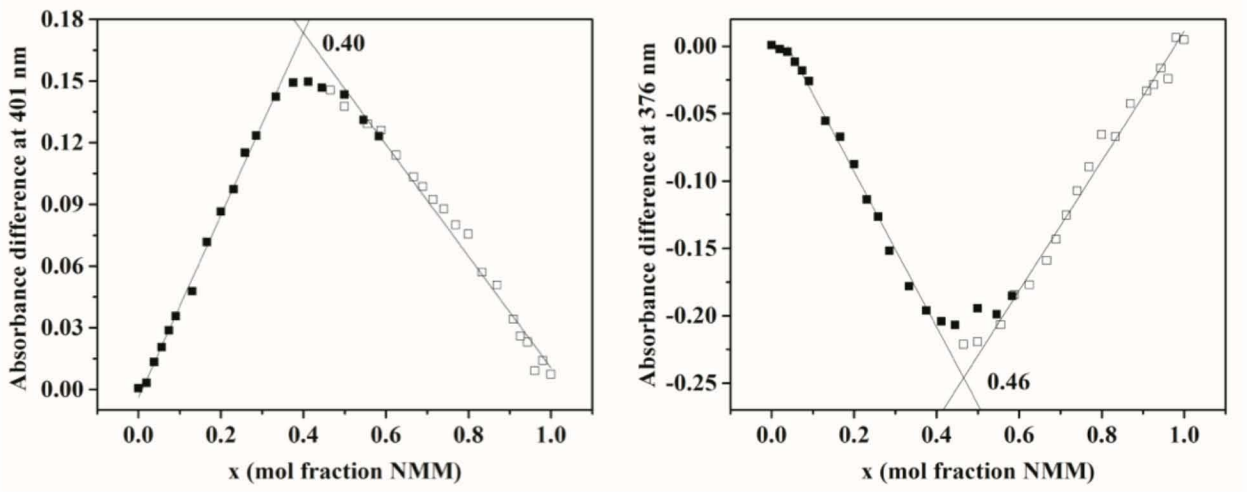

Figure 3.4. Job Plot titration for VEGF-NMM system. Titrations of NMM into VEGF are represented by solid squares, and titrations of VEGF into NMM in 5K are represented by open squares. The data indicate either a 1:1 or 1:2 NMM:VEGF binding stoichiometry.

In order to further confirm the results of the competition fluorescence titration, reverse competition experiments were also performed. Here, increasing amounts of either CT DNA in 5K buffer or C1A:C1B duplex in TB buffer were added to a solution of NMM containing a 10-fold excess of VEGF (Figure 3.5). Results show no change in fluorescence upon the addition of either duplex sequence, further demonstrating NMM's exceptional selectivity for quadruplexes vs. duplex DNA and how NMM is able to detect quadruplexes in the background of high concentrations of ds DNA.

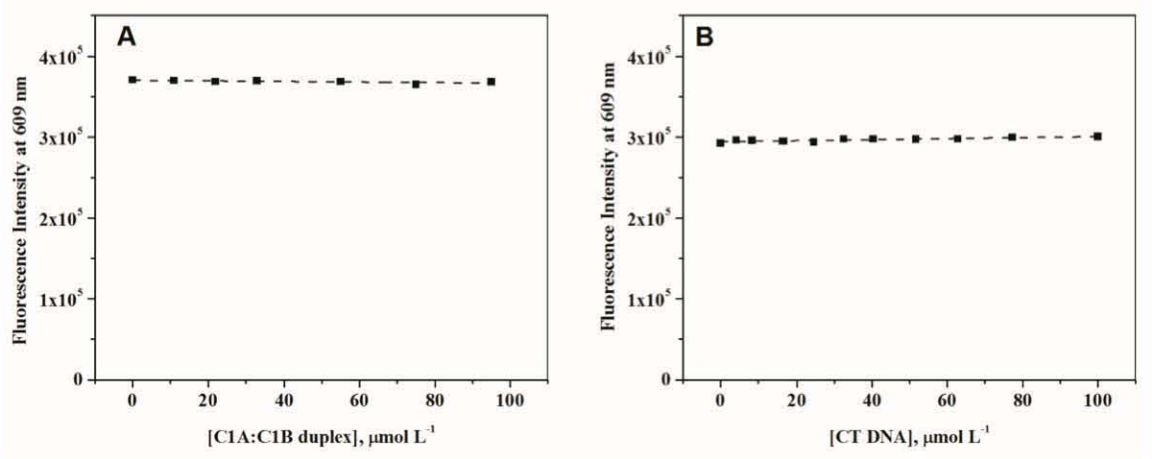

Figure 3.5. Representative titration of (A) C1A:C1B duplex and (B) CT DNA in 5K buffer and (B) into a solution of 1 μM NMM containing 10.0 μM VEGF.

Fluorescent lifetime studies indicate solvent exclusion as the mechanism of fluorescent enhancement

We next set out to elucidate the mechanism of NMM fluorescent enhancement in the presence of quadruplexes. We hypothesized that exclusion of water molecules from the porphyrin environment causes NMM's fluorescence to increase in the presence of quadruplexes. In order to test this hypothesis, NMM's fluorescent lifetime was measured

in the presence of the the GQs G4 (5K, TB), G8 (5K, TB), VEGF (5K), cMyc (5K), cKit2 (5K), Tel22 (5K, 50Na), $G_4T_4G_4$ (5K, 50Na), and TBA (5K). The fluorescent lifetime of a molecule is a measure of the average time that the molecule spends in the excited state before emitting a photon and returning to the ground state. Because fluorescence is governed by first-order kinetics, the following expression is obtained for the fluorescent lifetime:

$$\frac{n^*(t)}{n^*(0)} = e^{-t/\tau} \quad \textbf{eq. 10}$$

Here, *n*(t)* is the number of molecules in the excited state at some time *t*; *n*(0)* is the original number of molecules in the excited state immediately following excitation; and τ is the fluorescence lifetime. From this equation, it can be seen that the fluorescence lifetime may also be thought of as the time it takes to for the number of excited molecules decay to 1/e (36.8%) of their original population. Non-radiative processes, such as the collisions between solvent and NMM molecules, are expected to shorten the fluorescence lifetime by increasing the rate of decay of excited molecules. Consequently, if the solvent exclusion model were true, we would expect to see a correlation between the fluorescence lifetime and fluorescence enhancement of NMM bound to various GQs

The results (Figure 3.6A) indicate a relatively strong correlation (adj. $R^2 = 85.4$) between the fluorescence enhancement and lifetime, suggesting that the GQs are protecting the porphyrin's fluorescence from quenching by water. Fluorescent experiments with NMM in deuterium oxide (D_2O) and H_2O were conducted to confirm the results of the fluorescent lifetime study. The vibrational energy of a two atoms in a bond can be approximated with the following equation,

$$E_n = h\left(n + \frac{1}{2}\right)\frac{1}{2\pi}\sqrt{\frac{k}{\mu}} \qquad \textbf{eq. 11}$$

where n is the quantum number, k is the force constant, and μ is the reduced mass. D_2O has a greater mass than H_2O, meaning that D_2O should quench the excited state less efficiently than water and that NMM's fluorescence intensity should be higher in a solution of D_2O compared to a solution of H_2O. It was found that the steady-state fluorescence intensity of a 2.42 μM solution of NMM in D_2O is indeed higher than that in H_2O (Figure 3.6B), which is further consistent with solvent exclusion as the mechanism of fluorescent enhancement

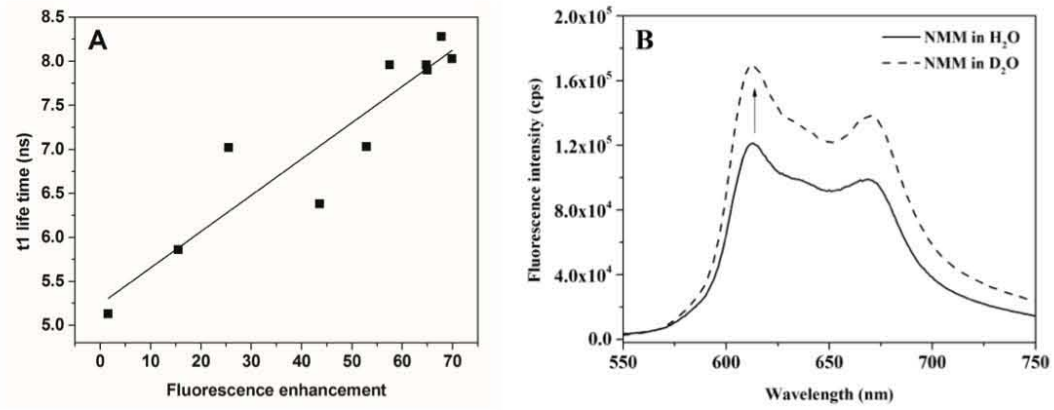

Figure 3.6. (A) Correlation graph between NMM fluorescent enhancement and fluorescent lifetime in the presence of various quadruplex structures. Adjusted R^2 is 85.4 signifying good correlation. (B) Fluorescence of a 2.42 μM sample of NMM is higher in D_2O than in H_2O.

Conclusion and Future Directions

In this work, we systematically showed that NMM fluorescencence increases selectively in the presence of parallel quadruplexes; the molecule displays a fluorescence enhancement in the rage of ~40 to 70, a value statistically significantly greater than those for anti-parallel and mixed hybrid GQs, which have fluorescence enhancement values in the ranges of ~2 to 18 and 35 to 60, respectively, and single-stranded, duplex, and i-motif DNA, which lead to essentially no increase in NMM fluorescence. Additionally, competition titration experiments illustrate that the porphyrin is able to probe parallel GQs even in the presence of excess duplex competitor, a key result given duplex DNA is the predominant form of DNA found in the cell. Combined, these results indicate that NMM meets the stringent criteria for an ideal fluorescent GQ probe. Finally, we were also able to demonstrate that solvent exclusion is the most likely mechanism of fluorescence enhancement.

Future experiments include examining a wider range of DNA sequences and topologies, including triplex DNA and RNA quadruplexes, in order to further probe NMM selectivity. Additionally, experiments may be devised to corroborate fluorescence lifetime and D_2O substitution studies performed to understand the mechanism of NMM fluorescence enhancement. Indeed, the studies presented here have not disproved the possibility that other factors, such as the alteration of the porphyrins electronic structure upon DNA binding, are also responsible for fluorescence enhancement in addition to the solvent exclusion that we were able to show. Comparing NMM fluorescence enhancement upon the addition of GQ DNA in both H_2O and D_2O buffers could investigate this possibility; if solvent exclusion were the primary mechanism of

fluorescence enhancement, one would expect a larger increase in fluorescence in the H_2O buffer compared to the D_2O one. If the fluorescence enhancement values are similar, however, it is possible that solvent exclusion only plays a minor role and that another factor is responsible for the dramatic increase in fluorescence emission observed. NMM fluorescence could also be measured in a greater number of solvents with varying vibrational energies; a strong, negative correlation between solvent vibrational energy and NMM fluorescence would verify the D_2O studies and point to solvent exclusion as a significant factor contributing to fluorescence enhancement. Finally, cells should be stained with NMM and its fluorescence should be measured using a technique such as confocal microscopy to determine the location of topologies of GQs in the cell.

Author Contributions

This project was carried out in collaboration with Dr. Veronika Szalai and Victoria Savikhin at the Center for Nanoscale Science and Technology at the National Institute of Standards and Technology (NIST) in Gaithersburg, MD. I collected and analyzed all data with the following exceptions. Fluorescence and CD data on the sequences C1A, C1B, IL1, G4, and G8 (all TB buffer), titrations with G4 and G8 and NMM (Fig. 2B of appended paper), and LiOH GQ unfolding experiments (Figs. S1 and S9 of appended paper) were collected by Dr. Veronika Szalai and Victoria Savikhin. Joshua Turek-Herman'16 performed Job Plot experiments with VEGF and NMM, collected some fluorescent and CD data in high potassium conditions (Fig.S5A of appended paper), and performed some repeats of titrations with $G_4T_4G_4$ and NMM (Fig. 2B of appended paper). I conducted the fluorescence lifetime experiments at NIST under the supervision of Dr. Szalai.

Chapter IV: TMPyP4 metalloporphyrins as GQ ligands

This chapter investigates how Pt(II) and Pd(II) derivatives of the well-studied TMPyP4 (PtTMPyP4 and PdTMPy4, respectively) interact with Tel22. Metallation of the TMPy4 core with a variety of metals, including Zn(II), Co(II), Fe(III), Pt(II), Pd(II), and Mg(II) is a simple modification that has been described thoroughly in the literature[77] and may alter the porphyrin's electronic and geometric structure, affecting GQ affinity, specificity, and telomerase inhibition.[78] For instance, it has been demonstrated that the Zn(II) derivative of TMPyP4 can stabilize, induce, and speed the folding of the parallel GQ d[TAGGG]$_2$.[79] Pt(II) and Pd(II) porphyrins are of particular interest because the metals are expected to have a square planar coordination geometry (the two metals have d^8 electronic configuration), and studies have revealed that square planar metalloporphyrins have an unhindered face for stacking and thus tend to display a greater degree of telomerase inhibition.[78] We are especially interested in Pt(II) complexes because they are known to have powerful photoluminescent properties[80] and, like NMM, may have potential as luminescent probes for the detection of GQ structures. We characterized the porphyrin-Tel22 interaction by UV-Vis, fluorescence, and circular dichroism spectroscopies, and FRET assays.

PtTmPyP4 and PdTmPyP4 do not aggregate onto themselves

Porphyrins can aggregate due to π-π stacking,[81] complicating the binding studies. UV-Vis dilution studies can test Beer's Law and identify this phenomenon. Aggregation is assumed to be insignificant if the absorbance at the Soret maximum increases linearly with the concentration of porphyrin. The linear dependence of absorbance in the concentration range from 0.5 to 20 μM and 0.5 to 50 μM for PtTMPyP4 and PdTMPyP4, respectively, indicates that the porphyrins do not aggregate under these conditions (Figure 2.1).

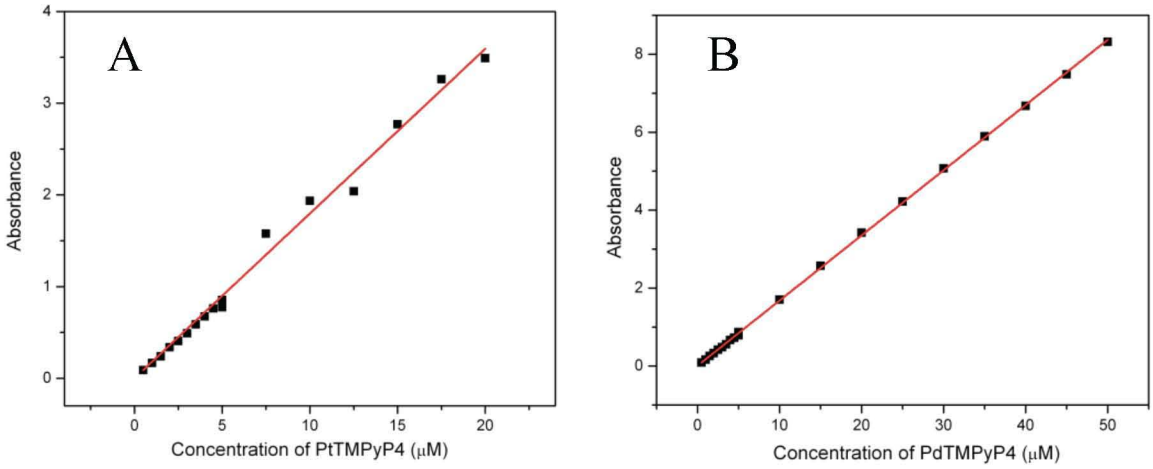

Figure 4.1. Results of the aggregation study for (A) PtTMPyP4 in H_2O and (B) PdTMPyP4 in 5K buffer. Using the measured absorbance values at the Soret band, known concentration values, and Beer's law, the extinction coefficient of PtTMPyP4 was determined to be 1.73×10^5 $M^{-1}cm^{-1}$ at 401 nm, compared to $\varepsilon_{401} = 1.72 \times 10^5$ $M^{-1}cm^{-1}$ determined by Pasternack et al.,[67] and the extinction coefficient of PdTMPyp4 was determined to be 1.67×10^5 $M^{-1}cm^{-1}$ at 418 nm, compared to the $\varepsilon_{418} = 1.68 \times 10^5$ $M^{-1}cm^{-1}$ reported in literature.[68]

Porphyrin-Tel22 binding explored by UV-Vis titrations

UV-Vis titrations provide a convenient means to quantitatively characterize GQ-porphyrin binding interactions. Three titrations were performed for each porphyrin. Because the two porphyrins were found to behave similarly, only the data for PtTMPyP4 is reported here in the main text (Figure 4.2); the data for PdTMPyP4 can be found in the Supplementary Information section (Figure S2).

Data analysis yielded percent hypochromicities of 46.2 ± 0.2 and 51.0 ± 1.6 and red shifts of 13.0 ± 0.1 nm and 14.7 ± 1.2 nm for PtTMPyP4 and PdTMPyP4, respectively (Figures 4.2A, S2A). Studies on duplex and poly dA DNA suggest that hyperchromicities greater than 35% and red shifts larger than 13 nm are indicative of intercalation between DNA bases.[67] Thus, these high hypochromicity and red shift values may be consistent with an intercalative binding mode between guanine quartets as the binding mode. Further support for the this model comes from the fact that PdTMPyP4 and PtTMPyP4 are both expected to have square planar geometry, so their lack of axial ligands would allow for intercalation.[67] Moreover, there is precedence for an intercalative mode of binding in the literature for the non-metallated TMPyP4 to various GQ-forming sequences including Bcl-2[52,82]and c-Myc;[83] this mode of binding was established using spectroscopic methods. It is worth noting, however, that while spectroscopic methods suggest intercalation as a porphyrin binding mode in the literature, there is no published X-ray crystallography structure to date that demonstrates intercalation between porphyrin and GQ.

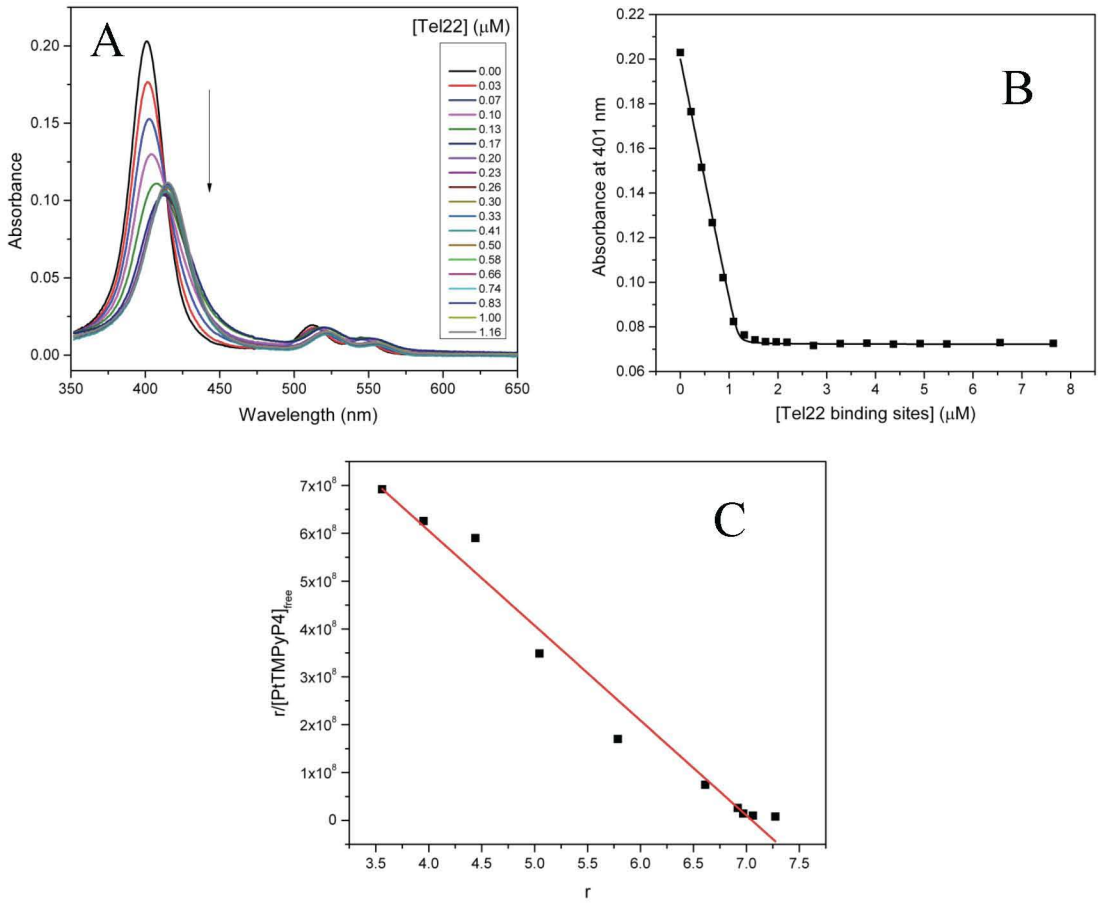

Figure 4.2 Summary of the results of titration studies with 1.18 μM PtTMPyP4 and 0.03 mM Tel22 in KPi buffer. (A) Representative UV-Vis absorption spectra for the titration. (B) Plot of the absorbance at the Soret peak (401 nm) as a function of the concentration of DNA used to calculate the binding constant from direct fitting. (C) Scatchard plot of r / [PtTMPyP4]free vs. r used to determine the binding affinity and binding ratio.

Direct fitting of our titration data using equations 5 and 6 yields a binding affinity of $(2.8 \pm 2.6) \times 10^8\ M^{-1}$ for PtTMPyP4 (Figure 4.2B) and $(1.1 \pm 0.3) \times 10^7\ M^{-1}$ for PdTMPyP4 (Figure S2B), high values which are indicative of tight binding between ligand and quadruplex. Titration data was also analyzed using linear Scatchard fits

(equations 7 and 8) which yielded K_a of $(1.4 \pm 0.2) \times 10^8\ M^{-1}$ for PtTMPyP4 (Figure 4.2C) and $(0.78 \pm 0.03) \times 10^7\ M^{-1}$ for PdTMPyP4 (Figure S2C), in excellent agreement with the direct fitting results. The binding stoichiometry was determined to be 6.7:1 and 6.5:1 ligand:GQ for PtTMPyP4 and PdTMPyP4, respectively. High values of binding stoichiometry suggest that if the porphyrin can indeed intercalate, additional binding modes such as end-stacking, loop binding, or groove binding, must also occur.

The method of continuous variation (Job's method)[84] was utilized to independently verify the binding stoichiometry. In these experiments, the total concentration of porphyrin and DNA were kept constant but the mole fractions of the porphyrin and DNA were varied. The change in absorbance was plotted against the mole fraction, and the peak of this plot was taken to indicate the binding stoichiometry. The average binding stoichiometry was found to be 6.6:1 ligand:GQ (Figure 4.3A), in excellent agreement with Scratchard fits. Subsequent titrations performed at a higher resolution give two binding ratios of 3.6:1 and 8.4:1 (Fig 4.3B), values which are also in agreement with the results of resonance light scattering (RLS) studies performed (data not shown).

The first ratio of 3.6:1 porphyrin to GQ could signify the intercalation of two porphyrins between the three G-tetrads and the end-stacking of two porphyrins to the two ends of the GQ structure. The second value (8.4:1) may result from four additional PtTMPyP4 molecules binding to the loops or grooves of the GQ structure or stacking on top of end-stacked porphyrin molecules. This hypothesis is supported by the fact that TMPyP4 molecules were found to bind to one of the TTA propellor loops in the crystal

structure of the TMPyP4-Tel22 complex.[85] Nonetheless, precise structural data from X-ray crystallography is needed to confirm these hypothesized binding modes.

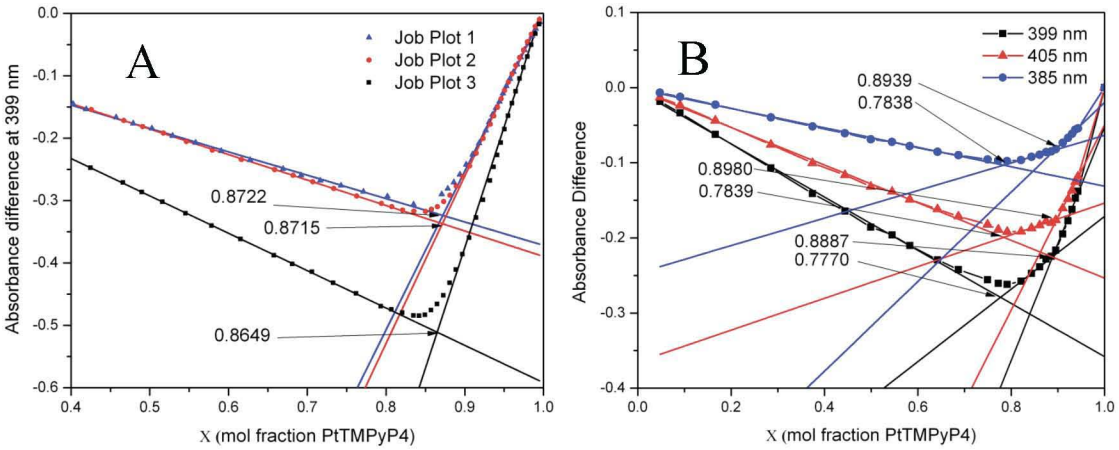

Figure 4.3. Job Plot titrations for PtTMPyP4 with Tel22 in KPi buffer. (A) Initial titrations show a ligand:GQ ratio of 6.6:1. (B) High resolution titration reveals two porphyrin:GQ binding stoichiometry values of 3.6:1 and 8.4:1.

PtTMPyP4 binding to and selectivity for Tel22 examined by fluorescence spectroscopy

Fluorescence titrations were performed in order to further elucidate the porphyrin-GQ binding interaction and determine whether PtTMPyP4 is a viable fluorescent probe for GQ DNA. As in the case of NMM, PtTMPyP4 fluoresces weakly alone, but π-π stacking between the porphyrin and G-quartet greatly increases this fluorescence intensity, most likely as a result of solvent exclusion.

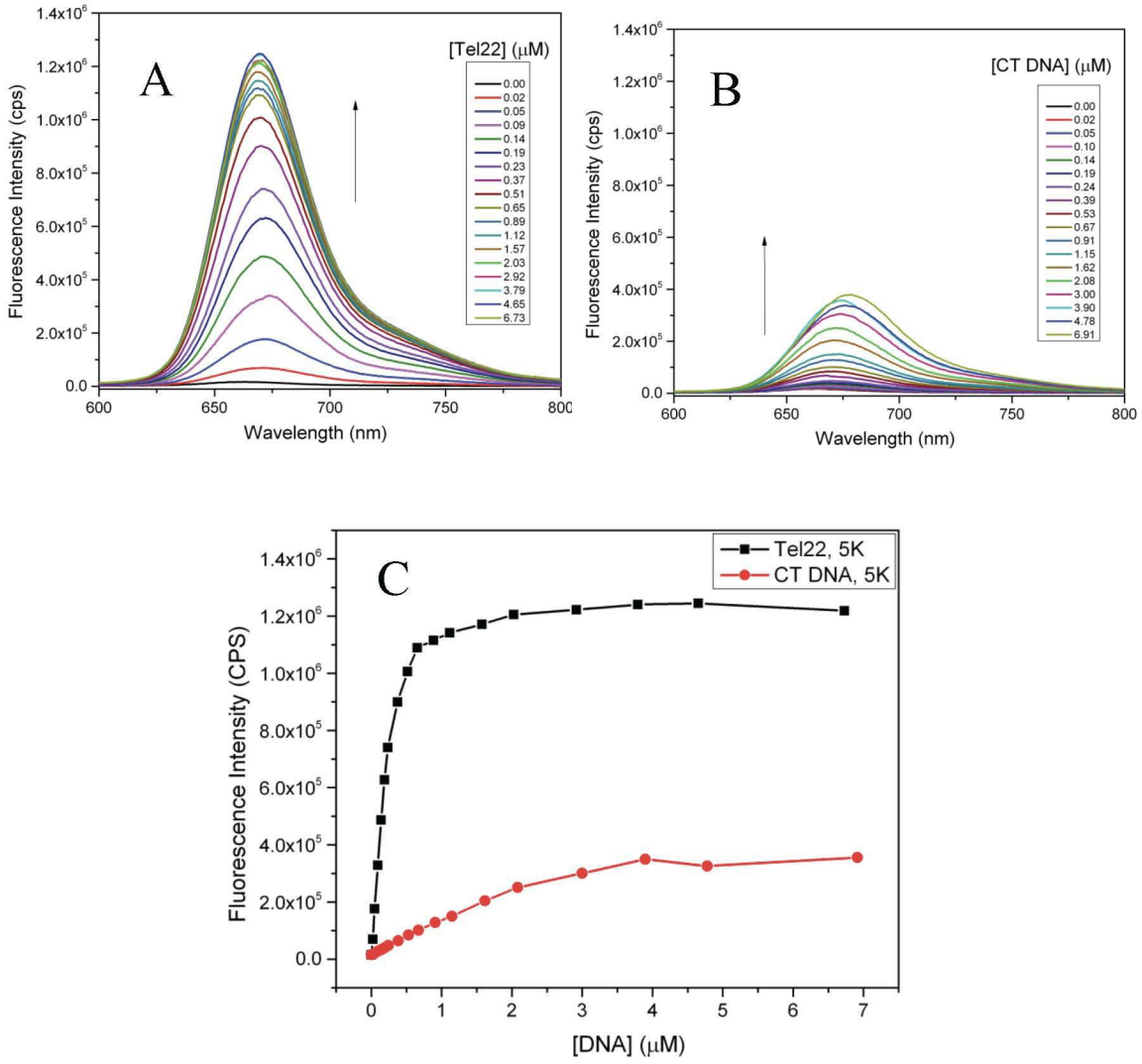

Figure 4.4. Representative spectra for fluorescent titrations of 1.69 μM PtTMPyP4 with (A) 0.094 mM Tel22 and (B) 0.097 mM CT DNA in 5K buffer. (C) Plot of PtTMPyP4 fluorescence intensity as a function of DNA concentration.

In order to determine the extent to which porphyrin fluorescence is selective for GQ DNA over duplex DNA, three titrations of PtTMPyP4 were performed with Tel22 and CT DNA under identical conditions in 5K buffer. Titrations were run in parallel to ensure that lamp fluctuation and other experimental errors would not bias the results of one titration. The results shown in Figure 4.4 indicate that the porphyrin fluorescence increases dramatically in the presence of Tel22 and must less in the presence of CT DNA.

This result suggests that PtTMPyP4 is selectively interacting with GQ DNA and that the porphyrin's fluorescence is able to discriminate between duplex and quadruplex DNA. Thus, the porphyrin may have promise as a fluorescent probe to visualize the location of GQs. Like UV-Vis titration data, fluorescence titration data may be analyzed to yield a value for K_a. Direct fitting of fluorescence data gives a binding constant of $(2.3 \pm 1.2) \times 10^6$ M^{-1}, a value somewhat lower than the binding constant value obtained from UV-Vis titration data, which is on the order of 10^8. Nonetheless, this high affinity constant value is still indicative of tight binding between porphyrin and quadruplex.

In order to systematically investigate the ability of PtTMPyP4 to fluoresce selectively in the presence of variety of GQ structure over other secondary DNA structures, we performed detailed fluorescent enhancement studies designed similarly to those discussed in Chapter III. In these experiments, the fluorescence of PtTMPyP4 was measured before and after the addition of DNA, and the fluorescence enhancement was calculated as described in the Materials and Methods section. Titrations studies indicate that the fluorescence signal of the porphyrin is saturated after the addition of ~ 1 equivalent of quadruplex. Thus, to ensure that all the porphyrin was bound to quadruplex, 5 equivalents of DNA were added in these fluorescence enhancement studies. The results shown in Figure 4.5 indicate that ss DNA (ds12A and ds12B sequences) and duplex DNA (ds12 and ds26 sequences) cause porphyrin fluorescence to increase to only a small degree, with the single-stranded sequences displaying an average fluorescence enhancement of 17.9 ± 4.0 and the duplex sequences displaying an average fluorescent enhancement of 16.0 ± 3.4. In the presence of the mixed hybrid Tel22 GQ formed in 5K buffer, however, the fluorescent enhancement is found to be 85.8 ± 5.5,

suggesting that PtTMPyP4 can discriminate between quadruplex and duplex structure and has a promise as a fluorescent probe for GQ structures. Unpaired two-sided t-tests confirm this conclusion; the difference in fluorescence enhancement between Tel22 and ssDNA and Tel22 and dsDNA is found to be statistically significant at the 95% confidence interval, with 2-sided p-values < 0.0001 for both tests.

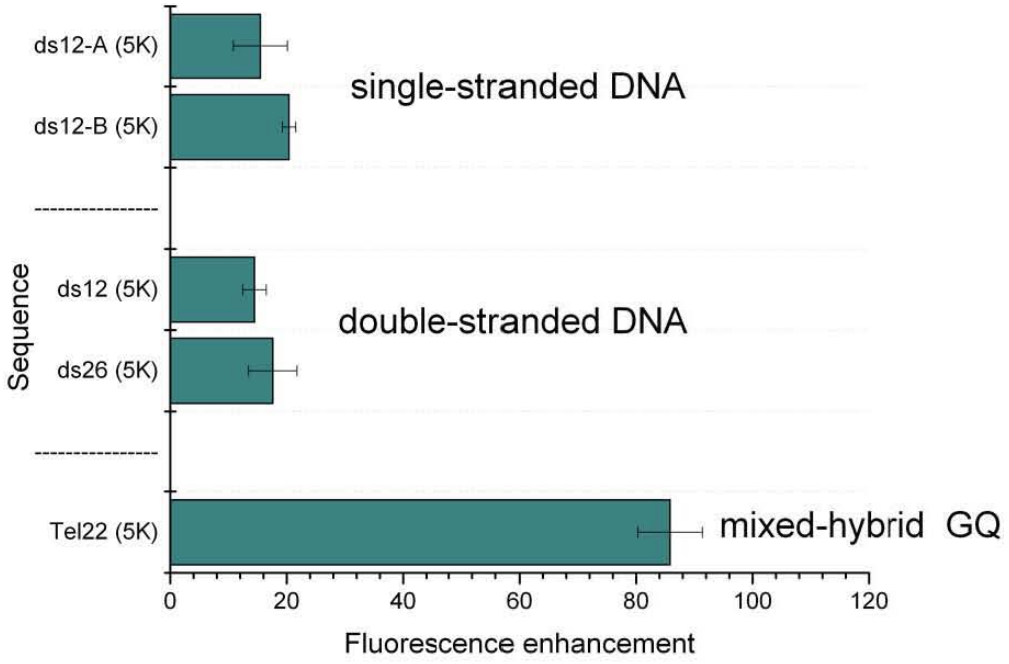

Figure 4.5. Results of the fluorescent enhancement study for PtTMPyP4. The porphyria's fluorescence increases selectively in the presence of the Tel22 mixed-hybrid GQ over

Stabilizing properties of PtTMPyP4 and PdTMPyP4 and selectivity toward Tel22 assessed through FRET

FRET assays provide a semi-quantitative measurements of quadruplex stabilizing ability and selectivity.[46] Similar to the UV-Vis titration studies, both porphyrins exhibit similar behavior, so only the FRET data for PtTMPyP4 is shown here in the main text; data for PdTMPyP4 is found in the supplemental information. The addition of 0 - 4 μM of PtTMPyP4 or PdTMPyP4 (the standard concentration range used in FRET studies in our laboratory) to 0.2 μM F21D in 5K yielded concentration-dependent melting curves whose fluorescence values do not flatten out at the maximum temperature of 95 °C (Figure S3), suggesting that the ligand-stabilized GQ has a T_m greater than 95 °C (hence, incomplete GQ melting). Therefore, experiments were repeated with a reduced concentration of 0 - 0.6 μM PtTMPyP4 and 0 - 0.4 μM PdTMPyP4. Both porphyrins exhibited similar behavior, with ΔT_m of 30.7 ± 0.6 °C for PtTMPyP4 (Figure 4.6A) and 30.0 ± 1.6 for PdTMPyP4 (Figure S4) at 0.4 μM ligand concentration in 5K buffer. In general, these porphyrins stabilize GQ's stronger than other similar porphyrins studied in our laboratory, such as TMPyP4, it's Cu(II) and Zn(II) derivatives,[79] and NMM.[56] In order to ensure that the measured fluorescence is due to the labeled GQ and not the natural fluorescence of the metalloporphyrins alone, control FRET experiments with both porphyrins were run using unlabeled Tel22 instead of F21D. No significant fluorescence was observed in both cases (Figure S5).

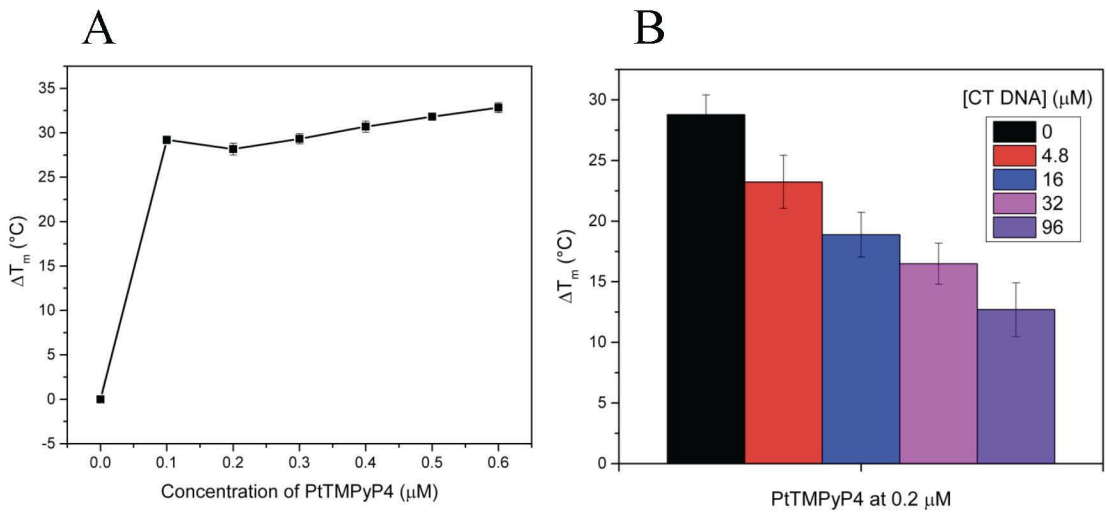

Figure 4.6. Summary of FRET experiments with PtTMPyP4 and F21D in 5K buffer. (A) Concentration-dependent increase in melting temperature of 0.2 μM F21D stabilized by 0 to 0.6 μM ligand. The increase in melting temperature at 0.6 μM relative to NMM alone (ΔT_m) is found to be 30.7 ± 0.6 °C. (B) Results of the competition study indicate a decrease in melting temperature with increasing concentrations of duplex DNA, suggesting moderate selectivity for the GQ structure.

Peculiarly, the melting curves for F21D in the presence of 0.1 μM PtTMPyP4 and PdTMPyP4 are biphasic (Figure S6A,B). Biphasic melting curves represent melting of two distinct DNA conformations with different thermal stabilities.[86] Indeed, the first derivative of the biphasic curve yielded a graph with two distinct peaks (Figure S6C,D), one most likely corresponding to the melting temperature of F21D alone and the second to the melting temperature of DNA bound to the porphyrin. These discrete peaks suggest a lack of equilibrium between the GQ DNA and porphyrin and confirm the exceptionally tight binding interaction implied by fluorescent experiments.

FRET competition studies with CT DNA were performed to assess the porphyrins' selectivity for GQ DNA over duplex DNA. Results indicate that both PtTMPyP4 and PdTMPyP4 are modestly selective for GQ. The selectivity ratio, defined as the excess of competitor necessary for a 50% decrease in ΔT_m, was 177 and 188, for

PtTMPyP4 and PdTMPyP4, respectively, in 5K. This selectivity ratio is similar to that measured for TMPyP4 and it's other metallated derivatives[79] but much lower than that of NMM (Figure 2.10A, B).[56] Overall, FRET results suggest that both porphyrins are extremely robust stabilizers of human telomeric DNA in the presence of potassium, but like TMPyP4 they exhibits only modest selectivity for GQ over duplex DNA. This modest selectivity may be due to the fact that the porphyrin is cationic and able to attract the negatively-charged phosphate groups of duplex DNA.

Effect of PtTMPyP4 on GQ structure assessed by CD spectroscopy

To determine the effect of PtTMPyP4 on the quadruplex structure, this porphyrin titrated into a solution of annealed Tel22 or cMyc in 5K buffer. Tel22 alone in 5K produces peaks at 294 nm and 255 nm and a trough at 235 nm, consistent with the mixed hybrid structure.[26,87] In the presence of PtTMPyP4, the overall CD signature does not change, but signal intensity decreases dramatically suggesting that the porphyrin is interrupting quartet stacking and potentially destabilizing the molecule (Figure 2.11A).

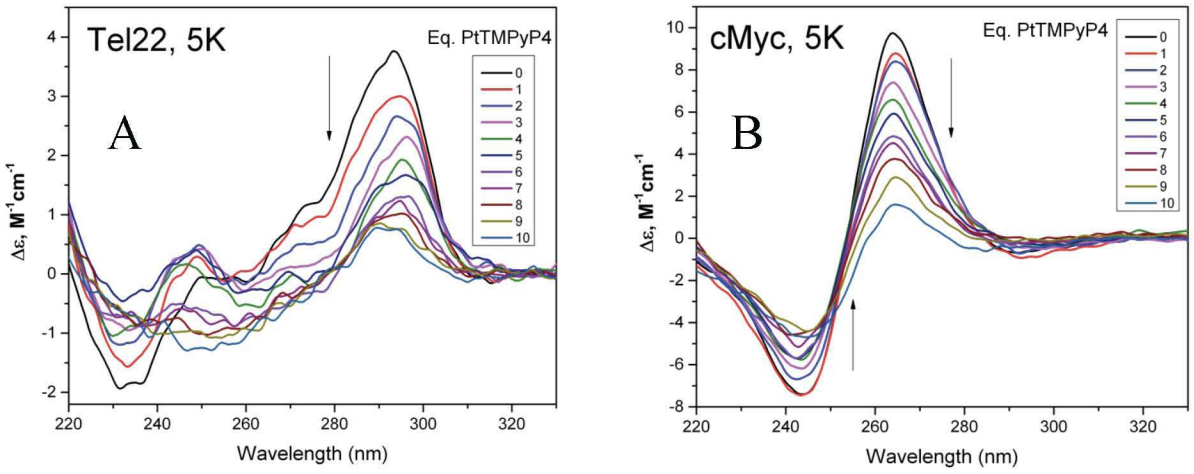

Figure 2.11. CD spectra of (A) Tel22 and (B) cMyc with increasing amounts of PtTMPyP4 in 5K buffer.

The cMyc GQ is parallel in 5K buffer as evidenced by a peak at 265 nm and a trough at 245 nm. This signal flattens out upon addition of PtTMPyP4, similar to Tel22 case (Fig. 2.11B). If one assumes that the porphyrin is interrupting G-tetrad stacking and thus destabilizing the GQ, such interpretation of the data is inconsistent with FRET results, which suggest strong stabilization of interaction between the porphyrin and human telomeric DNA. It is possible, however, that the low fluorescence values observed in preliminary FRET studies that we interpreted to be incomplete melting (Figure S3) may actually be due to destruction of the quadruplex. It is worth noting that the decrease in CD signal could be due to precipitation, which was not observed upon careful visual examination. Nonetheless, light scattering experiments do suggest the formation of small aggregates at 1 GQ to ~ 8 porphyrins, suggesting that some small precipitates may be forming.

Conclusion and Future Directions

Combined, our data suggest that both porphyrins bind tightly to Tel22 with an overall binding stoichiometry of ~7:1 and a binding constant on the order of ~10^6 to 10^8. Both porphyrins are found to be excellent stabilizers of human telomeric DNA, increasing its melting temperature by ~31 °C at only 2-fold excess of the porphyrin. They are also modestly selective for GQ over duplex DNA, with a selectivity ratio of 180-190. Because the fluorescence of PtTMPyP4 increases selectively upon addition of Tel22 as compared to ds or ssDNA, this porphyrin is a promising candidate for a photoluminescent GQ probe.

Future work should focus on better elucidating the modes of binding between porphyrin and GQ, ideally from a high resolution X-ray crystallography or NMR

structure of the PtTMPyP4-Tel22 complex. It is also essential to reconcile the contradictory results given by FRET and CD experiments and determine whether the GQ is being stabilized or destroyed. Tel22 could be titrated into a solution of PtTMPyP4 in a buffer with a high concentration of a GQ denaturing agent, such as LiOH, a strong base which will deprotonate the guanine molecules and cause repulsion between negatively charged guanines and thus destruction of the GQ structure, to help resolve this discrepancy. If high fluorescence values are observed and a strong binding constant is obtained from this titration in LiOH, it can be inferred that the high fluorescence seen during titrations and FRET melts is actually a result of GQ destruction by the ligand as suggested by CD. On the other hand, a flattened fluorescence signal upon addition of DNA would corroborate the results of FRET and imply that the GQ structure is indeed stabilized by the ligand. Finally, like NMM, PtTMPyP4 may be stained in the cell and its fluorescence measured by confocal microscopy to determine the location of cellular quadruplexs.

Author Contributions

This project was initiated by John M. Nicoludis'12, who performed the UV-Vis titrations, Job plots, RLS, and aggregation studies on PtTMPyP4. I completed the FRET stability and competition studies on PtTMPyP4 and PdTMPyP4, fluorescence titrations and fluorescence enhancement studies on PtTMPyP4, and UV-Vis titrations on PdTMPyP4. This project was also done in collaboration with Dr. Oscar Mendoza of the Institut Européen de Chimie et Biologie, (Bordeaux, France), who performed the CD studies on PtTMPyP4 and performed some repeats of the PtTMPyP4 fluorescent enhancement studies.

Chapter V: A spermine-derivatized porphyrin as a GQ ligand

This chapter details preliminary steps taken toward investigating the interactions between the porphyrin TCCPSpm4 and Tel22. TCCPSpm4 (Fig 5.1A) consists of meso-tetra(4-carboxyphenyl) porphyrin (TCPP, Figure 5.1B) substituted with four,spermine groups at the carboxylic acid to form amides. Such porphyins with long side chains, also known as tentacle porphyrins, have been synthesized as far back as the 1990s and their interactions with duplex DNA have been studied extensively.[88] Studies with quadruplex DNA, however, are needed. The spermine side chains are intended to bind to the grooves or loops of the quadruplex structure, thereby increasing the stabilizing interaction between ligand and GQ. The goal of this study is to determine if this porphyrin is a promising GQ stabilizer and if substituting ligands with long side chains is a valid strategy in the design of novel, better-stabilizing GQ ligands. This project, which was only recently begun, is currently being carried out in collaboration with Dr. Alessandro D'Urso of the University of Catania in Catania, Italy, who provided the porphyrin and is also studying the porphyrin's interactions with TG_3AG, a tetramolecular quadruplex currently being investigated as an anti-HIV drug.[89,90]

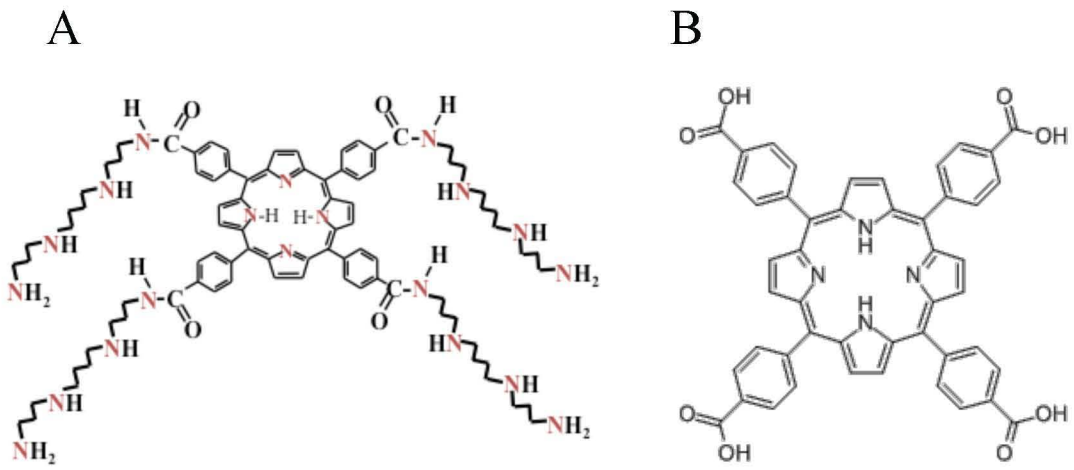

Figure 5.1. Structure of (A) TCCPSpm4, the porphyrin under investigation and (B) TCPP, the porphyrin from which TCPPSpm4 is derived.

TCCPSpm4 does not aggregate

Before proceeding to examining the interactions between TCCPSpm4 and quadruplex DNA, we tested for aggregation of the porphyrin alone using dilution studies that test Beer's law as was done for PtTMPyP4 and PdTMPyP4. The absorbance was found to increase linearly between concentrations of 0.5 and 50 μM TCCPSpm4, indicating that the porphyrin does not aggregate in this concentration range (Figure 5.2). A value of 2.24 x 10^5 $M^{-1}cm^{-1}$ is obtained for the extinction coefficient at 415 nm, the Soret peak.

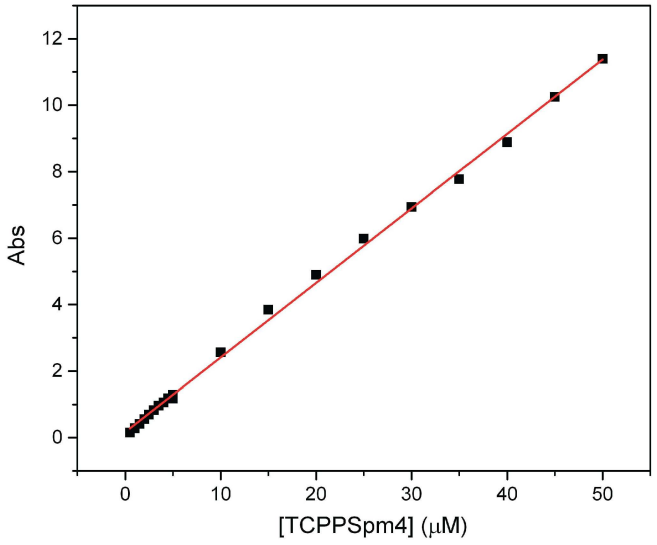

Figure 5.2. Results of the aggregation study for TCCPSpm4. A linear relationship between absorbance and concentration indicates no aggregation.

Porphyrin-Tel22 binding assessed by UV-Vis spectroscopy

UV-Vis titrations were then performed to quantify the porphyrin-GQ interaction.. For the titration between TCCPSpm4 and Tel22 in 5K, the average percent hypochromicity value is 62.9 ± 4.3 and the red shift is 13.0 ± 1.4 nm (Figure 5.3A).

These large values seem to suggest that intercalation is the main binding mode between the porphyrin and GQ. However, the loops of the mixed hybrid structure of Tel22 might block the grooves, making intercalation unlikely. In addition, intercalation implies breaking of pi-pi interaction between two G-tetrads, which is energetically very costly. Moreover, as discussed in Chapter IV, despite extensive spectroscopic evidence pointing toward intercalation as the binding mode for numerous porphyrins, including the well-studied TMPyP4, X-ray crystallography[85] and NMR[91] structural data have pointed to either loop binding or end-stacking[53] as the method of binding and not intercalation.

Titration data also allows for the calculation of the binding constant using the direct fitting method; a value of $(6.0 \pm 1.5) \times 10^6$ M^{-1} was determined for the association constant K_a, which is indicative of a somewhat tight binding interaction (Fig 5.3).

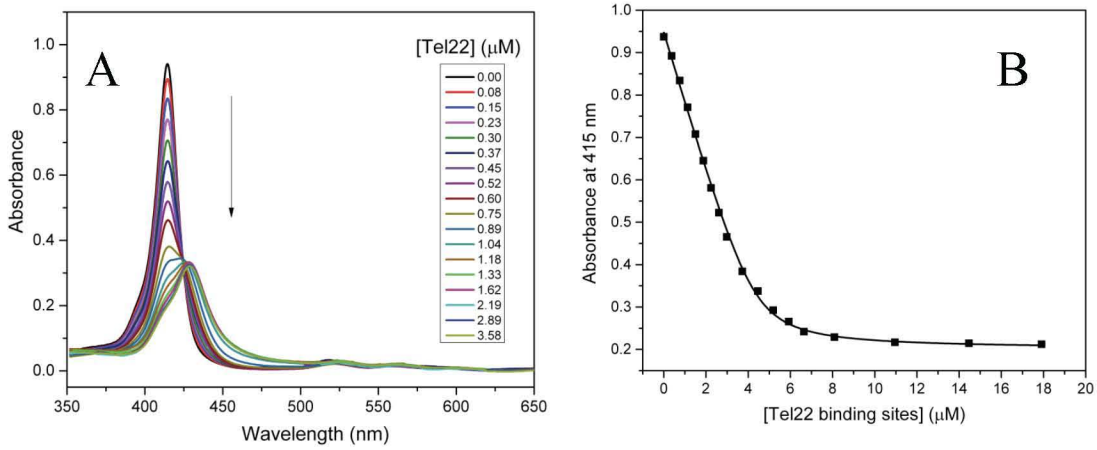

Figure 5.3 Summary of the results of titration studies with 4.34 μM TCPPSpm4 and 0.075 mM Tel22 in 5K buffer. (A) Representative UV-Vis absorption spectra for the titration. (B) Plot of the absorbance at the Soret peak (415 nm) as a function of the concentration of DNA used to calculate the binding constant from direct fitting.

It is important to note that a reasonable fit (as judged by the value of R^2) was only obtained assuming a ligand:DNA concentration of 5:1, suggesting that this may be the binding ratio. Nonetheless, an independent means of assessing binding stoichiometry, such as Job plot, is needed to elucidate the binding stoichiometry. Moreover, resonance light scattering fluorescent methods may be employed to identify more complex binding interactions that are occurring.

Stabilizing properties of H_2TCCPSpm4 assessed through FRET

The FRET melting assay discussed in Chapter IV was employed to investigate the extent to which H_2TCCPSpm4 is capable of stabilizing the quadruplex formed by the human telomeric DNA sequence. Experiments were subsequently performed with a ligand concentration range of 0 - 2μM TCCPSpm4 added to 0.2 μM F21D to obtain quantitative stabilization data (Fig. 5.5).

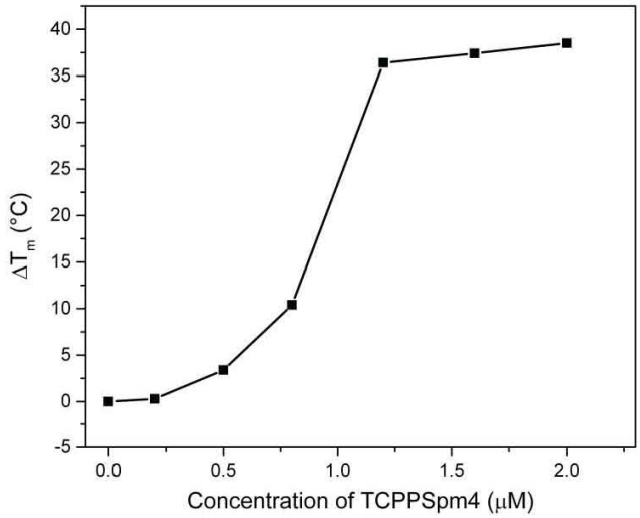

Fig. 5.5. Dependence of T_m versus concentration ligand for TCPPspm4 in 5K buffer. An increase in T_m of 38.5 °C is observed for 0.2 μM F21D at 2 μM ligand concentration.

An increase in stabilization temperature of F21D of 38.5 °C is found at a 2 μM concentration of ligand, which is indicative of a strong stabilizing interaction. Peculiarly, the graph of ΔTm vs. concentration of ligand appears sigmoidal; the change in melting temperature initially increases slowly from 0 to ~ 1μM ligand, increases rapidly from ~1 μM ligand to ~1.25 μM ligand, and then increases slowly again. This sigmoidal curve

may be indicative of cooperative binding between GQ and ligand. More data points should be obtained in the rapidly increasing range, however, before this assertion can be made confidently.

Porphyrin effect on GQ structure investigated by CD spectroscopy

In order to determine the of TCPPSpm4 on the secondary structure of Tel22, we completed annealing studies. Specifically, CD spectra were collected on Tel22 annealed alone or with 1 – 2 equivalents of porphyrin in 5K buffer (Fig 5.6).

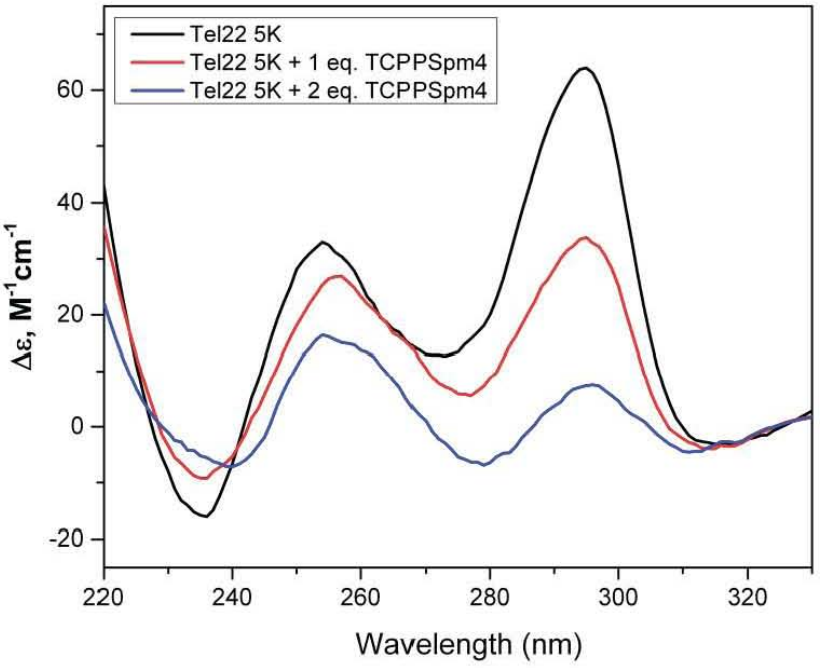

Figure 5.6. CD spectra of a solution of 2.82 μM Tel22 alone (black), and with one (red) or two (blue) equivalents of TCPPSpm4 in 5K buffer.

The slight decrease in molar ellipticity at 265 nm and dramatic decrease in signal at 295 nm suggest that the porphyrin may actually be destabilizing the quadruplex structure, a result which is in contradiction to the FRET data discussed earlier, which suggest a strong stabilizing interaction. As in the case of PtTMPyP4, it is possible that the decrease in CD signal is due to the formation of precipitates in the solution. Although no precipitates were visually observed in the cuvette, there may be smaller precipitates invisible to the unaided eye; resonance light scattering experiments are necessary to further investigate this possibility. CD melting studies, in which the CD signal of the quadruplex is monitored as the temperature is increased, can also provide a value for the melting temperature and should thus be employed to corroborate the values of the melting temperature obtained from FRET.

Conclusion and Future Directions

This chapter reveals the preliminary work on the investigation of the interactions between TCPPSpm4 and Tel22. The ligand appears to bind to the quadruplex with somewhat high affinity on the order of ~10^6 and appears to be an excellent stabilizer of the compound, resulting in a change in melting temperature of F21D at 38.5 °C. Interestingly, FRET studies suggest a sigmoidal graph of ΔT_m vs. ligand concentration, which may be indicative of cooperative porphyrin binding. A work in progress, future studies for this project should focus on obtaining more precise melting data via FRET and investigating to see if the binding is indeed cooperative. Given that ideal quadruplex binders are selective for GQ DNA, porphyrin selectivity for quadruplex over duplex competitors should be examined through FRET competition studies. Moreover, the binding ratio should be verified through an independent means, such as Job's method, so

as to obtain more accurate values for the binding constant and more fully characterize the porphyrin-GQ interaction. As in the case of PtTMPyP4, CD and FRET give contradictory results. CD melting studies, which provide an independent and alternate means of assessing the change in melting temperature of GQs in the presence of varying concentrations of porphyrin, may verify FRET experiments and thus potentialy shed light on this discrepancy. Finally, it would be interesting to quantify the extent to which the spermine side chains play a role in this ligand's unique activity. If molecules with 1, 2, and 3 spermine side chains could be synthesized, their binding affinities and stabilities could be measured and compared to evaluate the direct effect of each spermine side chain.

References

1. Watson, J. D.; Crick, F. H., Molecular structure of nucleic acids; a structure for deoxyribose nucleic acid. *Nature* **1953,** *171* (4356), 737-8.
2. Mirkin, S. M., Discovery of alternative DNA structures: a heroic decade (1979-1989). *Front Biosci* **2008,** *13*, 1064-71.
3. Frank-Kamenetskii, M. D.; Mirkin, S. M., Triplex DNA structures. *Annu Rev Biochem* **1995,** *64*, 65-95.
4. Huppert, J. L., Four-stranded nucleic acids: structure, function and targeting of G-quadruplexes. *Chem Soc Rev* **2008,** *37* (7), 1375-84.
5. Phan, A. T., Human telomeric G-quadruplex: structures of DNA and RNA sequences. *FEBS J* **2010,** *277* (5), 1107-17.
6. Bera, P. P.; Schaefer, H. F., (G-H)*-C and G-(C-H)* radicals derived from the guanine.cytosine base pair cause DNA subunit lesions. *Proc Natl Acad Sci U S A* **2005,** *102* (19), 6698-703.
7. Leroy, J. L.; Guéron, M.; Mergny, J. L.; Hélène, C., Intramolecular folding of a fragment of the cytosine-rich strand of telomeric DNA into an i-motif. *Nucleic Acids Res* **1994,** *22* (9), 1600-6.
8. Rajendran, A.; Nakano, S.; Sugimoto, N., Molecular crowding of the cosolutes induces an intramolecular i-motif structure of triplet repeat DNA oligomers at neutral pH. *Chem Commun (Camb)* **2010,** *46* (8), 1299-301.
9. Sun, D.; Hurley, L. H., The importance of negative superhelicity in inducing the formation of G-quadruplex and i-motif structures in the c-Myc promoter: implications for drug targeting and control of gene expression. *J Med Chem* **2009,** *52* (9), 2863-74.
10. Kendrick, S.; Akiyama, Y.; Hecht, S. M.; Hurley, L. H., The i-motif in the bcl-2 P1 promoter forms an unexpectedly stable structure with a unique 8:5:7 loop folding pattern. *J Am Chem Soc* **2009,** *131* (48), 17667-76.
11. Phan, A. T.; Mergny, J. L., Human telomeric DNA: G-quadruplex, i-motif and Watson-Crick double helix. *Nucleic Acids Res* **2002,** *30* (21), 4618-25.
12. Blackburn, E., Switching and signaling at the telomere. *Cell* **2001,** *106* (6), 661-673.
13. Muller, H. J., The remaking of chromosomes. *Collecting Net* **1938,** *13*, 181 - 198.
14. Muller, H. J., Induced mutations in Drosophila. *Cold Spring Harbor Symposia on Quantitative Biology* **1941,** *9*, 151-167.
15. McClintock, B., The Behavior in Successive Nuclear Divisions of a Chromosome Broken at Meiosis. *Proc Natl Acad Sci U S A* **1939,** *25* (8), 405-16.
16. McClintock, B., The Stability of Broken Ends of Chromosomes in Zea Mays. *Genetics* **1941,** *26* (2), 234-82.
17. Aubert, G.; Lansdorp, P. M., Telomeres and aging. *Physiol Rev* **2008,** *88* (2), 557-79.
18. Hayflick, L.; Moorhead, P. S., The serial cultivation of human diploid cell strains. *Exp Cell Res* **1961,** *25*, 585-621.
19. Cohen, S. B.; Graham, M. E.; Lovrecz, G. O.; Bache, N.; Robinson, P. J.; Reddel, R. R., Protein composition of catalytically active human telomerase from immortal cells. *Science* **2007,** *315* (5820), 1850-3.

20. Wyatt, H. D.; West, S. C.; Beattie, T. L., InTERTpreting telomerase structure and function. *Nucleic Acids Res* **2010,** *38* (17), 5609-22.
21. Hiyama, E.; Hiyama, K., Telomere and telomerase in stem cells. *Br J Cancer* **2007,** *96* (7), 1020-4.
22. Kim, N. W.; Piatyszek, M. A.; Prowse, K. R.; Harley, C. B.; West, M. D.; Ho, P. L.; Coviello, G. M.; Wright, W. E.; Weinrich, S. L.; Shay, J. W., Specific association of human telomerase activity with immortal cells and cancer. *Science* **1994,** *266* (5193), 2011-5.
23. Shay, J. W.; Bacchetti, S., A survey of telomerase activity in human cancer. *Eur J Cancer* **1997,** *33* (5), 787-91.
24. Wang, Y.; Patel, D. J., Solution structure of the human telomeric repeat d[AG3(T2AG3)3] G-tetraplex. *Structure* **1993,** *1* (4), 263-82.
25. Parkinson, G. N.; Lee, M. P.; Neidle, S., Crystal structure of parallel quadruplexes from human telomeric DNA. *Nature* **2002,** *417* (6891), 876-80.
26. Luu, K. N.; Phan, A. T.; Kuryavyi, V.; Lacroix, L.; Patel, D. J., Structure of the human telomere in K+ solution: an intramolecular (3 + 1) G-quadruplex scaffold. *J Am Chem Soc* **2006,** *128* (30), 9963-70.
27. Xu, Y.; Noguchi, Y.; Sugiyama, H., The new models of the human telomere d[AGGG(TTAGGG)3] in K+ solution. *Bioorg Med Chem* **2006,** *14* (16), 5584-91.
28. Bochman, M. L.; Paeschke, K.; Zakian, V. A., DNA secondary structures: stability and function of G-quadruplex structures. *Nat Rev Genet* **2012,** *13* (11), 770-80.
29. Croce, C., Molecular origins of cancer: Oncogenes and cancer. *New England Journal of Medicine* **2008,** *358* (5), 502-511.
30. Nishimura, S.; Sekiya, T., Human cancer and cellular oncogenes. *Biochem J* **1987,** *243* (2), 313-27.
31. Yokota, J., Tumor progression and metastasis. *Carcinogenesis* **2000,** *21* (3), 497-503.
32. Prendergast, G. C., Mechanisms of apoptosis by c-Myc. *Oncogene* **1999,** *18* (19), 2967-87.
33. Adams, J. M.; Cory, S., The Bcl-2 protein family: arbiters of cell survival. *Science* **1998,** *281* (5381), 1322-6.
34. Patel, D.; Phan, A.; Kuryavyi, V., Human telomere, oncogenic promoter and 5'-UTR G-quadruplexes: Diverse higher order DNA and RNA targets for cancer therapeutics. *Nucleic Acids Research* **2007,** *35* (22), 7429-7455.
35. Yuan, L.; Tian, T.; Chen, Y.; Yan, S.; Xing, X.; Zhang, Z.; Zhai, Q.; Xu, L.; Wang, S.; Weng, X.; Yuan, B.; Feng, Y.; Zhou, X., Existence of G-quadruplex structures in promoter region of oncogenes confirmed by G-quadruplex DNA cross-linking strategy. *Sci Rep* **2013,** *3*, 1811.
36. Siddiqui-Jain, A.; Grand, C. L.; Bearss, D. J.; Hurley, L. H., Direct evidence for a G-quadruplex in a promoter region and its targeting with a small molecule to repress c-MYC transcription. *Proc Natl Acad Sci U S A* **2002,** *99* (18), 11593-8.
37. Cogoi, S.; Xodo, L. E., G-quadruplex formation within the promoter of the KRAS proto-oncogene and its effect on transcription. *Nucleic Acids Res* **2006,** *34* (9), 2536-49.
38. Shirude, P. S.; Okumus, B.; Ying, L.; Ha, T.; Balasubramanian, S., Single-molecule conformational analysis of G-quadruplex formation in the promoter DNA duplex of the proto-oncogene c-kit. *J Am Chem Soc* **2007,** *129* (24), 7484-5.

39. Vummidi, B. R.; Alzeer, J.; Luedtke, N. W., Fluorescent probes for G-quadruplex structures. *Chembiochem* **2013,** *14* (5), 540-58.
40. Ma, D. L.; Shiu-Hin Chan, D.; Yang, H.; He, H. Z.; Leung, C. H., Luminescent G-quadruplex probes. *Curr Pharm Des* **2012,** *18* (14), 2058-75.
41. Georgiades, S. N.; Abd Karim, N. H.; Suntharalingam, K.; Vilar, R., Interaction of metal complexes with G-quadruplex DNA. *Angew Chem Int Ed Engl* **2010,** *49* (24), 4020-34.
42. Biffi, G.; Tannahill, D.; Balasubramanian, S., An intramolecular G-quadruplex structure is required for binding of telomeric repeat-containing RNA to the telomeric protein TRF2. *J Am Chem Soc* **2012,** *134* (29), 11974-6.
43. Biffi, G.; Tannahill, D.; McCafferty, J.; Balasubramanian, S., Quantitative visualization of DNA G-quadruplex structures in human cells. *Nat Chem* **2013,** *5* (3), 182-6.
44. Nikan, M.; Di Antonio, M.; Abecassis, K.; McLuckie, K.; Balasubramanian, S., An acetylene-bridged 6,8-purine dimer as a fluorescent switch-on probe for parallel G-quadruplexes. *Angew Chem Int Ed Engl* **2013,** *52* (5), 1428-31.
45. Sexton, A. N.; Collins, K., The 5' guanosine tracts of human telomerase RNA are recognized by the G-quadruplex binding domain of the RNA helicase DHX36 and function to increase RNA accumulation. *Mol Cell Biol* **2011,** *31* (4), 736-43.
46. De Cian, A.; Cristofari, G.; Reichenbach, P.; De Lemos, E.; Monchaud, D.; Teulade-Fichou, M. P.; Shin-Ya, K.; Lacroix, L.; Lingner, J.; Mergny, J. L., Reevaluation of telomerase inhibition by quadruplex ligands and their mechanisms of action. *Proc Natl Acad Sci U S A* **2007,** *104* (44), 17347-52.
47. Harrison, R. J.; Cuesta, J.; Chessari, G.; Read, M. A.; Basra, S. K.; Reszka, A. P.; Morrell, J.; Gowan, S. M.; Incles, C. M.; Tanious, F. A.; Wilson, W. D.; Kelland, L. R.; Neidle, S., Trisubstituted acridine derivatives as potent and selective telomerase inhibitors. *J Med Chem* **2003,** *46* (21), 4463-76.
48. Tauchi, T.; Shin-Ya, K.; Sashida, G.; Sumi, M.; Nakajima, A.; Shimamoto, T.; Ohyashiki, J. H.; Ohyashiki, K., Activity of a novel G-quadruplex-interactive telomerase inhibitor, telomestatin (SOT-095), against human leukemia cells: involvement of ATM-dependent DNA damage response pathways. *Oncogene* **2003,** *22* (34), 5338-47.
49. Benimetskaya, L.; Takle, G. B.; Vilenchik, M.; Lebedeva, I.; Miller, P.; Stein, C. A., Cationic porphyrins: novel delivery vehicles for antisense oligodeoxynucleotides. *Nucleic Acids Res* **1998,** *26* (23), 5310-7.
50. Izbicka, E.; Wheelhouse, R. T.; Raymond, E.; Davidson, K. K.; Lawrence, R. A.; Sun, D.; Windle, B. E.; Hurley, L. H.; Von Hoff, D. D., Effects of cationic porphyrins as G-quadruplex interactive agents in human tumor cells. *Cancer Res* **1999,** *59* (3), 639-44.
51. Monchaud, D.; Teulade-Fichou, M. P., A hitchhiker's guide to G-quadruplex ligands. *Org Biomol Chem* **2008,** *6* (4), 627-36.
52. Le, V. H.; Nagesh, N.; Lewis, E. A., Bcl-2 promoter sequence G-quadruplex interactions with three planar and non-planar cationic porphyrins: TMPyP4, TMPyP3, and TMPyP2. *PLoS One* **2013,** *8* (8), e72462.
53. Nicoludis, J. M.; Miller, S. T.; Jeffrey, P. D.; Barrett, S. P.; Rablen, P. R.; Lawton, T. J.; Yatsunyk, L. A., Optimized end-stacking provides specificity of N-methyl mesoporphyrin IX for human telomeric G-quadruplex DNA. *J Am Chem Soc* **2012,** *134* (50), 20446-56.

54. De Matteis, F.; Gibbs, A. H.; Smith, A. G., Inhibition of protohaem ferro-lyase by N-substituted porphyrins. Structural requirements for the inhibitory effect. *Biochem J* **1980,** *189* (3), 645-8.
55. Ragazzon, P. A.; Garbett, N. C.; Chaires, J. B., Competition dialysis: a method for the study of structural selective nucleic acid binding. *Methods* **2007,** *42* (2), 173-82.
56. Nicoludis, J. M.; Barrett, S. P.; Mergny, J. L.; Yatsunyk, L. A., Interaction of human telomeric DNA with N-methyl mesoporphyrin IX. *Nucleic Acids Res* **2012,** *40* (12), 5432-47.
57. Jaumot, J.; Gargallo, R., Experimental Methods for Studying the Interactions between G-Quadruplex Structures and Ligands. *Current Pharmaceutical Design* **2012,** *18* (14), 1900-1916.
58. Vorlíčková, M.; Kejnovská, I.; Bednářová, K.; Renčiuk, D.; Kypr, J., Circular dichroism spectroscopy of DNA: from duplexes to quadruplexes. *Chirality* **2012,** *24* (9), 691-8.
59. Paramasivan, S.; Rujan, I.; Bolton, P. H., Circular dichroism of quadruplex DNAs: applications to structure, cation effects and ligand binding. *Methods* **2007,** *43* (4), 324-31.
60. Masiero, S.; Trotta, R.; Pieraccini, S.; De Tito, S.; Perone, R.; Randazzo, A.; Spada, G. P., A non-empirical chromophoric interpretation of CD spectra of DNA G-quadruplex structures. *Org Biomol Chem* **2010,** *8* (12), 2683-92.
61. De Cian, A.; Guittat, L.; Kaiser, M.; Sacca, B.; Amrane, S.; Bourdoncle, A.; Alberti, P.; Teulade-Fichou, M.; Lacroix, L.; Mergny, J., Fluorescence-based melting assays for studying quadruplex ligands. *Methods* **2007,** *42* (2), 183-195.
62. Simonsson, T.; Sjöback, R., DNA tetraplex formation studied with fluorescence resonance energy transfer. *J Biol Chem* **1999,** *274* (24), 17379-83.
63. Mergny, J. L.; Lacroix, L., Analysis of thermal melting curves. *Oligonucleotides* **2003,** *13* (6), 515-37.
64. Förster, T., **Zwischenmolekulare Energiewanderung und Fluoreszenz**. *Annalen der Physik* **1948,** *437*, 55-75.
65. Stryer, L., Fluorescence energy transfer as a spectroscopic ruler. *Annu Rev Biochem* **1978,** *47*, 819-46.
66. Ren, J.; Chaires, J. B., Sequence and structural selectivity of nucleic acid binding ligands. *Biochemistry* **1999,** *38* (49), 16067-75.
67. Pasternack, R.; Brigandi, R.; Abrams, M.; Williams, A.; Gibbs, E., Interactions of porphyrins and metalloporphyrins with single-sranded poly(DA). *Inorganic Chemistry* **1990,** *29* (22), 4483-4486.
68. Roza-Fernández, M.; Valencia-González, M. J.; Díaz-García, M. E., Room-temperature phosphorescent palladium-porphine probe for DNA determination. *Anal Chem* **1997,** *69* (13), 2406-10.
69. Polo, C. F.; Frisardi, A. L.; Resnik, E. R.; Schoua, A. E.; Batlle, A. M., Factors influencing fluorescence spectra of free porphyrins. *Clin Chem* **1988,** *34* (4), 757-60.
70. Arthanari, H.; Basu, S.; Kawano, T.; Bolton, P., Fluorescent dyes specific for quadruplex DNA. *Nucleic Acids Research* **1998,** *26* (16), 3724-3728.
71. Paramasivan, S.; Bolton, P. H., Mix and measure fluorescence screening for selective quadruplex binders. *Nucleic Acids Res* **2008,** *36* (17), e106.

72. Uttamlal, M.; Holmes-Smith, A. S., The excitation wavelength dependent fluorescence of porphyrins. *Chemical Physics Letters* **2008,** *454* (4-6), 223-228.
73. Jameson, D. M.; Gratton, E.; Hall, R. D., The Measurement and Analysis of Heterogeneous Emissions by Multifrequency Phase and Modulation Fluorometry. Taylor and Francis group: 1984; Vol. 20, pp 55-106.
74. Scatchard, G., The attractions of proteins for small molecules and ions. *Annals of the New York Academy of Sciences* **1949,** *51* (4), 660-672.
75. Haq, I.; Trent, J.; Chowdhry, B.; Jenkins, T., Intercalative G-tetraplex stabilization of telomeric DNA by a cationic porphyrin. *Journal of the American Chemical Society* **1999,** *121* (9), 1768-1779.
76. Sabharwal, N. C.; Savikhin, V.; Turek-Herman, J. R.; Nicoludis, J. M.; Szalai, V. A.; Yatsunyk, L. A., N-methylmesoporphyrin IX fluorescence as a reporter of strand orientation in guanine quadruplexes. *FEBS J* **2014**.
77. Pasternack, R. F.; Gibbs, E. J.; Villafranca, J. J., Interactions of porphyrins with nucleic acids. *Biochemistry* **1983,** *22* (10), 2406-14.
78. Shi, D. F.; Wheelhouse, R. T.; Sun, D.; Hurley, L. H., Quadruplex-interactive agents as telomerase inhibitors: synthesis of porphyrins and structure-activity relationship for the inhibition of telomerase. *J Med Chem* **2001,** *44* (26), 4509-23.
79. Bhattacharjee, A. J.; Ahluwalia, K.; Taylor, S.; Jin, O.; Nicoludis, J. M.; Buscaglia, R.; Brad Chaires, J.; Kornfilt, D. J.; Marquardt, D. G.; Yatsunyk, L. A., Induction of G-quadruplex DNA structure by Zn(II) 5,10,15,20-tetrakis(N-methyl-4-pyridyl)porphyrin. *Biochimie* **2011,** *93* (8), 1297-309.
80. Ma, D. L.; Che, C. M.; Yan, S. C., Platinum(II) complexes with dipyridophenazine ligands as human telomerase inhibitors and luminescent probes for G-quadruplex DNA. *J Am Chem Soc* **2009,** *131* (5), 1835-46.
81. Tanaka, S.; Shirakawa, M.; Kaneko, K.; Takeuchi, M.; Shinkai, S., Porphyrin-based organogels: control of the aggregation mode by a pyridine-carboxylic acid interaction. *Langmuir* **2005,** *21* (6), 2163-72.
82. Nagesh, N.; Buscaglia, R.; Dettler, J. M.; Lewis, E. A., Studies on the site and mode of TMPyP4 interactions with Bcl-2 promoter sequence G-Quadruplexes. *Biophys J* **2010,** *98* (11), 2628-33.
83. Freyer, M. W.; Buscaglia, R.; Kaplan, K.; Cashman, D.; Hurley, L. H.; Lewis, E. A., Biophysical studies of the c-MYC NHE III1 promoter: model quadruplex interactions with a cationic porphyrin. *Biophys J* **2007,** *92* (6), 2007-15.
84. Job, P., Studies on the formation of complex minerals in solution and on their stability. *Annales De Chimie France* **1928,** *9*, 113-203.
85. Parkinson, G. N.; Ghosh, R.; Neidle, S., Structural basis for binding of porphyrin to human telomeres. *Biochemistry* **2007,** *46* (9), 2390-7.
86. Risitano, A.; Fox, K. R., Stability of intramolecular DNA quadruplexes: comparison with DNA duplexes. *Biochemistry* **2003,** *42* (21), 6507-13.
87. Ambrus, A.; Chen, D.; Dai, J.; Bialis, T.; Jones, R. A.; Yang, D., Human telomeric sequence forms a hybrid-type intramolecular G-quadruplex structure with mixed parallel/antiparallel strands in potassium solution. *Nucleic Acids Res* **2006,** *34* (9), 2723-35.

88. McClure, J. E.; Baudouin, L.; Mansuy, D.; Marzilli, L. G., Interactions of DNA with a new electron-deficient tentacle porphyrin: meso-tetrakis[2,3,5,6-tetrafluoro-4-(2-t rimethylammoniumethyl-amine)phenyl]porphy rin. *Biopolymers* **1997,** *42* (2), 203-17.
89. Chou, S. H.; Chin, K. H.; Wang, A. H., DNA aptamers as potential anti-HIV agents. *Trends Biochem Sci* **2005,** *30* (5), 231-4.
90. Hotoda, H.; Koizumi, M.; Koga, R.; Kaneko, M.; Momota, K.; Ohmine, T.; Furukawa, H.; Agatsuma, T.; Nishigaki, T.; Sone, J.; Tsutsumi, S.; Kosaka, T.; Abe, K.; Kimura, S.; Shimada, K., Biologically active oligodeoxyribonucleotides. 5. 5'-End-substituted d(TGGGAG) possesses anti-human immunodeficiency virus type 1 activity by forming a G-quadruplex structure. *J Med Chem* **1998,** *41* (19), 3655-63.
91. Phan, A. T.; Kuryavyi, V.; Gaw, H. Y.; Patel, D. J., Small-molecule interaction with a five-guanine-tract G-quadruplex structure from the human MYC promoter. *Nat Chem Biol* **2005,** *1* (3), 167-73.

Appendix

Table of Contents

Supplementary Figures

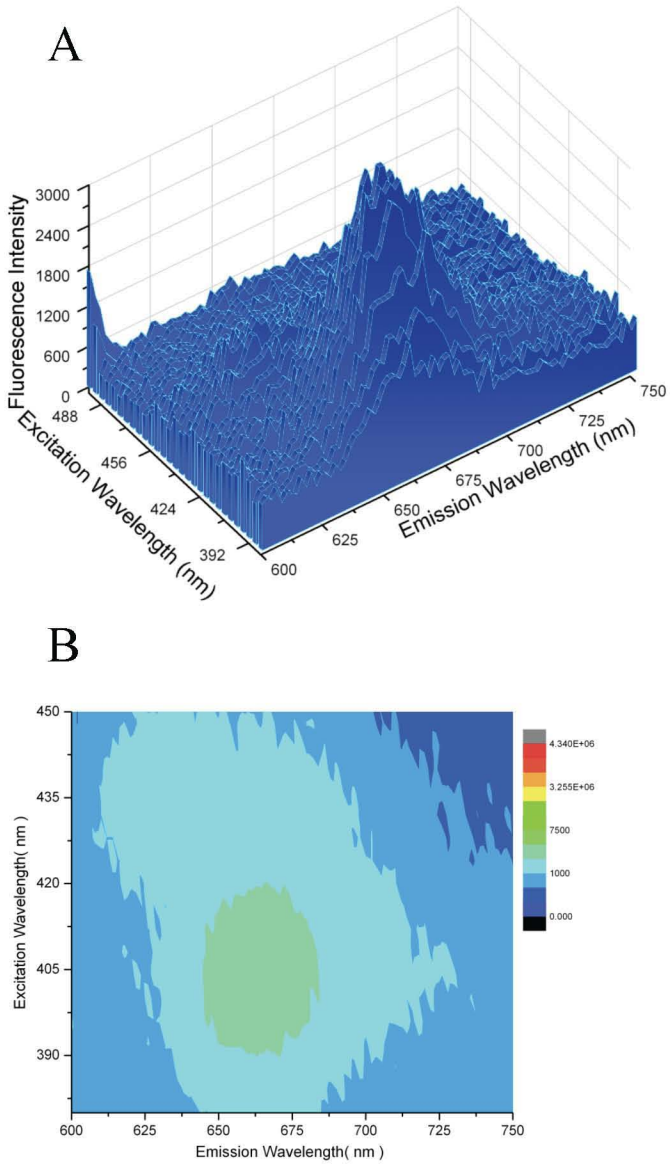

Figure S1. (A) 3D and (B) contour plot of excitation wavelength vs. emission wavelength vs. fluorescence intensity for a sample of PtTMPyP4 in dd H_2O. The maximum fluorescence intensity was found using a 412 nm excitation wavelength, which was the value that was subsequently used for future fluorescence studies with the porphyrin. Scan parameters were as follows: increment = 4 nm; integration time = 0.1 sec; slit length = 2 nm for excitation and 5 nm for emission.

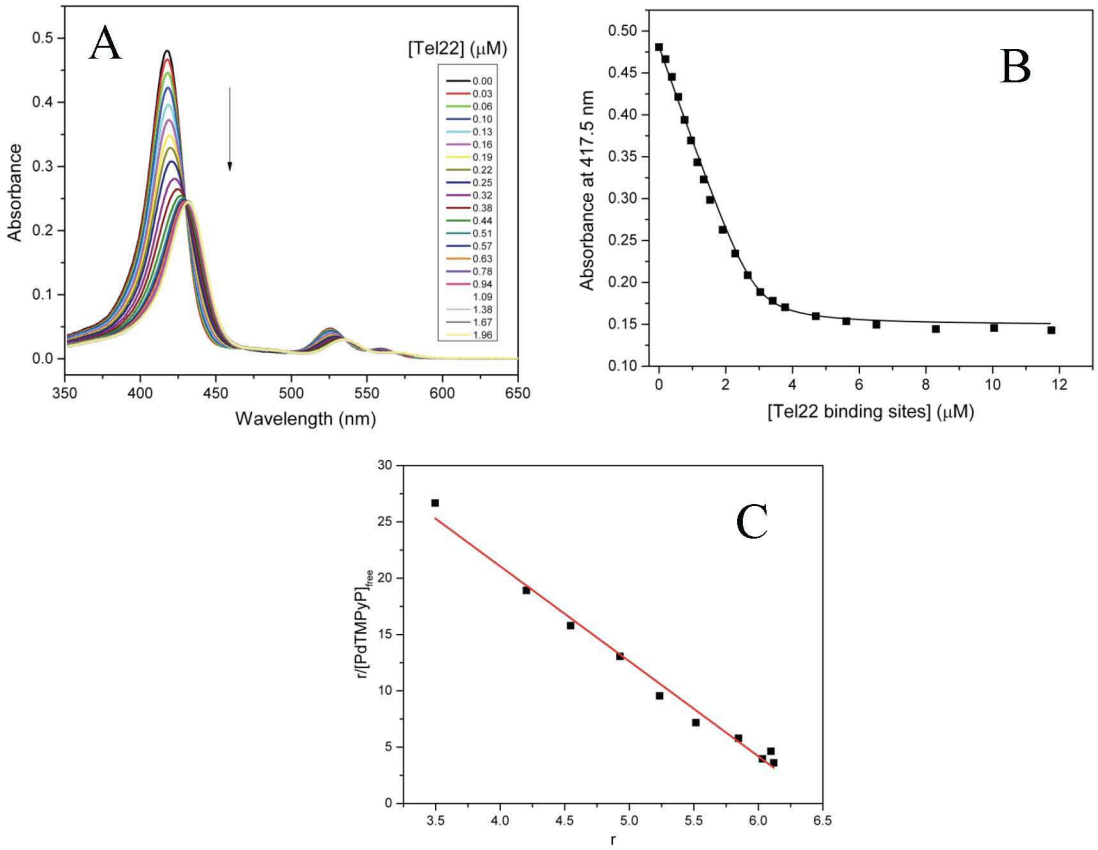

Figure S2. Summary of the results of titration studies with 2.87 μM PdTMPyP4 and 0.03 mM Tel22 in 5K buffer. (A) Representative UV-Vis absorption spectra for the titration. (B) Plot of the absorbance at the Soret peak (401 nm) as a function of the concentration of DNA used to calculate the binding constant from direct fitting. (C) Scatchard plot of r / [PtTMPyP4]free vs. r used to determine the binding affinity and binding ratio.

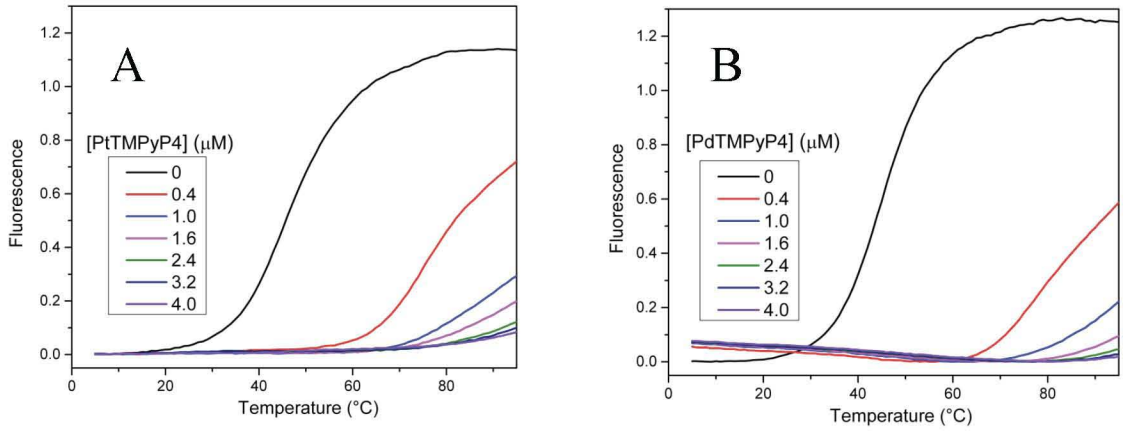

Figure S3. FRET melting curves for F21D in the presence of 0 to 4 μM of (A) PtTMPyP4 and (B) PdTMPyP4 in 5K buffer. The low fluorescence values of F21D in the presence of > 0.4 μM ligand indicate incomplete melting of the qudruplex.

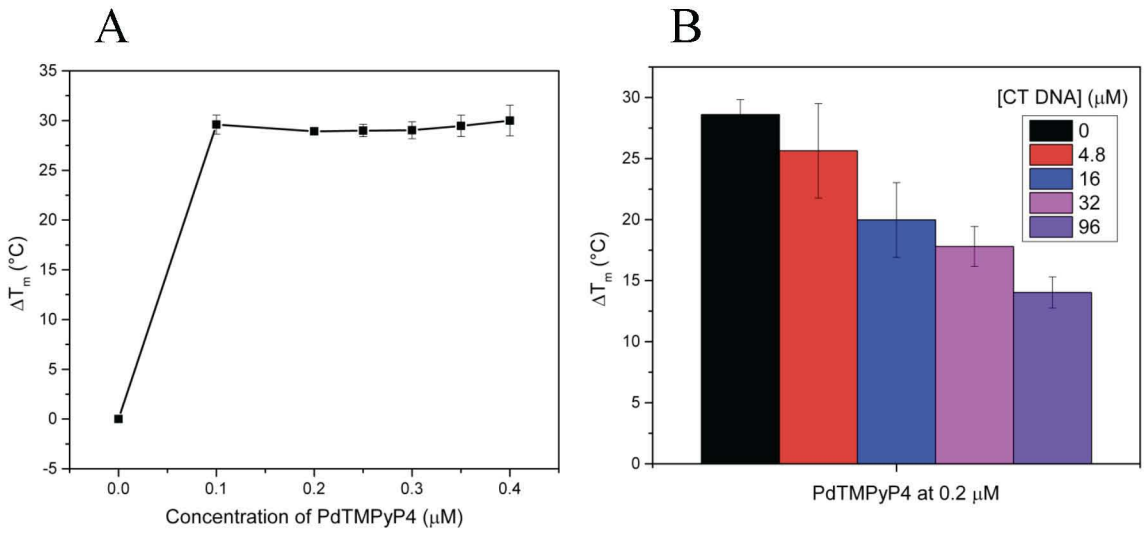

Figure S4. Summary of FRET experiments with PdTMPyP4 and F21D in 5K buffer. (A) Concentration-dependent increase in melting temperature of 0.2 μM F21D stabilized by 0 to 0.4 μM ligand. The increase in melting temperature at 0.4 μM relative to NMM alone (ΔT_m) is found to be 30.0 ± 1.6 °C. (B) Results of the competition study indicate a decrease in melting temperature with increasing concentrations of duplex DNA, suggesting moderate selectivity for the GQ structure.

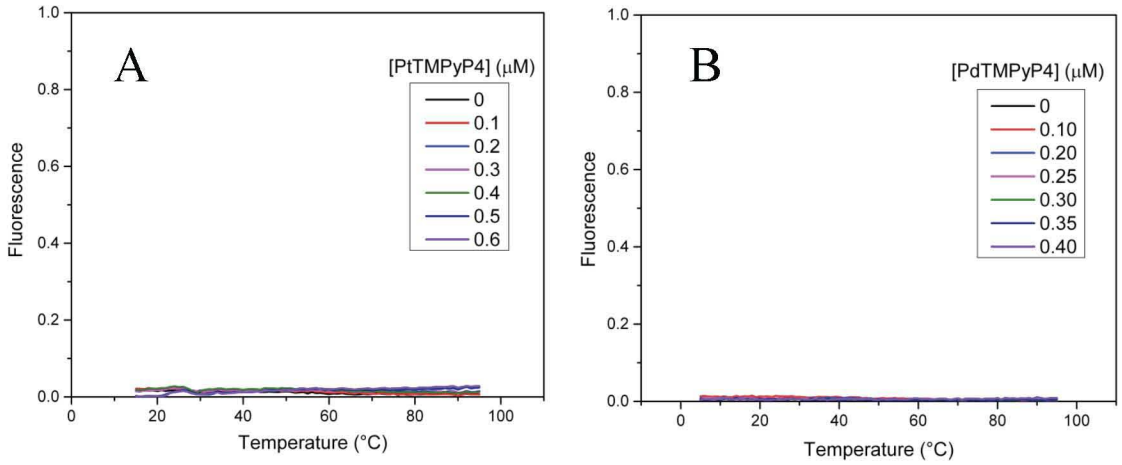

Figure S5. Absence of fluorescence emitted by (A) PtTMPyP4 and (B) PdTMPyP4 in the presence of Tel22 indicates that the natural porphyrin fluorescence is not responsible for the fluorescence observed in FRET experiments.

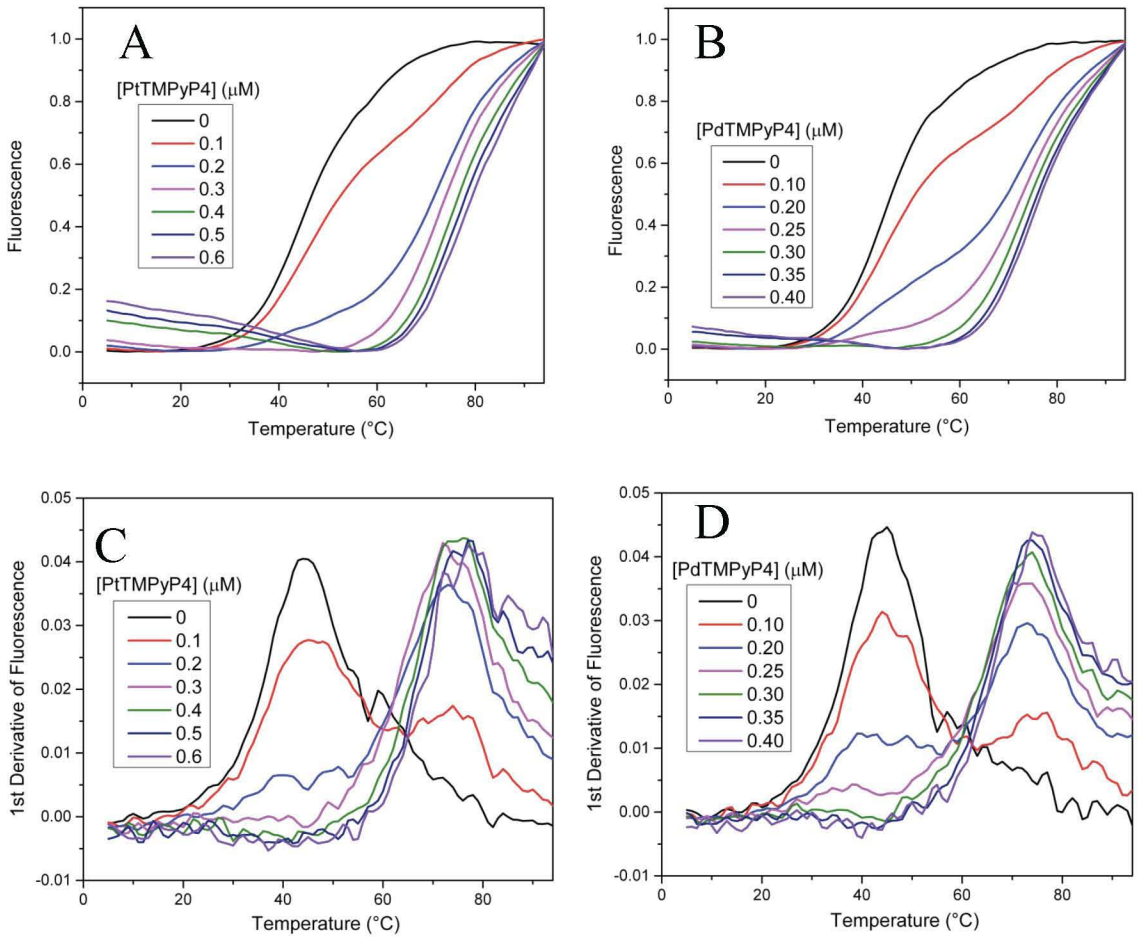

Figure S6. FRET melting curves for F21D in the presence of (A) 0 to 0.6 μM PtTMPyP4 and (B) 0 to 0.4 μM PdTMPyP4 in 5K buffer are biphasic. Graph of first derivative of fluorescence of the melting curves vs. temperature for (A) PtTMPyP4 and (B) PdTMPyP4 display contain two distinct peaks.

FRET sample setup for stabilization and competition studies

Table S1. FRET tray setup for stabilization studies with 0 to 20 equivalents (eq.) of either PtTMPyP4 of PdTMPyP4.

Well	Sample Description	Volume 0.25 µM F21D (µL)	Volume 20 µM porphyrin (µL)	Volume 5K buffer (µL)
A	Blank	0	0	50
B	F21D alone	40	0	10
C	2 eq. ligand	40	1	9
D	5 eq. ligand	40	2.5	7.5
E	8 eq. ligand	40	4	6
F	12 eq. ligand	40	6	4
G	16 eq. ligand	40	8	2
H	20 eq. ligand	40	10	0

Table S2. FRET tray setup for stabilization studies with 0 to 3 eq. of PtTMPyP4.

Well	Sample Description	Volume 0.25 µM F21D (µL)	Volume 5 µM PtTMPyP4 (µL)	Volume 5K buffer (µL)
A	Blank	0	0	50
B	F21D alone	40	0	10
C	0.5 eq. PtTMPyP4	40	1	9
D	1 eq. PtTMPyP4	40	2	8
E	1.5 eq. PtTMPyP4	40	3	7
F	2 eq. PtTMPyP4	40	4	6
G	2.5 eq. PtTMPyP4	40	5	5
H	3 eq. PtTMPyP4	40	6	4

Table S3. FRET tray setup for stabilization studies with 0 to 2 eq. of PdTMPyP4.

Well	Sample Description	Volume 0.25 µM F21D (µL)	Volume 5 µM PdTMPyP4 (µL)	Volume 5K buffer (µL)
A	Blank	0	0	50
B	F21D alone	40	0	10
C	0.5 eq. PdTMPyP4	40	1	9
D	1 eq. PdTMPyP4	40	2	8
E	1.25 eq. PdTMPyP4	40	2.5	7.5
F	1.5 eq. PdTMPyP4	40	3	7
G	1.75 eq. PdTMPyP4	40	3.5	6.5
H	2 eq. PdTMPyP4	40	4	6

Table S4. FRET tray setup for stabilization studies with 0 to 10 eq. of TCPPSpm4.

Well	Sample Description	Volume 0.25 µM F21D (µL)	Volume 10 µM TCPPSpm4 (µL)	Volume 5K buffer (µL)
A	Blank	0	0	50
B	F21D alone	40	0	10
C	1 eq. TCPPSpm4	40	1	9
D	2.5 eq. TCPPSpm4	40	2.5	7.5
E	4 eq. TCPPSpm4	40	4	6
F	6 eq. TCPPSpm4	40	6	4
G	8 eq. TCPPSpm4	40	8	2
H	10 eq. TCPPSpm4	40	10	0

Table S5. FRET tray setup for competition studies with 1 eq. PtTMPyP4 or PdTMPyP4 and 0 to 480 eq. of CT DNA competitor.

Well	Sample Description	Volume 0.25 µM F21D (µL)	Volume 800 µM CT DNA (µL)	Volume 5 µM ligand (µL)	Volume 5K buffer (µL)
A	Blank	0	0	0	50
B	F21D alone	40	0	0	10
C	1 eq. ligand, 0 eq. CT DNA	40	0	2	8
D	1 eq. ligand, 24 eq. CT DNA	40	3 (of 80 µM CT DNA)	2	5
E	1 eq. ligand, 80 eq. CT DNA	40	1	2	7
F	1 eq. ligand, 160 eq. CT DNA	40	2	2	6
G	1 eq. ligand, 480 eq. CT DNA	40	6	2	2
H	0 eq. ligand, 80 eq. CT DNA	40	1	0	9

Copy of the paper "N-methylmesoporphyrin IX fluorescence as a reporter of strand orientation in guanine quadruplexes"

Reference:

Sabharwal, N.C.; Savikhin, V.; Turek-Herman, J.R.; Nicoludis, J.M.; Szalai, V.A.; Yatsunyk, L.A. N-methylmesoporphyrin IX fluorescence as a reporter of strand orientation in guanine quadruplexes. *FEBS J.*, **2014**, *281*, 1726 - 1737

the FEBS Journal

N-methylmesoporphyrin IX fluorescence as a reporter of strand orientation in guanine quadruplexes

Navin C. Sabharwal[1], Victoria Savikhin[2,*], Joshua R. Turek-Herman[1], John M. Nicoludis[1,†], Veronika A. Szalai[2] and Liliya A.Yatsunyk[1]

1 Department of Chemistry and Biochemistry, Swarthmore College, PA, USA
2 Center for Nanoscale Science & Technology, National Institute of Standards & Technology, Gaithersburg, MD, USA

Keywords
fluorescent probe; guanine quadruplex; human telomeric DNA; *N*-methylmesoporphyrin IX; selectivity

Correspondence
L. A. Yatsunyk, Department of Chemistry and Biochemistry, Swarthmore College, 500 College Ave., Swarthmore, PA 19081, USA
Fax: +1 610 328 7355
Tel: +1 610 328 8558
E-mail: lyatsun1@swarthmore.edu
V. A. Szalai, Center for Nanoscale Science and Technology, National Institute of Standards and Technology, 100 Bureau Drive, Gaithersburg, MD 20899, USA
Fax: +1 301 975 2303
Tel: +1 301 975 3792
E-mail: Veronika.Szalai@NIST.gov

Present addresses *Department of Electrical Engineering, Stanford University, Stanford, CA, USA
†Department of Chemistry and Chemical Biology, Harvard University, Cambridge, MA,USA

(Received 9 October 2013, revised 24 December 2013, accepted 30 January 2014)

doi:10.1111/febs.12734

Guanine quadruplexes (GQ) are four-stranded DNA structures formed by guanine-rich DNA sequences. The formation of GQs inhibits cancer cell growth, although the detection of GQs *in vivo* has proven difficult, in part because of their structural diversity. The development of GQ-selective fluorescent reporters would enhance our ability to quantify the number and location of GQs, ultimately advancing biological studies of quadruplex relevance and function. *N*-methylmesoporphyrin IX (NMM) interacts selectively with parallel-stranded GQs; in addition, its fluorescence is sensitive to the presence of DNA, making this ligand a possible candidate for a quadruplex probe. In the present study, we investigated the effect of DNA secondary structure on NMM fluorescence. We found that NMM fluorescence increases by about 60-fold in the presence of parallel-stranded GQs and by about 40-fold in the presence of hybrid GQs. Antiparallel GQs lead to lower than 10-fold increases in NMM fluorescence. Single-stranded DNA, duplex, or i-motif, induce no change in NMM fluorescence. We conclude that NMM shows promise as a 'turn-on' fluorescent probe for detecting quadruplex structures, as well as for differentiating them on the basis of strand orientation.

Introduction

DNA adopts numerous secondary structures in addition to the canonical Watson–Crick duplex. One example is G-quadruplex (GQ) DNA, a structure formed by π-π stacking of G-quartets, composed of four guanines held together by Hoogsteen hydrogen bonds [1–3] (Fig. 1). To form GQs, a DNA sequence must contain one or more regions of contiguous guanines, typically three or more. Monovalent cations, such as

Abbreviations
APD, acetylene-bridged purine dimer; CT, calf thymus DNA; dsDNA, double-stranded DNA; GQ, guanine quadruplex DNA; NMM, *N*-methylmesoporphyrin IX; ssDNA, single-stranded DNA; TBA, thrombin-binding aptamer; Tel22, human telomeric DNA repeat model sequence.

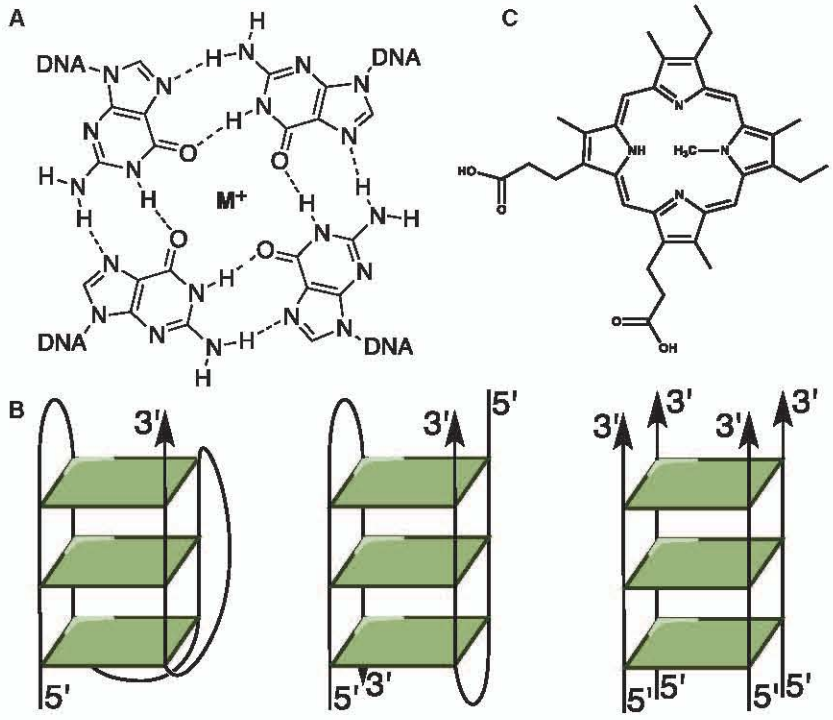

Fig. 1. Structures of GQ and NMM. (A) Structure of a G-tetrad. (B) Schematic representations of mixed-hybrid monomolecular GQ (left), antiparallel bimolecular GQ (middle) and tetramolecular parallel-stranded GQ (right). (C) Structure of NMM. Note that commercially available NMM is a mixture of four regioisomers that differ in the position of the N-Me group (only one isomer is shown); each isomer forms a pair of enantiomers with the N-Me group pointing up or down.

sodium, potassium or ammonium, stabilize GQ structures [1,4]. GQs can be uni-, bi- or tetramolecular and adopt parallel, antiparallel, or mixed-hybrid topology (Fig. 1B), depending on DNA composition, stabilizing cation and the presence of exogenous ligands [5–9].

G-rich DNA sequences with a propensity to form GQs have been identified throughout the human genome, including in telomeres, oncogenes (*c-MYC, c-MYB, c-FOS, c-ABL*), ribosomal DNA and immunoglobin switch regions [10–15]. GQs have been proposed to regulate gene expression, chromosomal alignment, recombination and DNA replication [16]. Conclusive correlation of GQs with cellular processes, however, has proved challenging, partly as a result of the structural diversity exhibited by GQs, and also because the available probes can induce GQ formation or alter their structures, making it unclear whether the GQs observed *in vivo* are present prior to probe addition. Accordingly, there is a need for new probes to clarify the physiological relevance of GQ DNA.

Selective quadruplex targeting and detection are both important and challenging. A variety of small-molecule probes display fluorescence that is modulated by the presence of GQs; such molecules are highlighted in a recent review [17]. The majority of these probes suffer from low selectivity for GQ versus double-stranded DNA (dsDNA) or toward a specific GQ geometry. It is important to discriminate GQs based on their geometry because it defines the biological roles and functions of GQs, such as interactions with proteins [18] and drugs [19,20]. The first example of a 'turn-on' fluorescent small molecule dye specific for parallel-stranded (but not antiparallel or mixed-hybrid GQs) was reported recently [21]. This acetylene-bridged purine dimer (APD) interacts with a variety of parallel-stranded GQ structures, displays strong emission in their presence, and exhibits topology-specific staining in agarose gels. Its synthesis, however, is not trivial. By contrast to this small molecule example, Balasubramanian's group reported immunofluorescence detection of GQs [22], thereby improving the ability to map GQs *in vivo*. The need remains for additional GQ selective probes that are either commercially available or easy to prepare and compatible with sensitive *in vivo* detection, primarily by fluorescence microscopy.

N-methylmesoporphyrin IX (NMM) (Fig. 1C) is highly selective for GQ over single-stranded DNA (ssDNA) and ssRNA, dsDNA, triplex DNA and DNA–RNA hybrids [23,24]. Previous studies have demonstrated that NMM fluorescence increases in the presence of GQ but not dsDNA [25,26]. Recently, NMM was shown to bind parallel but not antiparallel GQs [23,27]. The potential of NMM to discriminate between particular strand orientations of GQs using fluorescence, however, has not been systematically explored. NMM is water-soluble, chemically stable, and commercially available molecule with excellent optical and fluorescence properties. These attributes,

combined with the ability of NMM to preferentially recognize parallel-stranded GQ structures, make it a promising candidate for selective GQ detection. In the present study, we applied UV-visible, fluorescence and CD spectroscopies to evaluate the potential of NMM as a selective fluorescence GQ reporter in the presence of a wide selection of DNA structures.

Results and Discussion

In light of the exceptional selectivity of NMM for GQ DNA relative to other DNA secondary structures [24,25] and the unique ability of this ligand to discriminate between parallel versus antiparallel GQ conformation [23], we aimed to determine whether NMM could be used as a GQ-specific fluorescence probe. To achieve this goal, we measured the fluorescence of NMM in the presence of a variety of DNA sequences and secondary structures, including ssDNA, dsDNA and i-motif DNA, as well as carefully selected GQ DNA with representative folding topologies (Table 1). GQ secondary structures are usually defined as follows. Mixed-hybrid quadruplexes contain one strand running in the opposite direction from the other three strands (Fig. 1B, left). Antiparallel GQs contain two strands that run in opposite direction from the two remaining strands; for example, the bimolecular GQ shown in Fig. 1B (middle). A parallel-stranded GQ has all four DNA strands running in the same direction, as shown in Fig. 1B (right), for a tetramolecular GQ. The secondary struc-

Table 1. Oligonucleotide conformation and fluorescence enhancement and lifetime data.

	Conformation[a]			
Name	Without NMM	With NMM	Fluorescence enhancement[b]	Fluorescence lifetimes (τ_1; ns)[c]
C1A	ss	ss	0.69 ± 0.19 (TB)	
Tel22, 100Li	ss	ss	1.22 ± 0.21 (100Li)	
CT	ds	ds	0.00 ± 0.05	
			0.03 ± 0.07 (50Na)	
ds26	ds	ds	0.25 ± 0.06	
C1A:C1B	ds	ds	0.44 ± 0.22 (TB)	
C8	i	i	1.25 ± 0.65 (5K 5.8)	
i-cMyc	i	i	1.53 ± 0.12 (5K 5.8)	
$C_4T_4C_4$	i	i	0.45 ± 0.16 (5K 5.8)	
TC_4T	i	i	0.44 ± 0.00 (5K 5.8)	
IL1	P	P	55.7 ± 6.8 (TB)	
G4	P	P	67.8 ± 4.3	7.83 ± 0.01
			65 ± 11 (TB)	8.29 ± 0.01 in TB
G8	P	P	69.9 ± 3.7	8.00 ± 0.01
			57.5 ± 4.2 (TB)	7.97 ± 0.01 in TB
VEGF	P	P	52.9 ± 2.0	7.09 ± 0.01
cMyc	P	P	64.8 ± 3.8	7.96 ± 0.01
cKit2	P	P	46.3 ± 1.6	6.35 ± 0.01
cKit1	P/M	P	41.9 ± 2.5	
G4TERT	P/M	P	50.2 ± 6.1	
Bcl-2	P/M	P	47.9 ± 1.2	
Tel22	M	P	25.5 ± 2.4	τ_1 = 7.26 ± 0.02 (89)
				τ_2 = 2.00 ± 0.03 (11)
26TelG4	A/M	M	34.1 ± 4.6	
$G_4T_4G_4$	A/M	M	60.2 ± 4.6	7.13 ± 0.01
Tel22, 50Na	A	A	1.59 ± 0.18	τ_1 = 5.18 ± 0.01 (60 ± 2)
				τ_2 = 0.68 ± 0.002 (40 ± 2)
TBA	A	A	15.5 ± 1.4	τ_1 = 5.81 ± 0.01 (90 ± 4)
				τ_2 = 1.07 ± 0.01 (10 ± 4)
TBA, 50Na	A	A	5.15 ± 0.39	
26TelG4, 50Na	A	A	12.1 ± 1.3	
$G_4T_4G_4$, 50Na	A	A/M	16.0 ± 1.1	τ_1 = 6.85 ± 0.002 (88 ± 3)
				τ_2 = 1.34 ± 0.01 (12 ± 3)

[a] A, antiparallel; ds, double-stranded (duplex); I, i-motif; M, mixed; P, parallel; ss, single-stranded. [b] Buffer is 5K unless specified otherwise. [c] Population is given in parenthesis as a percentage and is 100% if not specified.

ture of each DNA in the present study was verified using CD spectroscopy (Figs S1 and S2).

Quadruplex sequences chosen in the present study include oncogene promoters, telomeric DNA and some synthetic sequences. Specifically, Tel22 [28] and 26TelG4 are human telomeric DNA sequences; $G_4T_4G_4$ is telomeric DNA from the ciliate *Oxytricha nova*. This latter sequence was chosen because it maintains antiparallel topology both in potassium [29] and sodium [30] buffers. G4TERT corresponds to a DNA sequence in the promoter of hTERT, a catalytic domain of telomerase [31]. Oncogene promoters tested in the present study include VEGF, Bcl-2, cKit and cMyc. VEGF is an oncogene promoter for vascular endothelial growth factor that is upregulated in a variety of cancers [14]; Bcl-2 inhibits cell apoptosis in B-cell lymphoma cancer cell lines [32]; cKit is a tyrosine kinase receptor that controls cell growth [33]; and cMyc is a transcriptional regulator of approximately 15% of human genes involved in a variety of cancers [34]. In addition, we tested nonphysiological DNA sequences that are models for GQs. The thrombin-binding aptamer (TBA) [35] was used in the present study because, similar to $G_4T_4G_4$, it forms an antiparallel topology regardless of buffer condition; G4 and G8 always form simple homogeneous tetramolecular parallel quadruplexes; and IL1 forms a parallel-stranded quadruplex with single-stranded overhangs that contain nucleotides other than thymine.

Titration of NMM with parallel and antiparallel GQs monitored by fluorescence to determine saturation limit and binding constants

NMM fluoresces weakly in aqueous solution, although its fluorescence increases dramatically in the presence of certain DNA structures [26]. Thus, NMM can serve as a 'turn-on' fluorescent probe. To determine the amount of DNA required to reach the fluorescence signal saturation point for NMM, we performed fluorescence titrations of NMM using a subset of DNA sequences. Titration data for the tetramolecular parallel quadruplexes, G4 and G8, and for the antiparallel/mixed-hybrid quadruplex $G_4T_4G_4$ are shown in Fig. 2; data for the intramolecular parallel quadruplex, VEGF, are shown in Fig. S3. These data indicate that at least five equivalents of GQ DNA are required to saturate NMM fluorescence. For consistency, 10 equivalents of DNA structural element were used per NMM molecule in all subsequent experiments.

Our titration data allowed determination of binding constants. The maximum fluorescence intensity as a function of added GQ DNA was fit to a 1:1 binding model, yielding K_a of $(1.4 \pm 0.2) \times 10^6$ L·mol^{-1} for G4, $(1.7 \pm 0.2) \times 10^6$ L·mol^{-1} for G8 and $(1.1 \pm 0.1) \times 10^6$ L·mol^{-1} for VEGF. Fits improved (as judged by residuals) for VEGF when the NMM to GQ binding ratio was changed to 1:2, yielding K_a of $(7.0 \pm 0.9) \times 10^6$ L·mol^{-1}. We utilized Job plot experiments (method of continuous variation) to verify independently the stoichiometry of the NMM–VEGF interaction. Analysis of the Job plot indicates either a 1:1 or 1:2 binding stoichiometry (Fig. S3B). From these data, we conclude that one molecule of NMM binds two molecules of VEGF when VEGF is in excess, although it binds only one molecule of VEGF when concentrations of DNA and NMM are comparable.

$G_4T_4G_4$ quadruplex, which adopts an antiparallel/mixed-hybrid topology in potassium buffer, displayed

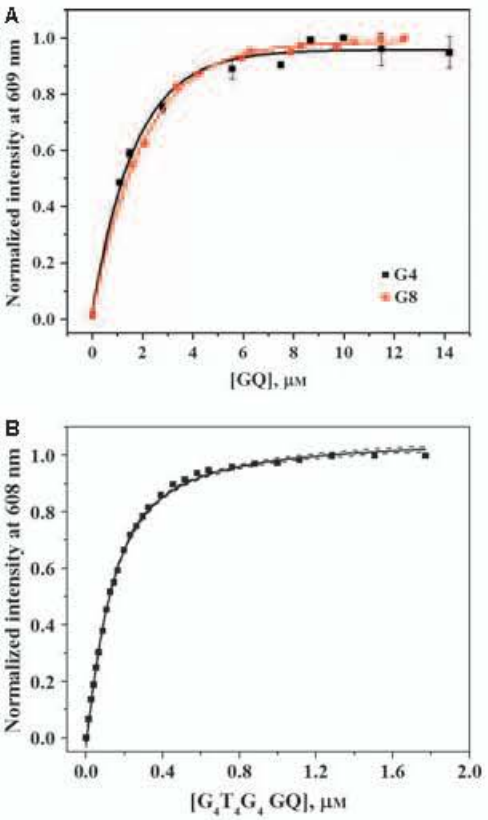

Fig. 2. Normalized fluorescence data for titration of (A) 1.0 μM NMM with G4 and G8 in TB buffer and (B) 0.1 μM NMM with $G_4T_4G_4$ in 5K buffer at 25 °C. Data for G4 and G8 are the average of three individual titrations. Solid lines represent global fits to a 1 : 1 binding model and dashed lines represent the 95% confidence interval. Binding constants were determined to be $(1.4 \pm 0.2) \times 10^6$, $(1.7 \pm 0.2) \times 10^6$ and $(1.26 \pm 0.07) \times 10^7$ L·mol^{-1} for G4, G8 and $G_4T_4G_4$, respectively. Note, the data for $G_4T_4G_4$ could be satisfactory fit to a 1 NMM : 2 GQ binding model with K_a of $(5.4 \pm 0.5) \times 10^7$ L·mol^{-1}.

tight binding to NMM with K_a of $(1.26 \pm 0.07) \times 10^7$ L·mol^{-1} using a 1 : 1 binding model. This affinity is two orders of magnitude higher than the previously reported binding affinity of NMM to a different mixed-hybrid quadruplex, Tel22, 1.0×10^5 L·mol^{-1} [23]. Overall, the affinity of NMM for the GQ structures decreases in the order: $G_4T_4G_4$ > VEGF ≈ G8 ≈ G4 > Tel22. This ordering correlates qualitatively with higher steady-state NMM fluorescence in the presence of $G_4T_4G_4$, G4, G8 and VEGF compared to Tel22 in 5K buffer (Fig. 3). The tight binding between NMM and $G_4T_4G_4$ is somewhat unexpected. In potassium buffer, $G_4T_4G_4$ forms an antiparallel dimer [29], which would leave no room for NMM binding. Currently, our laboratory is investigating the details of this interaction to uncover possible reasons for this apparently anomalous behavior.

When NMM was titrated with predominantly antiparallel $G_4T_4G_4$ and 26TelG4, both in 50Na buffer, the fluorescence intensity increased in a linear fashion not reaching saturation even at a >16-fold excess of DNA over NMM (Fig. S4). The observed increase in fluorescence is well below that obtained for $G_4T_4G_4$ in 5K buffer. The data suggest weak and/or nonspecific binding of NMM to these sequences.

The presence of parallel GQs increases NMM steady-state fluorescence intensity and fluorescence lifetime

To establish the utility of NMM as a fluorescent probe for quadruplex detection, we determined how the fluorescence of NMM changes in the presence of a 10-fold excess of a variety of DNA structures. Figure 3 shows that ssDNA and dsDNA have little effect on NMM fluorescence in agreement with previous equilibrium dialysis experiments [24]. These same equilibrium dialysis experiments indicated significant binding between NMM and the i-motifs TC_4T and $C_4T_4C_4$ [24]. By contrast, we did not observe fluorescence increases in the presence of any of the i-motifs that we tested (i-cMyc, C8, TC_4T and $C_4T_4C_4$). This discrepancy could be a result of the difference in experimental conditions and nature of techniques utilized to observe interaction between NMM and DNA. Specifically, the buffer used in the equilibrium dialysis experiments contained 6 mM Na_2HPO_4, 2 mM NaH_2PO_4, 1 mM Na_2EDTA, and 185 mM NaCl (pH 7.0), whereas our buffer, 5K 5.8, had lower ionic strength, lower pH and 5 mM KCl. The insensitivity of NMM to i-motifs (at least as reported by fluorescence and UV-visible spectroscopy) emphasizes its exceptional selectivity for GQ DNA structures.

The steady-state fluorescence of NMM increases in the presence of GQ DNA. We investigated the specificity of this increase by utilizing selected G-rich oligonucleotides that adopt well-defined secondary structures, including parallel, mixed-hybrid and antiparallel (Table 1). IL1, G4, G8, cMyc, cKit2 and VEGF sequences adopt parallel-stranded topology alone or in the presence of NMM on the basis of our CD spectra ([23] and Fig. S1). The addition of a 10-fold excess of these DNA structures to NMM leads to a fluorescence enhancement of more than 50

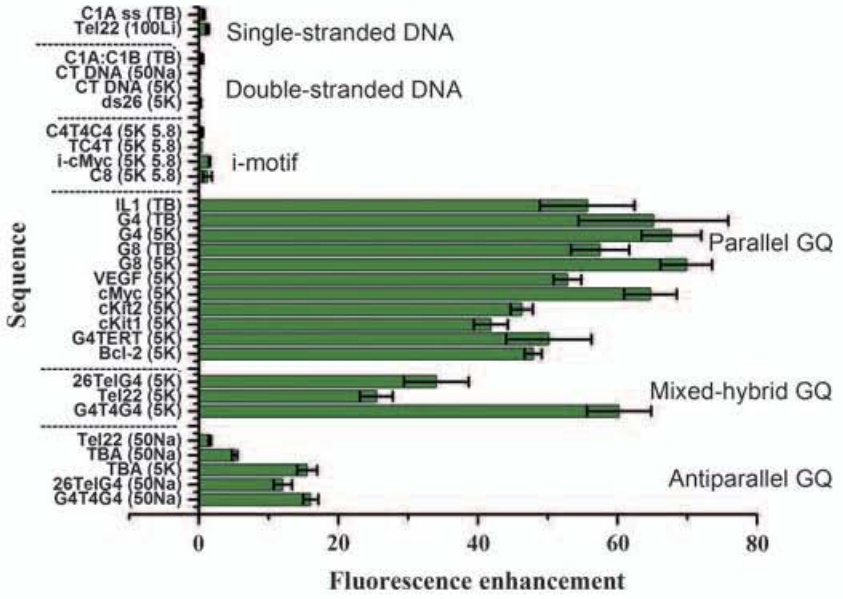

Fig. 3. Summary of steady-state fluorescence data for NMM incubated with a 10-fold molar excess of indicated sequences. Fluorescence enhancement is reported relative to the fluorescence of NMM alone. Error bars are 1 SD (confidence interval of 68.2%).

(Fig. 3 and Table 1) with the only exception being cKit2, for which fluorescence enhancement is 46. Sequences exhibiting starting parallel/mixed-hybrid conformations, such as cKit1, G4TERT and Bcl-2, generally lead to fluorescence enhancement of 42 to 50.

Sequences with predominantly mixed-hybrid GQ topology, such as Tel22 and 26TelG4 in 5K buffer, lead to a significantly smaller fluorescence enhancement of 25 and 34, respectively. As in the titration experiments, $G_4T_4G_4$ GQ in 5K buffer produces an anomalous result. This sequence adopts an antiparallel/mixed-hybrid topology (CD data; Fig. S2), yet leads to a fluorescence enhancement of 60, which is similar to that caused by parallel GQ structures. A large increase in the fluorescence of NMM upon the addition of $G_4T_4G_4$ in 10 mM HEPES buffer with 150 mM NaCl and 5 mM KCl was also reported previously [25]. A possible explanation is that NMM might convert $G_4T_4G_4$ to a structure (or a mixture) containing significant parallel component. Indeed, increased parallel component is detected by CD for this sequence under conditions of two-fold NMM excess (Fig. S2). It is important to note that the fluorescence samples contained 10-fold excess DNA (not excess NMM), leading us to expect that only a small fraction of GQ DNA could be structurally altered by NMM if it acts in a stoichiometric fashion.

Incubating NMM with predominantly antiparallel G-rich sequences resulted in only a small increase in fluorescence, the lowest of which was observed for Tel22 and TBA in 50Na, 1.6 and 5.2, respectively. Low fluorescence enhancements suggest a lack of interaction between NMM and these antiparallel structures, consistent with our previous study [23]. This interpretation is further supported by CD annealing studies in which NMM failed to induce changes in these DNA structures ([23] and Fig. S2). Other sequences in this group, $G_4T_4G_4$ and 26TelG4 in 50Na or TBA in 5K, caused small but significant increases in NMM fluorescence. These increases, however, are three- to six-fold lower than those observed for parallel GQ sequences. We tested whether NMM has an effect on the folds of these sequences by CD annealing ([23] and Fig. S2) and observed that the topologies of 26TelG4 in 50Na and TBA in 5K do not change in the presence of NMM. By contrast, the addition of NMM to $G_4T_4G_4$ in 50Na leads to an increase in the CD signal at 264 nm, consistent with an increase in parallel component of GQ structure. Our result differs from a previous study indicating that annealing of $G_4T_4G_4$ DNA with one equivalent of NMM in a buffer containing 140 mM NaCl does not change its CD signal [36]. This discrepancy is most likely a result of the lower amount of NMM and different buffer composition used in the latter study.

The presence of a high concentration of potassium ions shifts folding equilibria toward fully-folded GQ structures with a higher parallel component. Potassium is also known to significantly stablize GQ conformations minimizing the ability of ligands to affect quadruplex topology. To test this possibility, we performed fluorescence experiments in buffer with 150 mM KCl. (Fig. S5A). Under this condition, most of the DNA sequences (cKit1, cKit2, G4TERT, Bcl-2, 26TelG4 and $G_4T_4G_4$) displayed a significant increase in CD spectral intensity at 264 nm (Fig. S5B). Overall, the data collected in 150K buffer resemble those collected in 5K buffer. Notably, all of the parallel (or predominantly parallel) sequences (G4, G4TERT, Bcl-2, Kit2, cMyc, VEGF) generate a somewhat lower enhancement of NMM fluorescence in 150K versus 5K buffer; the only exception is cKit1, which exhibits an unchanged fluorescence. The small decrease in fluorescence enhancement observed in 150K buffer could be explained by weaker binding of NMM to DNA at this increased ionic strength. By contrast, NMM in the presence of mixed-hybrid (Tel22), antiparallel (TBA) or predominantly antiparallel (26TelG4) quadruplexes showed an increase in fluorescence enhancement in 150K versus 5K buffer, as would be expected for quadruplexes with an increased parallel component. $G_4T_4G_4$ GQ once again displayed anomalous behavior characteristic of parallel GQs and not mixed-hybrid GQs. It is important to emphasize that the overall trends of fluorescence enhancement were reproducible in buffers with low or high potassium ion concentrations.

Statistical analysis of the fluorescence enhancement data confirms the unique selectivity of NMM toward GQs versus nonquadruplex structures (Table S4). For example, the fluorescence of NMM at 610 nm is 150- and 390-fold higher on average in the presence of Tel22 and G8 (in 5K) versus dsDNA, respectively. More importantly, NMM can differentiate GQ structures based on their strand orientation. The fluorescence enhancement values increase in the order: antiparallel < mixed-hybrid < parallel. The ratio of fluorescence enhancements for predominantly parallel GQs (inter- or intramolecular) versus antiparallel GQ is 5.9 and for parallel GQs versus mixed-hybrid is 2.0 when the values in each category are averaged (Table S3). In previous equilibrium dialysis experiments, a discrimination ratio of 2 was reported [24]. This ratio appears to depend on the identity of the G-rich sequences and on buffer conditions.

When different conformations of Tel22 are compared (mixed-hybrid GQ in K^+-buffer, antiparallel GQ in Na^+-buffer and predominantly single-stranded in Li^+-buffer), the preference of NMM for mixed-hybrid (or possibly parallel GQ fold) is obvious (Fig. S6). The overall discrimination pattern for NMM is similar to that of another recently reported fluorescent probe, APD [21]. However, the fluorescence of APD did not increase in the presence of Tel22, in contrast to our observation with NMM; the effect of i-motifs on APD fluorescence was not reported.

We hypothesized that the observed increase in steady-state emission of NMM in the presence of GQs is a result of protection of NMM from dynamic quenching by water. To test this idea, we collected fluorescence lifetimes for NMM in the presence of representative quadruplex topologies (Table 1). The fluorescence lifetime of NMM is the longest (6–8 ns) in the presence of predominantly parallel-stranded GQs. By contrast, NMM exhibits two lifetimes (5–7 ns and 1–2 ns) when it interacts with antiparallel or mixed-hybrid GQ structures. The key result is that the steady-state fluorescence enhancement values correlate with fluorescence lifetimes (Fig. S7A). In another experiment, we used isotopic substitution of deuterium oxide (D_2O) for water because D_2O decreases dynamic quenching of fluorophores [37]. As predicted, the steady-state fluorescence intensity of NMM in D_2O increased relative to that in H_2O (Fig. S7B). The results of these experiments are consistent with our hypothesis that binding of NMM to a quadruplex protects it from solvent, leading to increased fluorescence.

NMM fluorescence detects parallel-stranded GQs in the presence of duplex DNA

It is important that quadruplex DNA should be recognized by its probe even in the context of a large background of dsDNA. To demonstrate that NMM is capable of such selective recognition, we performed two sets of competition experiments. A solution of NMM containing > 10-fold-excess of the parallel-stranded G4 or VEGF quadruplex was titrated with increasing amounts of C1A:C1B dsDNA or genomic CT dsDNA, respectively. In both cases, the fluorescence of NMM did not change even when a 100-fold excess of dsDNA was added (Fig. S8). This is consistent with previous experiments, where we observed that the melting temperature of NMM-stabilized Tel22 did not decrease even in the presence of 480-fold excess dsDNA [23]. In a reverse competition experiment, a solution of NMM with 100-fold excess duplex was titrated with increasing amounts of either G4 or VEGF quadruplex. In both cases, the titration data were practically indistinguishable from the titrations of NMM (alone, in the absence of duplex) with GQ (Fig. S3C for the VEGF case). The binding constants obtained for NMM–VEGF complex with or without CT DNA are within experimental error of each other $(6.9 \pm 1.5) \times 10^6$ L·mol^{-1} and $(7.0 \pm 0.9) \times 10^6$ L·mol^{-1}, respectively (assuming 2 : 1 GQ : NMM binding stoichiometry).

Disruption of GQ structure decreases NMM fluorescence

Treatment of GQ structures with LiOH dissociates DNA strands. This process is driven by deprotonation of the N1 site on guanine at a pH above its pK_a of 9.4, which leads to electrostatic repulsion of the strands. We observed unfolding of G4 or IL1 GQs upon treatment with LiOH via CD spectroscopy (for IL1, see Fig. S1). When NMM was incubated with G4 or IL1, its fluorescence increased as expected but fell to levels typical for NMM alone when DNA was treated with LiOH prior to addition of NMM (Fig. S9). These results further highlight the ability of NMM to discriminate between GQ DNA and other DNA structures (single-stranded DNA in this case).

NMM fluorescence is predominantly independent of pH and buffer composition

Physiological pH varies from 7 to 9; thus, it is ideal that the potential fluorescent probe remain insensitive to changes in pH in this range. To test the sensitivity of NMM to pH, an aqueous solution of NMM was titrated either with acid (HCl) or base (NaOH). The NMM fluorescence spectrum retained its overall shape but slightly increased in intensity (by 1.5- to 2.0-fold) when the pH was increased from 2.0 to 8.6 (Fig. S10A). Upon further pH increase, a new signal emerged at 636 nm that was at least 25-fold more intense than the signal in the original spectrum (Fig. S10B). Observed pH changes were reversible because the addition of acid to a basic solution of NMM regenerated the starting NMM fluorescence spectrum (Fig. S10C). Neutralization of the acidic solution of NMM lead to a relatively small change in spectral shape and intensity (Fig. S10D).

Because working with biological molecules requires buffered solutions, we tested the fluorescence of NMM in five commonly used buffers over a wide pH range: 8.3 (Tris), 7.2 and 5.8 (lithium cacodylate), and 4.9 and 4.0 (sodium acetate). Again, NMM displayed only a small (approximately 1.3-fold) decrease in fluorescence intensity with decreasing pH (Fig. S11).

We proceeded to test the fluorescence of NMM in the presence of selected DNA sequences in two potassium-containing buffers: lithium cacodylate at pH 7.2 (5K) and Tris at pH 8.3 (TB). Direct comparison of the increase in NMM fluorescence induced by G4 and G8 reveals that the values in TB are slightly lower than in 5K: 65 ± 11 versus 68 ± 4 for G4 and 58 ± 4 versus 70 ± 4 for G8. Both measurements show, however, that NMM fluorescence increases significantly and reproducibly in the presence of parallel quadruplex, indicating that the enhancement is observed easily over a range of experimental conditions.

In short, the fluorescence of NMM is only weakly sensitive to the nature of the buffer or the pH (in the physiological pH range), making it highly suitable for biological detection of quadruplex DNA. It is important to note that the amount and type of monovalent cation, as well as solution pH, can modulate DNA structure and, therefore, any DNA interactions with NMM thereby affecting the fluorescence of NMM.

Conclusions

For use in fluorescence microscopy, a candidate dye should possess a large extinction coefficient, be selective toward its target and have an acceptable quantum yield. NMM meets the first criterion: its extinction coefficient is 1.45×10^5 M^{-1}·cm^{-1} [38] and it shows a Soret band red shift of approximately 20 nm upon DNA binding [23]. Duplex-binding dyes, such as propidium iodide, which are used routinely for fluorescence microscopy of DNA, exhibit a 20- to 30-fold increase in fluorescence when bound to DNA. NMM displays little change in fluorescence intensity in the presence of ssDNA (regardless of G-content), dsDNA or i-motif DNA, and a modest increase in fluorescence in the presence of antiparallel quadruplexes. By marked contrast, the fluorescence of NMM increases more than 40-fold upon the addition of parallel-stranded GQ DNA, making it an attractive 'light-switch' fluorescent probe. The sequence Tel22, which is a fragment of the human telomeric repeat, leads to an enhancement of 28 ± 2 fold in the fluorescence of NMM in 5K buffer (where Tel22 exist in a mixed-hybrid form) but only an enhancement of 2.6 ± 0.2 fold in 50Na buffer (where Tel22 adopts antiparallel topology) or an enhancement of 2.2 ± 0.2 fold in 100Li buffer (where Tel22 is single-stranded), indicating that discrimination of the type of fold adopted by the human telomeric sequence *in vivo* could be achieved by fluorescence microscopy of NMM-stained samples.

Materials and methods

Porphyrins, oligonucleotides and buffers

NMM was purchased from Frontier Scientific (Logan, UT, USA), dissolved in water (resistivity 1.8×10^5 Ωm) at 0.3–1.3 mM, and stored at 4 °C. NMM stock solutions were freshly diluted with appropriate buffers. NMM concentrations were determined spectrophotometrically using $\varepsilon_{379\ nm} = 1.45 \times 10^5$ M^{-1}·cm^{-1} [38]. Tris(hydroxymethyl)amino methane (Tris), boric acid, hydrochloric acid, cacodylic acid, lithium hydroxide (LiOH), tetramethylammonium chloride (TMACl), potassium chloride and magnesium chloride were standard grade reagents and were used as received. The DNA oligonucleotide sequences used in the present study are provided in Table S1. All oligonucleotides were purchased from commercial vendors. Selected sequences were purified by ethanol precipitation as described in the Supporting information, Doc. S1. The buffers used were:

10 mM lithium cacodylate (pH 7.2), 5 mM KCl, 95 mM LiCl (5K);
10 mM lithium cacodylate (pH 7.2), 150 mM KCl (150K);
10 mM lithium cacodylate (pH 5.8), 5 mM KCl, 95 mM LiCl (5K 5.8);
10 mM lithium cacodylate (pH 7.2), 50 mM NaCl, 50 mM LiCl (50Na);
10 mM lithium cacodylate (pH 7.2), 100 mM LiCl (100Li);
50 mM Tris-borate (pH 8.3), 10 mM KCl, 1 mM $MgCl_2$ (TB); and
50 mM Tris-borate (pH 8.3), 10 mM TMACl, 1 mM $MgCl_2$ (TB-TMACl).

The complete list of buffers is provided in Table S2. TMACl was used in lieu of KCl because it minimizes GQ formation [39].

To induce the formation of the most thermodynamically stable GQ conformations, oligonucleotides were diluted in the desired buffer (with or without added salts) and melted at > 90 °C for 5 min. When required, aliquots of concentrated stock solutions of KCl and/or $MgCl_2$ were mixed into the heated solution, which was then allowed to heat for an additional 5 min, cooled to room temperature over 3 h, and incubated overnight at 4 °C. The i-motif structures were formed by preparing C-rich sequences in acidic pH 5.8 [40]. For experiments testing NMM interaction with rigorously single-stranded G-rich sequences, GQs assembled from IL1 or G4 in TB buffer were treated with 50 mM LiOH for 30 min, after which the pH was adjusted to neutral by the addition of HCl. The disruption of the quadruplex into single strands was verified using CD spectroscopy.

The C1A:C1B duplex was formed in solutions containing 120 μM of each strand in TB-TMACl buffer. The solution was heated to 95 °C for 10 min, and cooled to room temperature over a period of 3 h. The final duplex was either used as

generated or gel-purified on nondenaturing PAGE using TMACl in the running buffer as described previously [41]. A dry sample of calf-thymus (CT) DNA was dissolved in 10 mM lithium cacodylate and 1 mM Na_2EDTA to a concentration of approximately 1 mM (in base pairs) and placed on a nutator for 1 week at 4 °C. Before use, the sample was centrifuged extensively to remove insoluble components and the supernatant was transferred to a clean microcentrifuge tube. Stock DNA and NMM solutions were stored at −80 °C; samples in buffers were stored at either −20 °C or 4 °C depending on the length of time between sample preparation and use.

Concentrations of all DNA samples were determined spectrophotometrically at room temperature on two types of UV-visible spectrophotometers and are reported as the concentration of structural element: GQ, i-motif or duplex. For example, the concentration of a unimolecular GQ is equal to the concentration of oligonucleotide strand, whereas the concentration of a tetramolecular GQ is assumed to be one quarter of the oligonucleotide strand concentration. The concentration of genomic CT DNA is reported in base pairs. Extinction coefficients for all single-stranded oligonucleotides are provided in Table S1 and were calculated using the nearest-neighbor approximation [42,43]. Secondary structures of all DNA sequences were verified using CD wavelength scans.

CD spectroscopy

For CD experiments, DNA samples were prepared at 1–10 μM concentrations in desired buffers. Spectra were collected on two types of CD spectropolarimeters; one of which was equipped with a Peltier temperature control unit (error of ±0.3 °C). Samples were placed in cylindrical quartz cuvettes (pathlengths of 0.1 or 0.5 cm) or a 1-cm quartz cuvette. Three scans were collected from 330 to 220 nm with a 1-nm bandwidth and an average time of 1 s at 25 °C and averaged. CD data were treated as described previously [44]. CD spectra of selected sequences were collected in the presence of a two-fold excess of NMM to determine its effect on DNA secondary structure. For these experiments, samples were annealed with or without NMM at 90 °C for 10 min, slowly cooled to room temperature and stored at 4 °C overnight before collecting CD scans.

UV-visible and fluorescence spectroscopy

UV-visible spectra for absorption titrations were collected on a spectrophotometer with a Peltier-thermostatted cuvette holder (error of ±0.3 °C) using a 1-cm quartz cuvette. Spectra were collected in the range of 350–700 nm at 25 °C. All experiments were performed at least three times on independently prepared solutions.

Fluorescence experiments were performed on three types of commercially available spectrofluorometers. An NMM solution was prepared in the desired buffer at 1 μM and its steady-state fluorescence spectrum was measured. DNA was added to NMM at 10-fold excess, the sample was equilibrated at room temperature for up to 1 h and its fluorescence spectrum was remeasured. The amount of DNA required to saturate the NMM fluorescence signal was determined from fluorescence titrations, which also were used to obtain binding constants. Titrations of 1 μM NMM were conducted with G4 (in TB), G8 (in TB) and VEGF (in 5K), all of which are parallel-stranded GQs; with antiparallel/mixed-hybrid $G_4T_4G_4$ (5K); and with antiparallel $G_4T_4G_4$ (50Na) and 26TelG4 (50Na). Spectra of NMM in the presence of G4 and G8 were collected in 100-μL volume quartz cuvettes with excitation wavelength of 399 nm, emission wavelength range from 550 to 750 nm, slits of 0.5 nm, and an integration time of 1 or 2 s. Spectra of NMM in the presence of VEGF, $G_4T_4G_4$ and 26TelG4 were collected in a 1-cm quartz cuvette using excitation wavelength of 399 nm, emission wavelength range from 550 to 700 nm, increment of 1 nm, integration time of 0.5 s, slits of 2 nm, and temperature of 25 °C. Quadruplex $G_4T_4G_4$ in 5K displays tight binding to NMM ($K_a > 10^7$ M^{-1}); in this case, a solution of only 0.1 μM NMM was titrated with the quadruplex; data were collected at a single wavelength of 608 nm using two points per second and a 50-s duration (which corresponds to 100 scans with 0.5-s integration time) to improve the signal-to-noise ratio. All data were corrected for dilution and fit to extract the association constants, K_a, as described previously [23]. Reported errors originate from the global fit of two to three collected data sets. Both, 1 NMM:1 DNA and 1 NMM:2 DNA binding models were considered. Changes in fluorescence intensity at λ_{max} (610 nm for NMM and 607–609 nm for NMM bound to DNA) are reported as fluorescence enhancement and were calculated by taking the difference between the fluorescence intensity in the presence and absence of DNA divided by the fluorescence intensity recorded for NMM alone. Uncertainties in the fluorescence intensities arise predominantly from lamp intensity variation at the excitation wavelength from day to day and errors associated with pipetting small volumes. Error bars on fluorescence enhancement values are 1 SD (confidence interval of 68.2%), derived from replicate experiments. Statistical analysis performed on the fluorescence enhancement data are provided in Tables S3 and S4 and in Doc. S2.

Competition titrations via fluorescence

To determine the selectivity of NMM for GQ structures, two sets of competition titrations were performed. In one set, a solution of 1.0 μM NMM containing approximately 10 μM of G4 or VEGF was titrated with increasing amounts of dsDNA. In another set of experiments, a solution of 1.0 μM NMM containing up to 100 μM of dsDNA was titrated with an increasing amount of G4 or VEGF. These titrations were performed at 25 °C in TB (for G4) or 5K (for VEGF) buffers.

pH studies

To measure the effect of pH on NMM fluorescence, 1–2 μM NMM in H_2O was titrated with 0.1 M of either HCl or NaOH to achieve the desired pH. The pH, fluorescence and UV-visible data were collected after each addition of acid or base. The experiments were run either as titrations or using a batch method. For fluorescence, slits were 3.5–5 nm. Titrations were repeated four times.

To test the reversibility of the NMM fluorescence as a function of pH UV-visible and fluorescence spectra of two NMM samples were recorded at neutral pH. The pH of the first sample was brought down to approximately 3.2, then back up to neutral. The pH of the second sample was brought up to approximately 10.5, then back down to neutral. The solution pH was adjusted using either 0.25 M HCl or 0.25 M LiOH. These experiments were repeated twice.

The effect of pH and buffer type on the fluorescence of NMM was tested in five buffers that contained 10 mM of Tris (pH 8.3), lithium cacodylate (pH 7.2 and 5.8) or sodium acetate (pH 4.9 and 4.0). All buffers were supplemented with 5 mM KCl and 95 mM LiCl.

Fluorescence lifetime measurements

Fluorescence lifetimes were collected for NMM in the presence of representative GQ structures on a multi-frequency cross-correlation phase and modulation fluorometer at room temperature [45,46]. Samples were prepared at concentrations of NMM ranging from 0.7 to 2.3 μM with GQ ratios ranging from 1 : 4 to 1 : 30, depending on the sequence. The excitation wavelength was 399 nm; sample emission was filtered through a 550-nm longpass filter and referenced to a scatterer with counts that were matched to that of the sample. The frequency range over which data were collected was 1–250 MHz. The number of frequencies collected varied from 10 to 50, depending on the sample. Lifetimes were calculated from fits to the phase delay and modulation ratio data as described previously using commercially available software [47]. Errors are either associated with global fits to multiple scans or are 1 SD calculated from multiple lifetime measurements for a given sample. The low fluorescence intensity of free NMM in a buffer made it impossible to measure its lifetime accurately with our instrumentation.

Acknowledgements

This work was supported by the Swarthmore College Start-up grant; Howard Hughes Medical Institute (to NCS); Benjamin Franklin Travel Grants (to NCS); and National Institute of Standards and Technology Summer Undergraduate Research Fellowship (to VS). We thank Professors Lisa Kelly (University of Maryland, Baltimore County) and Richard B. Thompson (University of Maryland, Baltimore) for discussions regarding the fluorescence lifetime measurements. We thank Jean-Louis Mergny (the University of Bordeaux, IECB) for hosting LAY and NCS during the final stages of this project. Steve Wang, Michelle Ferreira and Vince Formica from Swarthmore are acknowledged for their help with the statistical analysis of fluorescence enhancement data.

Certain commercial entities, equipment or materials may be identified in this document to describe an experimental procedure or concept adequately. Such identification is not intended to imply recommendation or endorsement by the National Institute of Standards and Technology, nor is it intended to imply that the entities, materials or equipment are necessarily the best available for the purpose.

References

1 Williamson JR, Raghuraman MK & Cech TR (1989) Monovalent cation-induced structure of telomeric DNA: the G-quartet model. *Cell* **59**, 871–880.
2 Sen D & Gilbert W (1992) Guanine quartet structures. *Methods Enzymol* **211**, 191–199.
3 Kang C, Zhang X, Ratliff R, Moyzis R & Rich A (1992) Crystal structure of four-stranded Oxytricha telomeric DNA. *Nature* **356**, 126–131.
4 Sen D & Gilbert W (1990) A sodium-potassium switch in the formation of four-stranded G4-DNA. *Nature* **344**, 410–414.
5 Burge S, Parkinson GN, Hazel P, Todd AK & Neidle S (2006) Quadruplex DNA: sequence, topology, and structure. *Nucleic Acids Res* **34**, 5402–5415.
6 Esposito V, Galeone A, Mayol L, Oliviero G, Virgilio A & Randazzo L (2007) A topological classification of G-quadruplex structures. *Nucleosides Nucleotides Nucleic Acids* **26**, 1155–1159.
7 Li J, Correia JJ, Wang L, Trent JO & Chaires JB (2005) Not so crystal clear: the structure of the human telomere G-quadruplex in solution differs from that present in a crystal. *Nucleic Acids Res* **33**, 4649–4659.
8 Haider SM, Parkinson GN & Neidle S (2003) Structure of a G-quadruplex-ligand complex. *J Mol Biol* **326**, 117–125.
9 Parkinson GN, Lee MPH & Neidle S (2002) Crystal structure of parallel quadruplexes from human telomeric DNA. *Nature* **417**, 876–880.
10 Huppert JL & Balasubramanian S (2007) G-quadruplexes in promoters throughout the human genome. *Nucleic Acids Res* **35**, 406–413.
11 Di Antonio M, Rodriguez R & Balasubramanian S (2012) Experimental approaches to identify cellular G-quadruplex structures and functions. *Methods* **57**, 84–92.

12 Bugaut A & Balasubramanian S (2012) 5′-UTR RNA G-quadruplexes: translation regulation and targeting. *Nucleic Acids Res* **40**, 4727–4741.
13 Todd AK & Neidle S (2011) Mapping the sequences of potential guanine quadruplex motifs. *Nucleic Acids Res* **39**, 4917–4927.
14 Sun DK, Guo KX & Shin YJ (2011) Evidence of the formation of G-quadruplex structures in the promoter region of the human vascular endothelial growth factor gene. *Nucleic Acids Res* **39**, 1256–1265.
15 Mathad RI, Hatzakis E, Dai JX & Yang DZ (2011) c-MYC promoter G-quadruplex formed at the 5 '-end of NHE III1 element: insights into biological relevance and parallel-stranded G-quadruplex stability. *Nucleic Acids Res* **39**, 9023–9033.
16 Bochman ML, Paeschke K & Zakian VA (2012) DNA secondary structures: stability and function of G-quadruplex structures. *Nat Rev Genet* **13**, 770–780.
17 Vummidi BR, Alzeer J & Luedtke NW (2013) Fluorescent probes for G-quadruplex structures. *ChemBioChem* **14**, 540–558.
18 Biffi G, Tannahill D & Balasubramanian S (2012) An intramolecular G-quadruplex structure is required for binding of telomeric repeat-containing RNA to the telomeric protein TRF2. *J Am Chem Soc* **134**, 11974–11976.
19 Monchaud D & Teulade-Fichou M-P (2008) A hitchhiker's guide to G-quadruplex ligands. *Org Biomol Chem* **6**, 627–636.
20 Georgiades SN, Karim NHA, Suntharalingam K & Vilar R (2010) Interaction of metal complexes with G-quadruplex DNA. *Angew Chem Int Ed* **49**, 4020–4034.
21 Nikan M, Di Antonio M, Abecassis K, McLuckie K & Balasubramanian S (2013) An acetylene-bridged 6,8-purine dimer as a fluorescent switch-on probe for parallel G-quadruplexes. *Angew Chem Int Ed* **52**, 1428–1431.
22 Biffi G, Tannahill D, McCafferty J & Balasubramanian S (2013) Quantitative visualization of DNA G-quadruplex structures in human cells. *Nat Chem* **5**, 182–186.
23 Nicoludis JM, Barrett SP, Mergny J-L & Yatsunyk LA (2012) Interaction of human telomeric DNA with *N*-methyl mesoporphyrin IX. *Nucleic Acids Res* **40**, 5432–5447.
24 Ragazzon P & Chaires JB (2007) Use of competition dialysis in the discovery of G-quadruplex selective ligands. *Methods* **43**, 313–323.
25 Arthanari H, Basu S, Kawano TL & Bolton PH (1998) Fluorescent dyes specific for quadruplex DNA. *Nucleic Acids Res* **26**, 3724–3728.
26 Paramasivan S & Bolton PH (2008) Mix and measure fluorescence screening for selective quadruplex binders. *Nucleic Acids Res* **36**, e106.
27 Nicoludis JM, Miller ST, Jeffrey PD, Barrett SP, Rablen PR, Lawton TJ & Yatsunyk LA (2012) Optimized end-stacking provides specificity of *N*-methyl mesoporphyrin IX for human telomeric G-quadruplex DNA. *J Am Chem Soc* **134**, 20446–20456.
28 Phan AT (2010) Human telomeric G-quadruplex: structures of DNA and RNA sequences. *FEBS J* **277**, 1107–1117.
29 Haider S, Parkinson GN & Neidle S (2002) Crystal structure of the potassium form of an *Oxytricha nova* G-quadruplex. *J Mol Biol* **320**, 189–200.
30 Schultze P, Smith FW & Feigon J (1994) Refined solution structure of the dimeric quadruplex formed from the Oxytricha telomeric oligonucleotide d (GGGGTTTTGGGG). *Structure* **2**, 221–233.
31 Lim KW, Lacroix L, Yue DJE, Lim JKC, Lim JMW & Phan AT (2010) Coexistence of two distinct G-quadruplex conformations in the hTERT promoter. *J Am Chem Soc* **132**, 12331–12342.
32 Dai J, Dexheimer TS, Chen D, Carver M, Ambrus A, Jones RA & Yang D (2006) An intramolecular G-quadruplex structure with mixed parallel/antiparallel G-strands formed in the human BCL-2 promoter region in solution. *J Am Chem Soc* **128**, 1096–1098.
33 Phan AT, Kuryavyi V, Burge S, Neidle S & Patel DJ (2007) Structure of an unprecedented G-quadruplex scaffold in the human c-kit promoter. *J Am Chem Soc* **129**, 4386–4392.
34 Gonzalez V & Hurley LH (2010) The c-MYC NHE III1: function and regulation. *Annu Rev Pharmacol Toxicol* **50**, 111–129.
35 Macaya RF, Schultze P, Smith FW, Roe JA & Feigon J (1993) Thrombin-binding DNA aptamer forms a unimolecular quadruplex structure in solution. *Proc Natl Acad Sci* **90**, 3745–3749.
36 Paramasivan S, Rujan I & Bolton PH (2007) Circular dichroism of quadruplex DNAs: applications to structure, cation effects and ligand binding. *Methods* **43**, 324–331.
37 Förster T & Rokos K (1967) A deuterium isotope solvent effect on fluorescence. *Chem Phys Lett* **1**, 279–280.
38 Ren J & Chaires JB (1999) Sequence and structural selectivity of nucleic acid binding ligands. *Biochemistry* **38**, 16067–16075.
39 Fahlman RP & Sen D (1999) 'Synapsable' DNA double helices: self-selective modules for assembling DNA superstructures. *J Am Chem Soc* **121**, 11079–11085.
40 Leroy J-L, Guéron M, Mergny J-L & Hélène C (1994) Intramolecular folding of a fragment of the cytosine-rich strand of telomeric DNA into an i-motif. *Nucleic Acids Res* **22**, 1600–1606.
41 Sambrook J & Russell D (2001) Molecular Cloning A Laboratory Manual, 3rd edn. Cold Spring Harbor Laboratory Press, Cold Spring Harbor, NY.
42 Borer PN (1975) Optical properties of nucleic acids, absorption, and circular dichroism spectra. In

Handbook of Biochemistry and Molecular Biology (Fasman G, ed.), pp. 589. CRC Press, Cleveland, OH.
43 Tataurov AV, You Y & Owczarzy R (2008) Predicting ultraviolet spectrum of single stranded and double stranded deoxyribonucleic acids. *Biophys Chem* **133**, 66–70.
44 Bhattacharjee AJ, Ahluwalia K, Taylor S, Jin O, Nicoludis JM, Buscaglia R, Brad Chaires J, Kornfilt DJP, Marquardt DGS & Yatsunyk LA (2011) Induction of G-quadruplex DNA structure by Zn(II) 5,10,15,20-tetrakis(*N*-methyl-4-pyridyl)porphyrin. *Biochimie* **93**, 1297–1309.
45 Gratton E, Alcala JR & Barbieri B (1991) Frequency domain fluorometry. Handbook of Luminescence Techniques in Chemical and Biochemical Analysis. Marcel Dekker Inc., New York, NY.
46 Lackowicz JR (2006) Principles of Fluorescence Spectroscopy, 3rd edn. Springer Science + Business Media, New York, NY.
47 Jameson DM & Gratton E (1983) Analysis of heterogeneous emissions by multifrequency phase and modulation fluorometry. In New Directions in Molecular Luminescence (Eastwood D, ed.). pp. 67–81, ASTM STP 822. American Society of Testing and Materials, Philadelphia, PA.

Supporting information

Additional supporting information may be found in the online version of this article at the publisher's web site:

Doc. S1. Ethanol precipitation.
Doc. S2. Statistical analysis of fluorescence enhancement data.
Fig. S1. CD spectra of selected DNA sequences.
Fig. S2. CD annealing studies of DNA in the presence of a two-fold excess NMM.
Fig. S3. Fluorescence titration of NMM with VEGF in 5K buffer at 25 °C.
Fig. S4. Fluorescence titration of NMM with $G_4T_4G_4$ and with 26TelG4 in 50Na buffer at 25 °C.
Fig. S5. Fluorescence enhancement and CD study in 150K buffer.
Fig. S6. Fluorescence spectra of NMM alone and with Tel22 in different buffers.
Fig. S7. NMM fluorescence intensity is modulated by dynamic solvent quenching.
Fig. S8. Competition titration of (NMM + GQ DNA) with dsDNA.
Fig. S9. Effect of LiOH on fluorescence of NMM in the presence of G4 in TB buffer.
Fig. S10. Effect of pH on the fluorescence spectra of NMM.
Fig. S11. Effect of pH and buffer type on the fluorescence spectra of NMM.
Table S1. Oligonucleotide sequences, extinction coefficients and fluorescence enhancement data.
Table S2. Composition of buffers.
Table S3. Raw data used for statistical analysis.
Table S4. Summary of *t*-test statistics for pairwise comparison.

the FEBS Journal

WILEY Blackwell

www.febsjournal.org

N-methylmesoporphyrin IX fluorescence as a reporter of strand orientation in guanine quadruplexes

Navin C. Sabharwal, Victoria Savikhin, Joshua R. Turek-Herman, John M. Nicoludis, Veronika A. Szalai and Liliya A.Yatsunyk

DOI: 10.1111/febs.12734

Supporting Information for

N-methylmesoporphyrin IX fluorescence as a reporter of strand orientation in guanine quadruplexes

Navin C. Sabharwal[1], *Victoria Savikhin*[2,3], *Joshua R. Turek-Herman*[1], *John M. Nicoludis*,[1,4] *Veronika A. Szalai*[2*], *Liliya A. Yatsunyk*[1*]

[1]Department of Chemistry and Biochemistry, Swarthmore College, 500 College Ave., Swarthmore, PA 19081 USA

[2]Center for Nanoscale Science & Technology, National Institute of Standards & Technology, 100 Bureau Drive, Gaithersburg, MD 20899 USA

[3]Current address: Department of Electrical Engineering, Stanford University, Stanford, CA 94305 USA

[4]Current address: Department of Chemistry and Chemical Biology, Harvard University, 12 Oxford St.Cambridge MA 02138, USA

Doc. S1. Ethanol precipitation

Oligonucleotides (IL1, G8, C1A, and C1B) were suspended in 100 μL of polished H_2O (resistivity of 1.8×10^5 Ω-m). Half (50 μL) of the resuspended DNA was transferred to a separate microfuge tube and ethanol precipitated by addition of 50 μL of 2.5 mol L^{-1} tetramethylammonium chloride (TMACl) and 1 mL of ethanol. The mixture was shaken, placed at -80 °C for 30 min and then pelleted in a microcentrifuge for 20 min at 2.05939×10^5 m s^{-2} (21 000 g) in a 4 °C refrigerator. Ethanol supernatant was removed from the resultant pellet. The pellet was dried in a DNA concentrator and then resuspended in 40 μL to 100 μL of polished H_2O, depending on oligonucleotide sequence.

Table S1: Oligonucleotide sequences, extinction coefficients and fluorescence enhancement data

Name	Sequence 5′→ 3′	ε_{260}[a] ($L\ mol^{-1}\ m^{-1}$)	ε_{260} ($mM^{-1}\ cm^{-1}$)	Conformation		Fluorescence enhancement
				w/o NMM[b]	w/ NMM	
C1A	ACAGTAGAGATGCTGCTGATTCGTTCA TGTGCTTCAAGC	3.732×10^7	373.2	ss	ss	0.69 ± 0.19[c]
C1B	GCTTGAAGCACATGAACGAATCAGCA GCATCTCTACTGT	3.769×10^7	376.9	ss	ss	nm
C1A:C1B				ds	ds	0.44 ± 0.22[c]
IL1	GCAGCATCTCTACTGTTTTGGGGGGGG TTTTAGCAGTGCGAGAGTCGTGGC	4.816×10^7	481.6	P	P	55.7 ± 6.8[c]
G4	TTTTGGGGTTTT	1.064×10^7	106.4	P	P	65 ± 11[c] 67.8 ± 4.3[d] 60.1 ± 2.9[h]
G8	TTTTGGGGGGGGTTTT	1.468×10^7	146.8	P	P	57.5 ± 4.2[c] 69.9 ± 3.7[d]
CT	Genomic calf thymus DNA	1.22×10^6 (per bp)	12.2	ds	ds	0.00 ± 0.05[d] 0.03 ± 0.07[e]
ds26	CAATCGGATCGAATTCGATCCGATTG	2.532×10^7	253.2	ds	ds	0.25 ± 0.06
Tel22	AGGGTTAGGGTTAGGGTTAGGG	2.285×10^7	228.5	M[d] A[e] ss[g]	P[d] A[e] ss[g]	25.5 ± 2.4[d] 31.3 ± 2.7[h] 1.59 ± 0.18[e] 1.22 ± 0.21[g]

VEGF	GGGAGGGTTGGGGTGGG	1.714×10^7	171.4	P	P	52.9 ± 2.0^d 50.5 ± 0.9^h
cMyc	TGAGGGTGGGTAGGGTGGGTAA	2.287×10^7	228.7	P	P	64.8 ± 3.8^d 62.6 ± 3.5^h
C8	AAAACCCCCCCCAAAA	1.574×10^7	157.4	i	i	1.25 ± 0.65^f
i-cMyc	TTACCCACCCTACCCACCCTCA	2.287×10^7	228.7	i	i	1.53 ± 0.12^f
TC_4T	TCCCCT	4.56×10^6	45.6	i	i	0.44 ± 0.00
$C_4T_4C_4$	CCCCTTTTCCCC	9.02×10^6	90.3	i	i	0.45 ± 0.16
26TelG4	AGGGGTTAGGGGTTAGGGGTTAGGGG	2.689×10^7	268.9	A/M^d A^e	M^d A^e	34.1 ± 4.6^d 42.6 ± 2.7^h 12.1 ± 1.3^e
Bcl-2	GGGCGCGGGAGGGAATTGGGCGGG	2.374×10^7	237.4	P/M	P	47.9 ± 1.2^d 44.9 ± 2.7^h
cKit1	GGGAGGGCGCTGGGAGGAGGG	2.132×10^7	213.2	P/M	P	41.9 ± 2.5^d 42.4 ± 2.3^h
cKit2	GGGCGGGCGCGAGGGAGGGG	1.991×10^7	199.1	P	P	46.3 ± 1.6^d 43.6 ± 1.4^h
G4TERT	AGGGGAGGGGCTGGGAGGGC	2.029×10^7	202.9	P/M	P	50.2 ± 6.1^d 43.2 ± 0.9^h
TBA	GGTTGGTGTGGTTGG	1.433×10^7	143.3	$A^{d,e}$	$A^{d,e}$	15.5 ± 1.4^d 19.6 ± 1.7^h 5.15 ± 0.39^e

$G_4T_4G_4$	GGGGTTTTGGGG	1.152×10^7	115.2	A/M[d] A[e]	M[d] A/M[e]	60.2 ± 4.6[d] 51.2 ± 1.8[h] 16.0 ± 1.1[e]

[a]Extinction coefficients for single-stranded oligonucleotide in SI units (42)

[b]ss, single-stranded; P = parallel; A = antiparallel; ds = duplex; M = mixed; i = i-motif

c – TB buffer

d – 5K buffer

e – 50Na buffer

f – 5K 5.8 buffer

g – 100Li buffer

h – 150K buffer

nm – not measured

Table S2. Composition of buffers

Abbreviation	Buffer Composition
5K	10 mmol L^{-1} lithium cacodylate, pH 7.2, 5 mmol L^{-1} KCl, 95 mmol L^{-1} LiCl
150K	10 mmol L^{-1} lithium cacodylate, pH 7.2, 150 mmol L^{-1} KCl
5K 5.8	10 mmol L^{-1} lithium cacodylate, pH 5.8, 5 mmol L^{-1} KCl, 95 mmol L^{-1} LiCl
50Na	10 mmol L^{-1} lithium cacodylate, pH 7.2, 50 mmol L^{-1} NaCl, 50 mmol L^{-1} LiCl
100Li	10 mmol L^{-1} lithium cacodylate, pH 7.2, 100 mmol L^{-1} LiCl
TB	50 mmol L^{-1} Tris-borate, pH 8.3, 10 mmol L^{-1} KCl, 1 mmol L^{-1} $MgCl_2$
TB-TMACl	50 mmol L^{-1} Tris-borate, pH 8.3, 10 mmol L^{-1} TMACl, 1 mmol L^{-1} $MgCl_2$

Doc S2. Statistical analysis of fluorescence enhancement data

For statistical analysis we used an unpaired two-tailed t-test. Calculations were done with GraphPad Software QuickCalcs t-test calculator available online (http://graphpad.com/quickcalcs/ttest1.cfm). GQ sequences were split into three groups: predominantly parallel (IL1, G4, G8, VEGF, cMyc, cKit1, cKit2, G4TERT, and Bcl-2), mixed-hybrid (Tel22, 26TelG4, and $G_4T_4G_4$, all in 5K), and antiparallel (Tel22, 26TelG4, TBA and $G_4T_4G_4$, all in 50Na and TBA in 5K). $G_4T_4G_4$ in 5K buffer adopts an antiparallel conformation according to our CD data (Fig. S2), but behaves similar to the parallel sequences in the current work and thus was excluded from statistical analysis. We performed an Analysis of Variance to compare the three groups of quadruplex topology and found significant differences between them ($p < 0.0001$). This was followed by pairwise comparisons of GQ topologies to each other and parallel GQ topology to other DNA sturctures (ssDNA, dsDNA, and i-motif). The data used for calculations (the mean, standard deviation, and sample size (N) of each group) are shown in Table S3. The t-test statistics are reported in Table S4. To account for multiple comparisons, p-values were adjusted using a Bonferroni correction.

Table S3. Raw data used for statistical analysis

Group	Mean	Std dev.	N	Discrimination ratio[a]
Parallel GQ	57.72	10.35	50	--
Anti-parallel GQ	9.83	6.39	14	5.9
Mixed-hybrid GQ	40.46	16.46	11	1.4
Mixed-hybrid (excluding $G_4T_4G_4$)	29.15	5.57	7	2.0
i-motif	1.00	0.61	13	57.7
dsDNA	0.20	0.23	13	287
ssDNA	0.95	0.34	6	50.8

[a]Discrimination ratio was determined by dividing mean for parallel GQ (57.72) by the mean for each DNA topology.

Table S4. Summary of t-test statistics for pairwise comparison

Group 1	Group 2	p	t	DM	DF	SED	95% CI	SSD
Parallel	Antiparallel	< 0.001	16.4120	47.8918	62	2.918	42.0586 to 53.7250	Yes
Parallel	Mixed-hybrid	< 0.001	4.4648	17.2641	59	3.867	9.5268 to 25.0014	Yes
Parallel	Mixed-hybrid (excluding $G_4T_4G_4$)	< 0.001	7.1254	28.5703	55	4.010	20.5349 to 36.6058	Yes
Parallel	i-motif	< 0.001	19.6417	56.7186	61	2.888	50.9443 to 62.4928	Yes
Parallel	dsDNA	< 0.001	19.9284	57.5255	61	2.887	51.7534 to 63.2976	Yes
Parallel	ssDNA	< 0.001	13.3339	56.7715	54	4.258	48.2354 to 65.3077	Yes
Anti parallel	Mixed-hybrid	< 0.001	6.4037	30.6277	23	4.783	20.7337 to 40.5216	Yes
Anti parallel	Mixed-hybrid (excluding $G_4T_4G_4$)	< 0.001	6.7956	19.3214	19	2.843	13.3705 to 25.2723	Yes

DM is the difference in means between the two groups
DF - the degrees of freedom
SED - the standard error of difference
95% CI - the 95% confidence interval of the difference
SSD - statistically significantly different (i.e, is $p < 0.05$)

Figure S1

Figure S1. CD spectra of selected DNA sequences. Data for C1A ssDNA, and C1B:C1B dsDNA, were collected in TB buffer; C8, TC_4T, $C_4T_4C_4$ and i-cMyc were collected in 5K 5.8 buffer; IL1 DNA was collected in TB (GQ form), and TB-TMACl (single-stranded form) buffers, and after LiOH treatment (to induce GQ dissociation, CD scan is labeled Li). The similarity of CD data for LiOH-treated IL1 and IL1 in TB-TMACl buffer indicates that IL1 is single-stranded in both cases. If not mentioned otherwise, molar ellipticity is reported per strand.

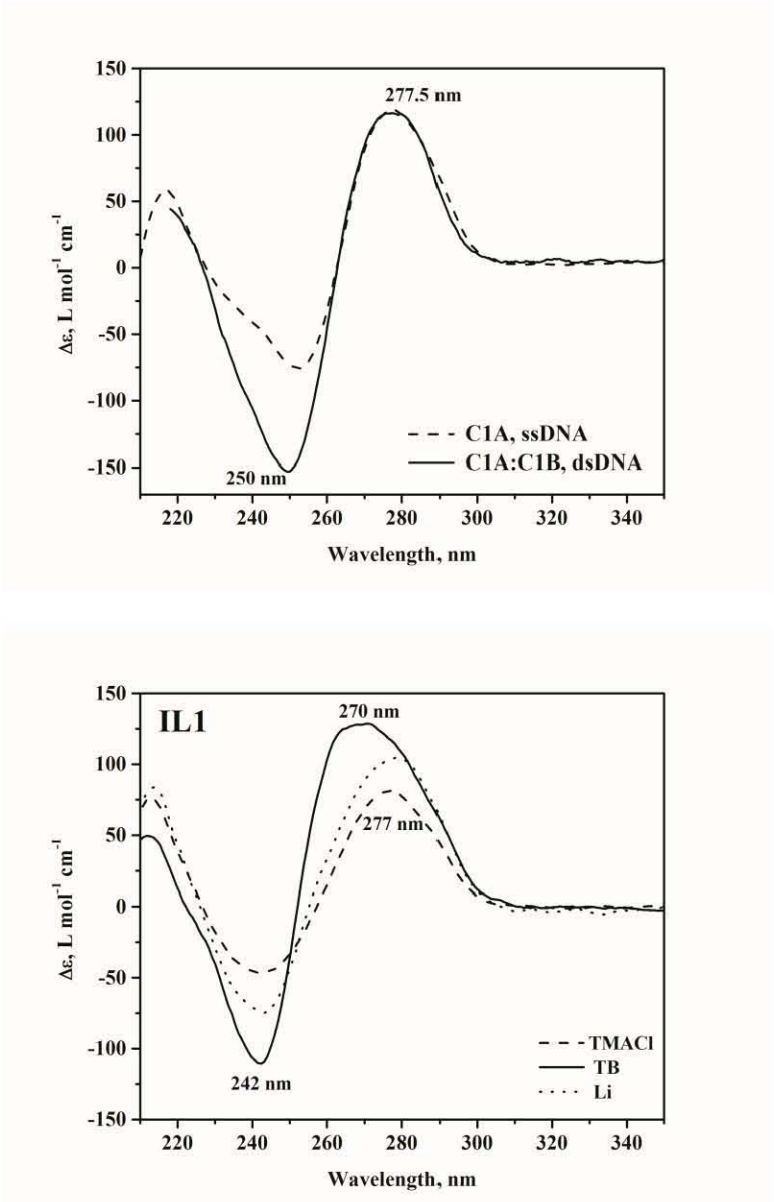

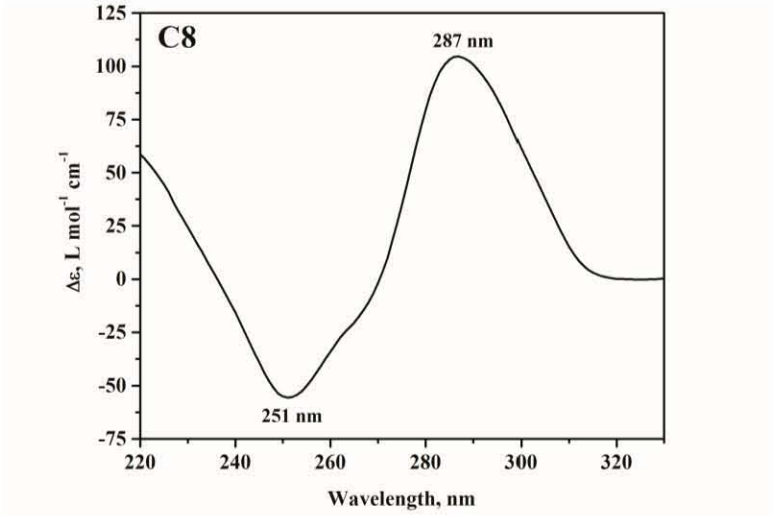
C8
287 nm
251 nm
Δε, L mol-1 cm-1
Wavelength, nm

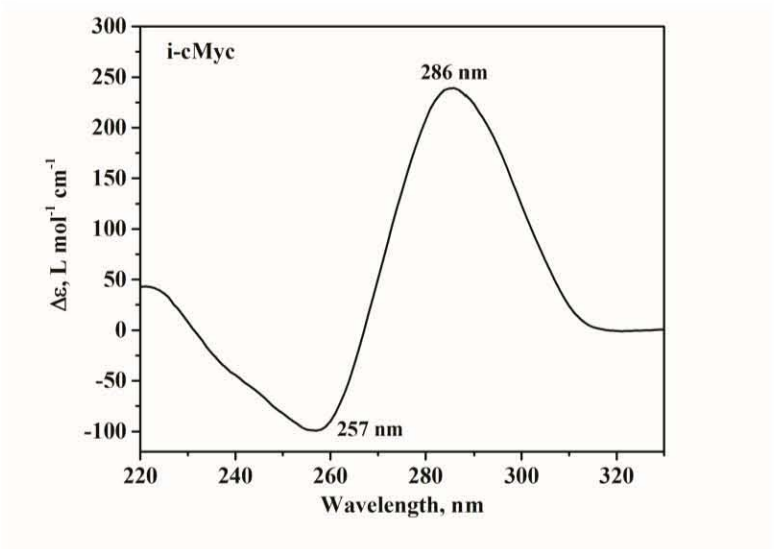
i-cMyc
286 nm
257 nm
Δε, L mol-1 cm-1
Wavelength, nm

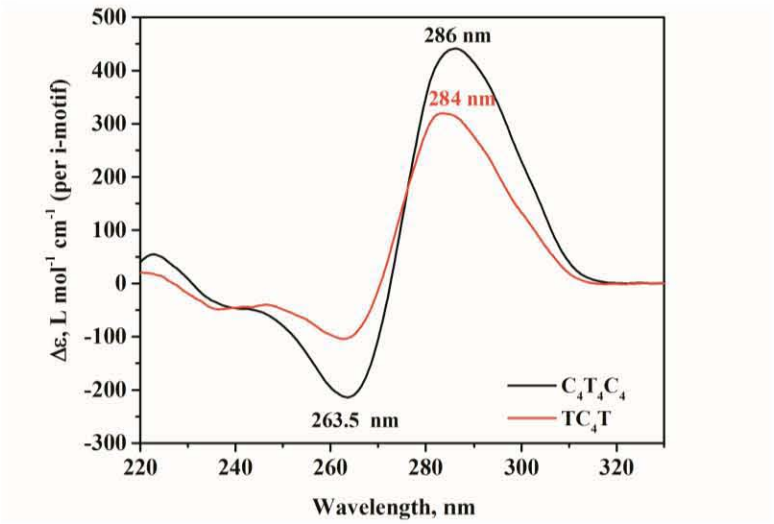
286 nm
284 nm
263.5 nm
C4T4C4
TC4T
Δε, L mol-1 cm-1 (per i-motif)
Wavelength, nm

Figure S2

Figure S2. CD annealing studies of DNA in the presence of a 2-fold excess NMM. DNA samples were annealed at 90 °C for 10 min with (dash lines) or without (solid lines) 2 equivalents of NMM, cooled for 3h and stored at 4 °C overnight. The concentrations of oligonucleotides were [TBA] = 2.5 μmol L^{-1}, [26TelG4, 50Na] = 2.5 μmol L^{-1}, [$G_4T_4G_4$, 5K] = 2.6 μmol L^{-1} (per bimolecular GQ), [$G_4T_4G_4$, 50Na] = 4.9 μmol L^{-1} (per bimolecular GQ). CD data were collected at 25 °C in 5K or 50Na buffer. For TBA or 26TelG4, there is little change in the CD spectra in the presence of NMM. It is important to note that TBA is rather unstable in 50Na buffer: it is completely unfolded above 37 °C (unpublished data). For $G_4T_4G_4$, NMM causes an increase in the fraction of parallel component in both 50Na and 5K buffers. The insets in the two figures are difference spectra between the spectrum of $G_4T_4G_4$ quadruplex with NMM and that of $G_4T_4G_4$ quadruplex alone. Molar ellipticity is reported per GQ.

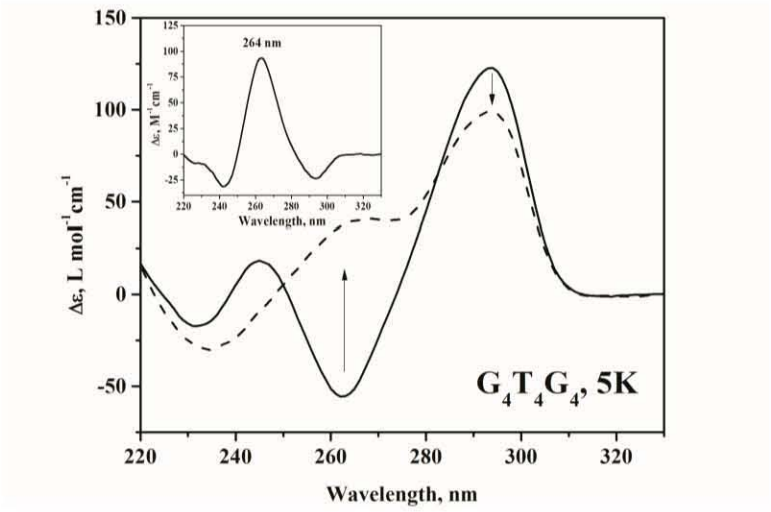

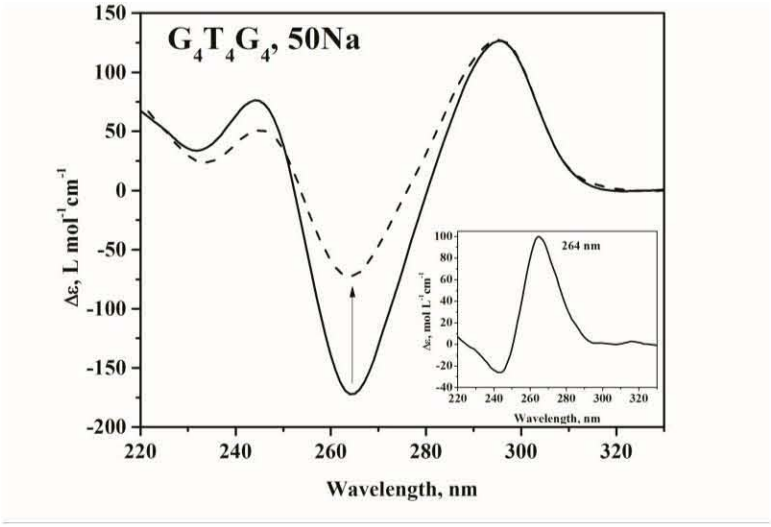
G4T4G4, 50Na
Δε, L mol-1cm-1
Wavelength, nm
264 nm

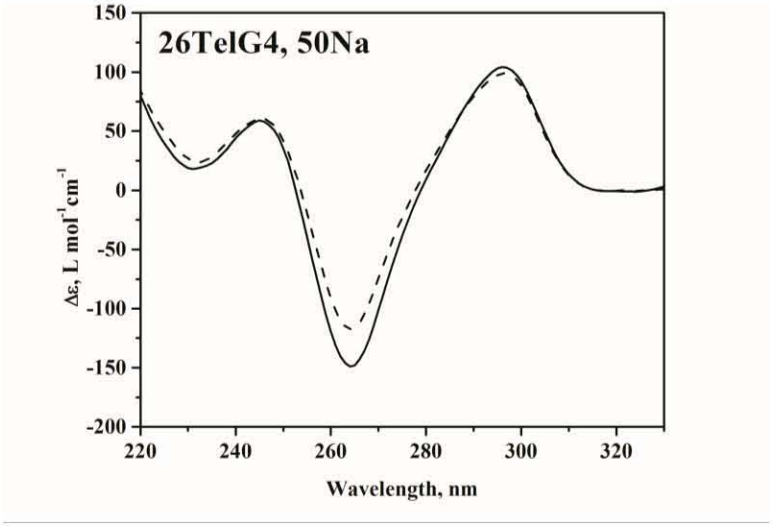
26TelG4, 50Na
Δε, L mol-1cm-1
Wavelength, nm

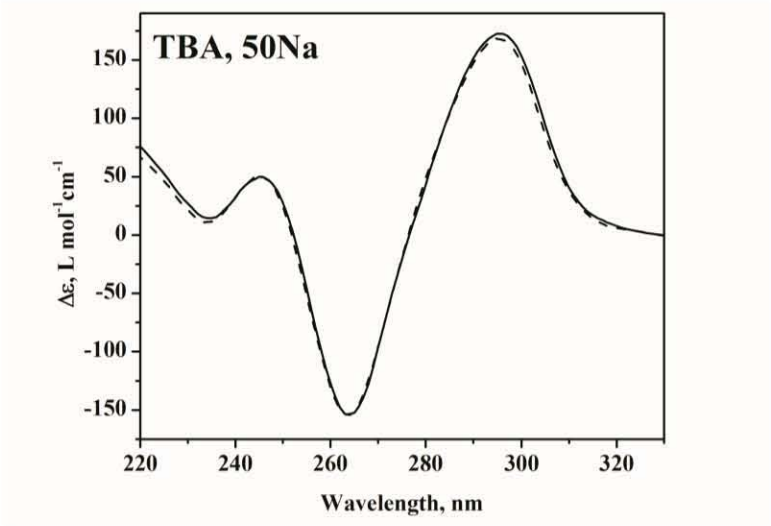
TBA, 50Na
Δε, L mol-1cm-1
Wavelength, nm

Figure S3

Figure S3. Fluorescence titration of NMM with VEGF in 5K buffer at 25 °C. (A) Normalized data for three fluorescence titrations. Solid line represents a global fit to a 1 NMM:2 GQ binding model; the dashed lines represent the 95% confidence interval. The concentration of binding sites corresponds to half of the VEGF GQ concentration. Titration experiments indicate that NMM fluorescence saturates above 5 eq of VEGF GQ (or 2.5 eq of VEGF binding sites), **(B)** Job plot data obtained from a titration of VEGF into a solution of NMM (open squares) and from a titration of NMM into a solution of VEGF (solid squares) at 401 nm (left) and 376 nm (right). Analysis of the Job plot indicates either a 1:1 or 1:2 binding ratio between NMM and VEGF. Experimental details and data analysis are described elsewhere (23). (**C**) Normalized data for titrations of NMM with VEGF or NMM in the presence of 100 μmol L^{-1} CT DNA with VEGF. Almost perfect overlap of both data sets suggests robust selectivity of NMM toward GQ DNA vs. dsDNA. Under our experimental conditions, VEGF adopts parallel quadruplex topology.

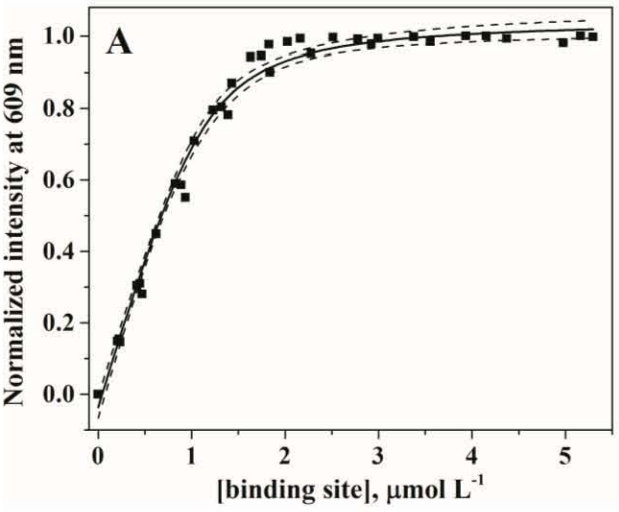

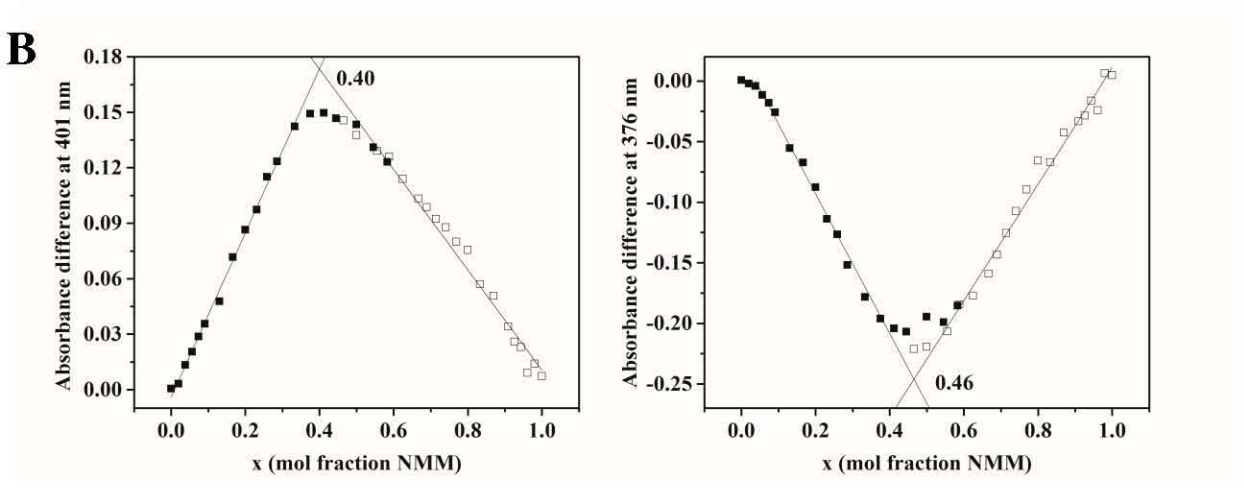
B
Absorbance difference at 401 nm
0.18
0.15
0.12
0.09
0.06
0.03
0.00
0.40
0.0
0.2
0.4
0.6
0.8
1.0
x (mol fraction NMM)
Absorbance difference at 376 nm
0.00
-0.05
-0.10
-0.15
-0.20
-0.25
0.46
0.0
0.2
0.4
0.6
0.8
1.0
x (mol fraction NMM)

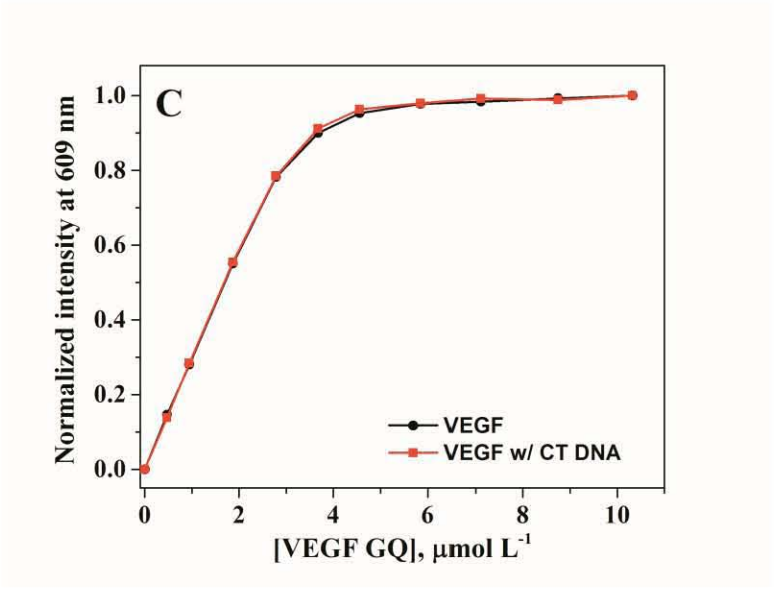
C
Normalized intensity at 609 nm
1.0
0.8
0.6
0.4
0.2
0.0
VEGF
VEGF w/ CT DNA
0
2
4
6
8
10
[VEGF GQ], μmol L-1

Figure S4

Figure S4. Fluorescence titration of NMM with $G_4T_4G_4$ and with 26TelG4 in 50Na buffer at 25 °C. Data for $G_4T_4G_4$ in 5K are shown for comparison. Under the experimental conditions, $G_4T_4G_4$ in 5K is antiparallel/mixed-hybrid, and both 26TelG4 and $G_4T_4G_4$ in 50Na are antiparallel. Concentration of NMM was 1.0 μmol L^{-1}.

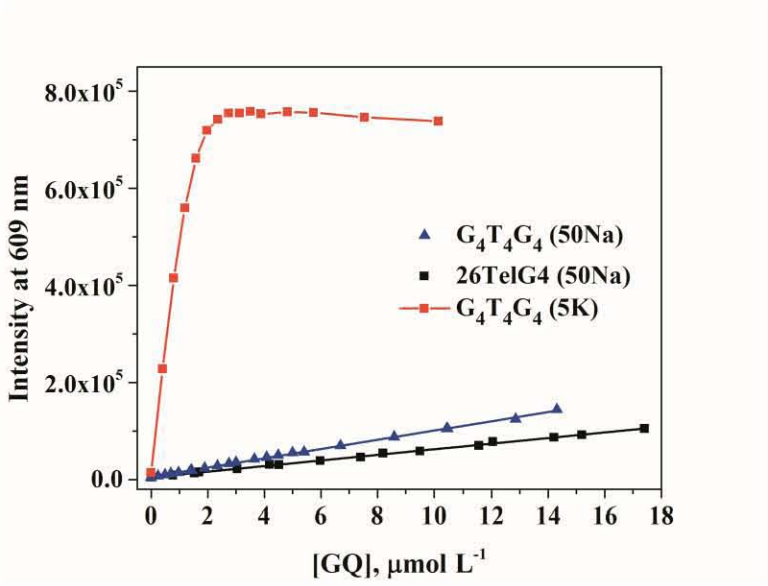

Figure S5

Figure S5. Fluorescence enhancement and CD study in 150K buffer. **(A)** Comparison of fluorescence data for NMM incubated with 10-fold molar excess of indicated sequences in 5K vs. 150K buffers. Fluorescence enhancement is reported relative to the fluorescence of NMM alone. Error bars are one standard deviation (confidence interval 68.2%). **(B)** Overlay of the CD wavelength scans for sequences presented in Fig. S5A in 5K, 150K buffers and after the fluorescence measurements in 150K buffer (usually, 1 eq. NMM and 10 eq. of DNA quadruplex).

A

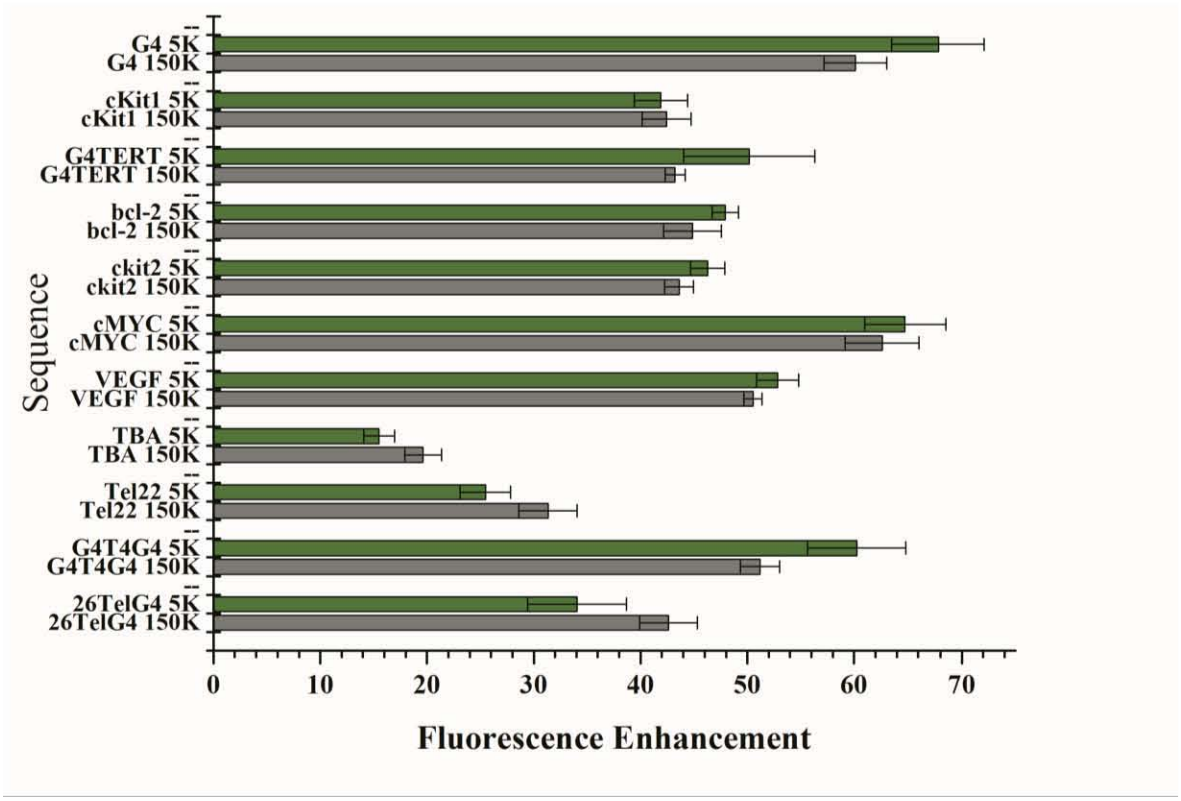

B

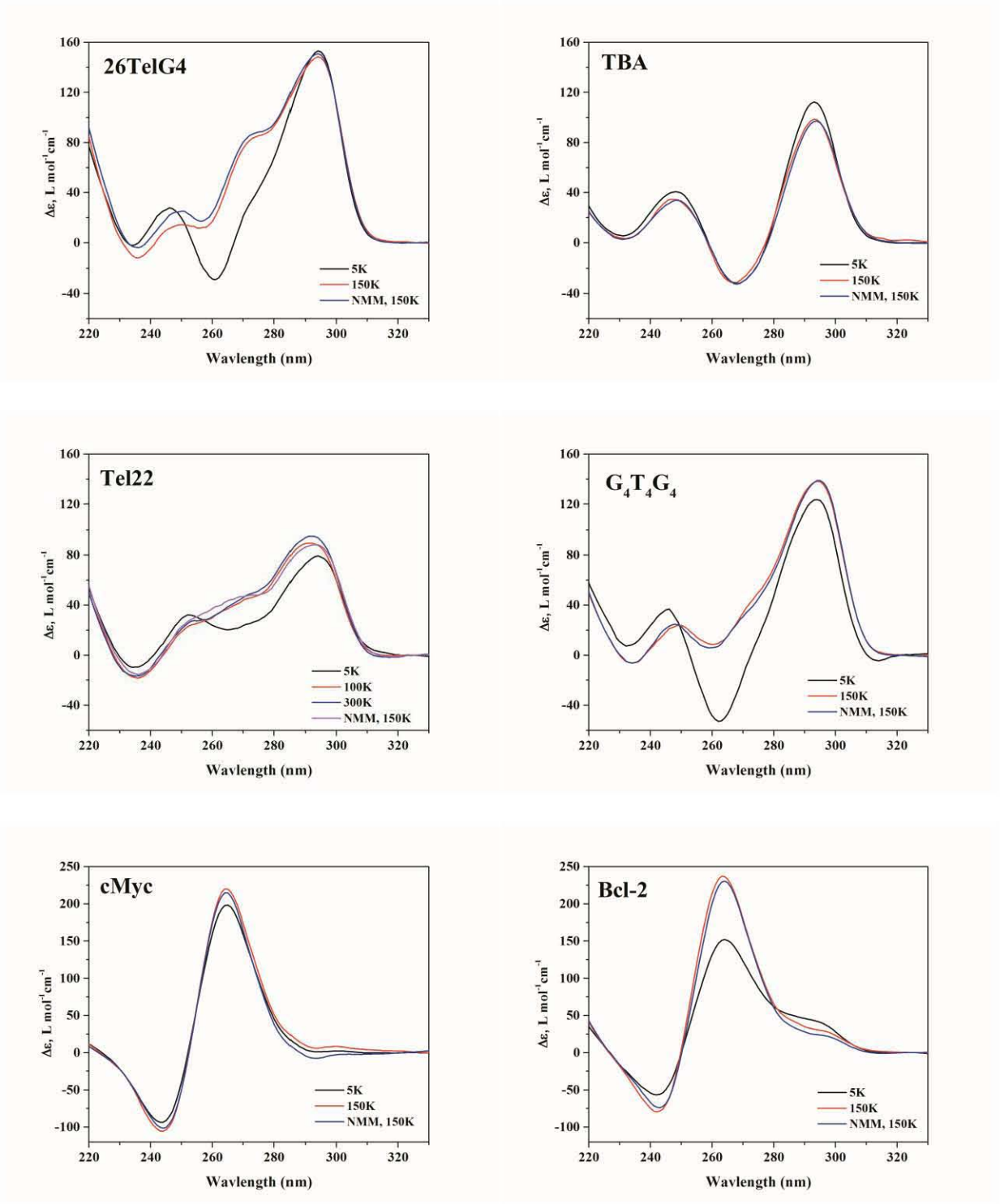
26TelG4
TBA
Tel22
$G_4T_4G_4$
cMyc
Bcl-2
Δε, L mol⁻¹cm⁻¹
Wavlength (nm)
5K
100K
150K
300K
NMM, 150K

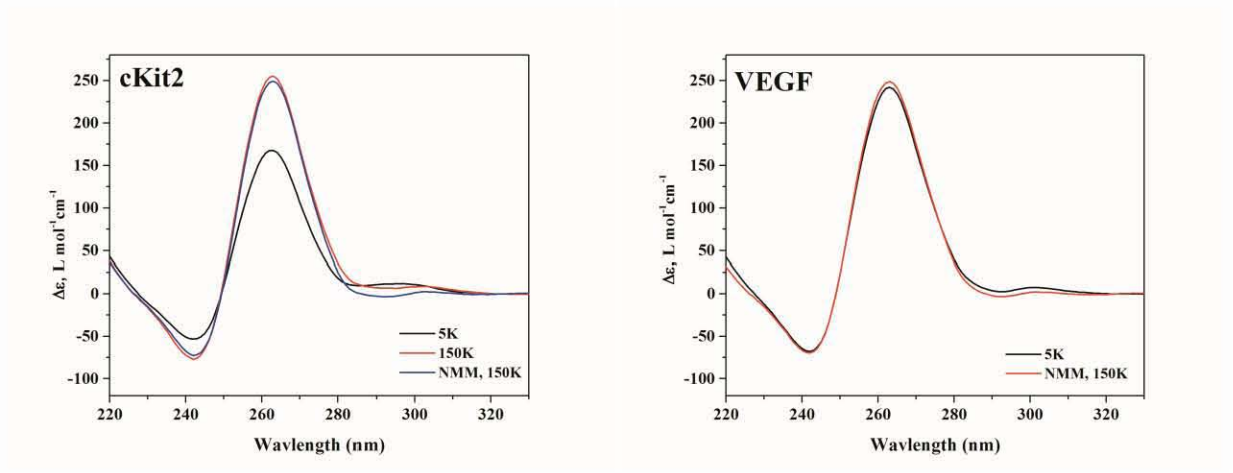
cKit2
VEGF
cKit1
G4TERT
Δε, L mol-1cm-1
Wavlength (nm)
5K
150K
NMM, 150K

Figure S6

Figure S6. Fluorescence spectra of NMM alone and with Tel22 in different buffers. Fluorescence intensity for 1.0 μmol L^{-1} NMM alone in 5K buffer and NMM in the presence of Tel22 in 5K, 50Na, and 100Li buffers where Tel22 adopts mixed-hybrid quadruplex, antiparallel quadruplex and single-stranded structures, respectively.

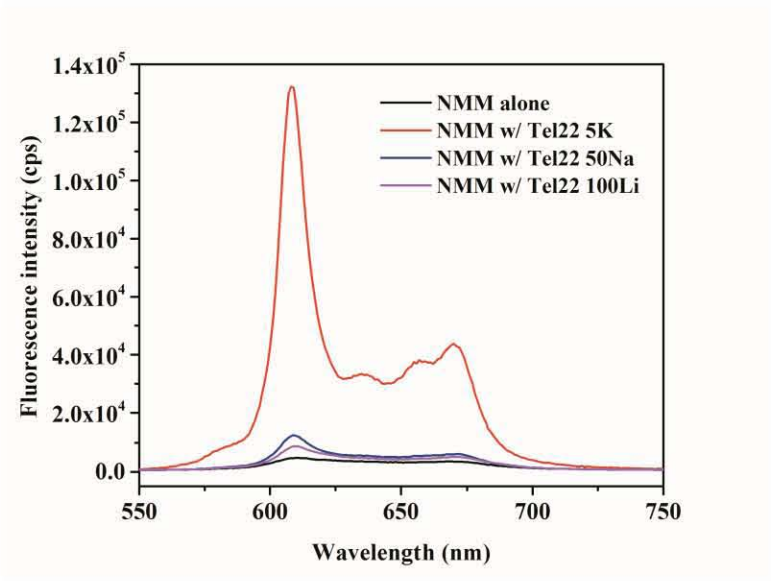

Figure S7

Figure S7. NMM fluorescence intensity is modulated by dynamic solvent quenching. (A) Correlation diagram for fluorescence lifetime vs. fluorescence enhancement; correlation coefficient (adjusted R^2) is 85.4. **(B)** Fluorescence spectra of NMM in H_2O and in D_2O, showing an increase in fluorescence intensity in the latter solvent.

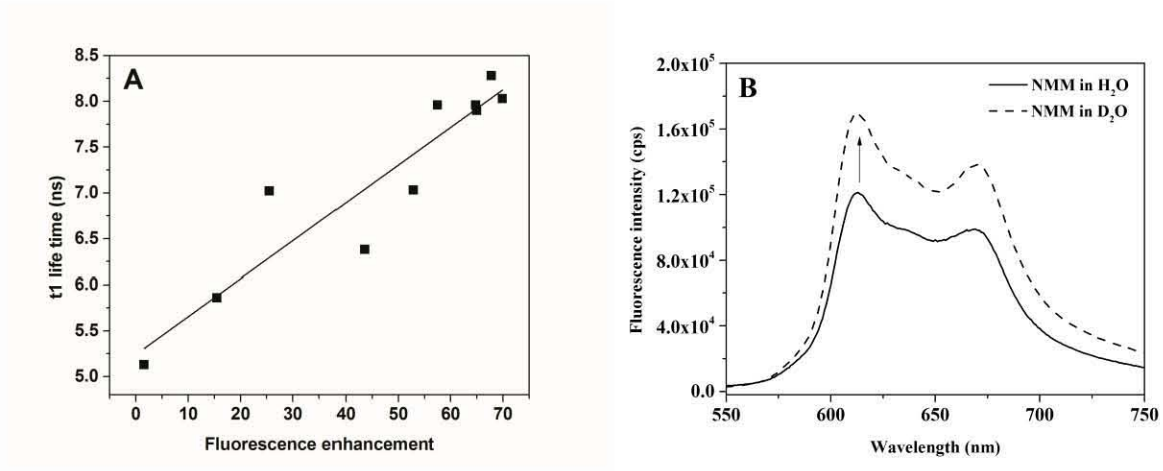

Figure S8

Figure S8. Competition titration of (NMM + GQ DNA) with dsDNA. **(A)** Representative titration of sample containing 1.0 μmol L^{-1} NMM and 14.2 μmol L^{-1} of G4 quadruplex with increasing concentration of C1A:C1B duplex at 25 °C in TB buffer. **(B)** Representative titration of sample containing 1.1 μmol L^{-1} NMM and 10.0 μmol L^{-1} of VEGF quadruplex with increasing amount of CT DNA at 25 °C in 5K buffer.

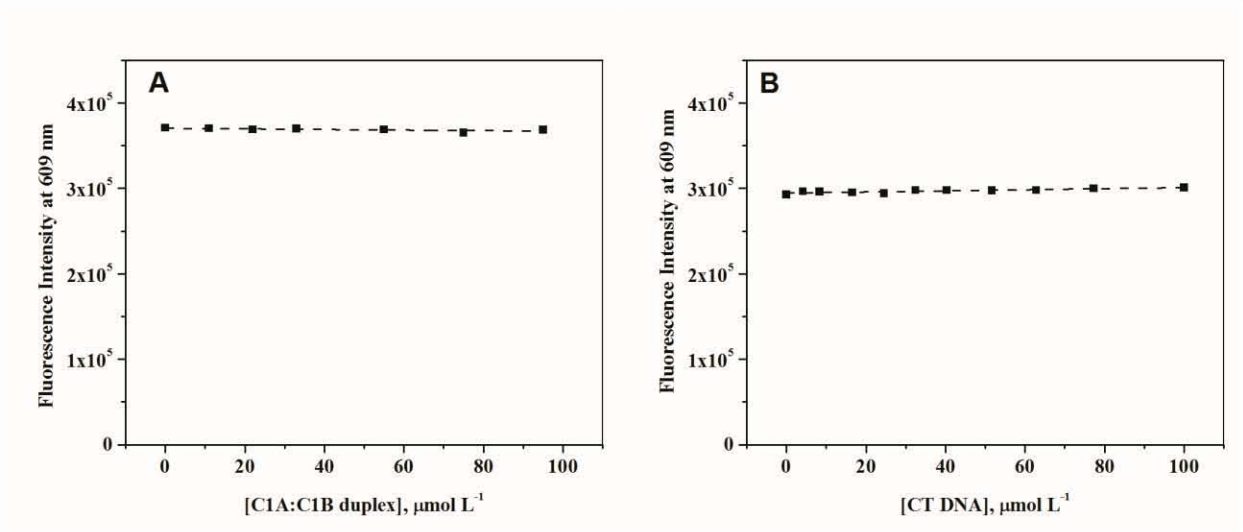

Figure S9

Figure S9. Effect of LiOH on fluorescence of NMM in the presence of G4 in TB buffer. Fluorescence intensity for 1.0 μmol L^{-1} NMM alone; NMM in the presence of 10 μmol L^{-1} G4 DNA (per quadruplex); and NMM in the presence of G4 treated with 50 mmol L^{-1} LiOH (and subsequently neutralized with HCl). LiOH treatment of GQ unfolds the quadruplex, which decreases the NMM fluorescence intensity to the level of NMM alone.

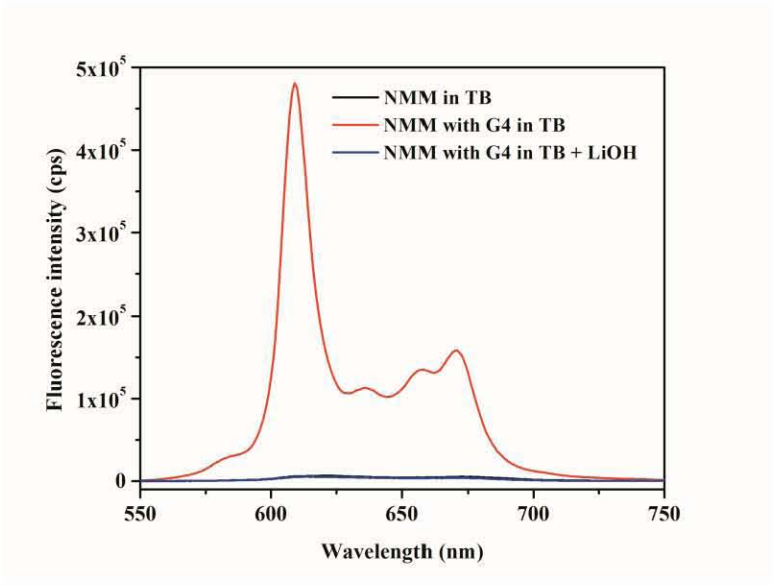

Figure S10

Figure S10. Effect of pH on the fluorescence spectra of NMM. pH titration of 1.0 μmol L^{-1} NMM with 0.1 mol L^{-1} HCl (pH range from 7.3 to 2.3) or 0.1 mol L^{-1} NaOH (pH range from 7.3 to 11.6). (**A**) The fluorescence of NMM increases gradually upon raising the pH from 2.3 to 7.3. The overall spectral shape does not change in this pH range. (**B**) When the pH is increased above 10, the spectral shape changes. Most noticeably, the maximum emission shifts from 610 nm to 636 nm and the intensity increases dramatically. (**C**) Reversibility study in the basic pH range. An NMM sample at neutral pH was brought to pH of 10.3 with NaOH and then back to 6.7 with HCl. Fluorescence changes were measured after each change of pH. (**D**) Reversibility study in the acidic pH range. An NMM sample at neutral pH was brought to pH of 3.3 with HCl and then back to 6.7 with NaCl. Fluorescence changes were measured after each change of pH. The small increase in spectral intensity might be related to partial loss of the N-Me group leading to formation of planar mesoporphyrin IX that can self-associate and increase the signal intensity. Note that neutralization increases the ionic strength, which could contribute to the observed signal change.

Our preliminary UV-vis data (not shown) indicate that NMM retains its spectral shape and displays increased intensity when the pH is increased from 4 to 11. Below pH 3 NMM's Soret maximum shifts from 379 nm to 406 nm and the peak becomes significantly sharper, possibly signifying loss of the N-methyl group. Commercially-available NMM is a mixture of 4 diastereomers with the methyl group positioned at one of the four core nitrogens (see Fig. 1C). Due to nonplanarity of the NMM macrocycle (27) each diastereomer exists as a pair of enantiomers where the methyl group protrudes from a different face of the macrocycle. Thus the UV-vis Soret band of NMM is rather broad. When the methyl group is lost, a single species is expected, consistent with the sharper Soret band.

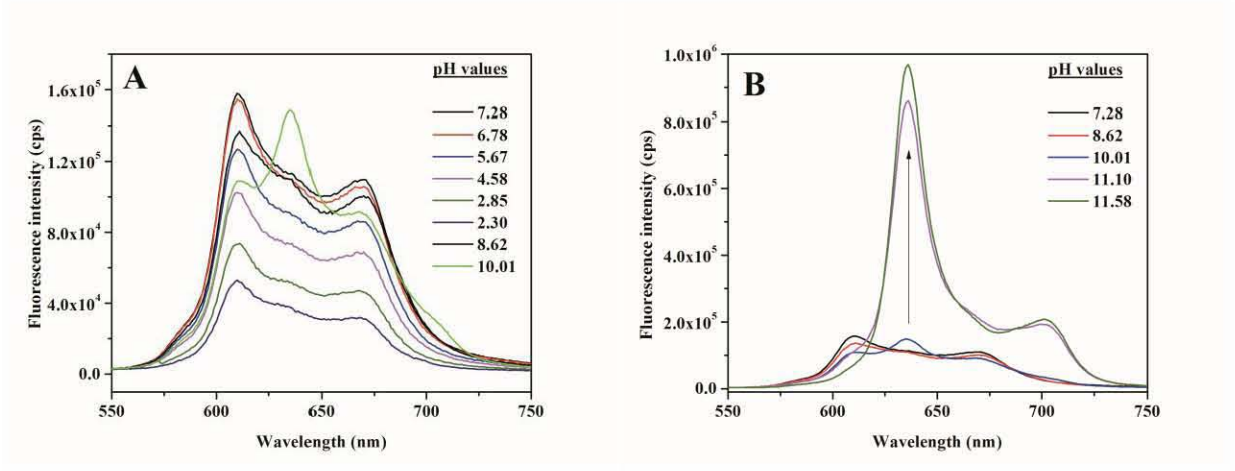

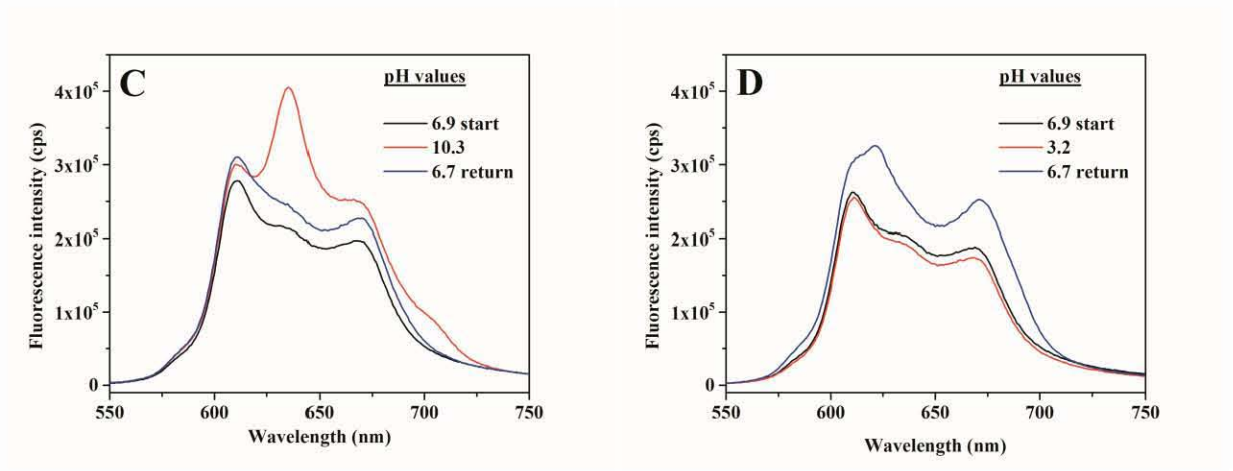
C
pH values
6.9 start
10.3
6.7 return
Fluorescence intensity (cps)
Wavelength (nm)
D
pH values
6.9 start
3.2
6.7 return
Fluorescence intensity (cps)
Wavelength (nm)

Figure S11

Figure S11. Effect of pH and buffer type on the fluorescence spectra of NMM. Fluorescence intensity of 1 μmol L^{-1} NMM solution in five buffers with pH values of 8.3 (Tris), 7.2 and 5.8 (lithium cacodylate), 4.9 and 4.0 (sodium acetate). Each buffer was present at 10 mmol L^{-1} and was supplemented with 5 mmol L^{-1} KCl and 95 mmol L^{-1} LiCl. A small 1.3-fold decrease in fluorescence intensity was observed upon changing the pH from 8.3 to 4.0.

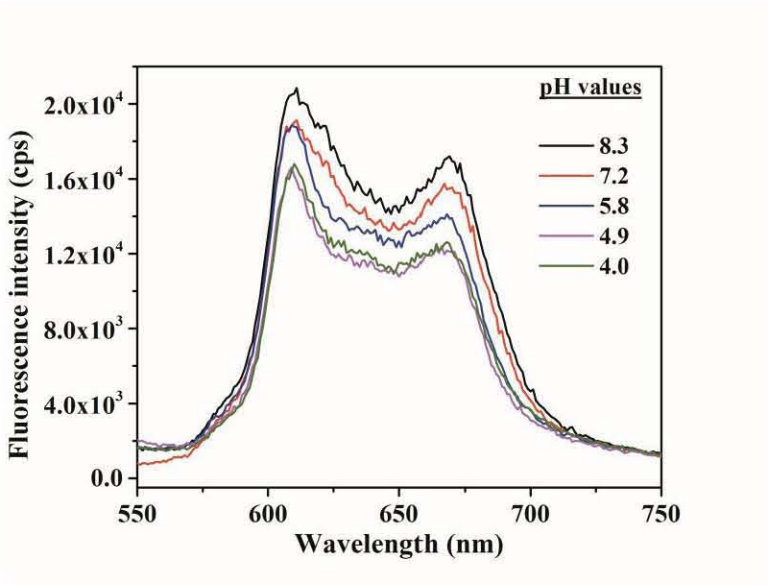

SI References

23. Nicoludis, J. M., Barrett, S. P., Mergny, J.-L., and Yatsunyk, L. A. (2012) Interaction of human telomeric DNA with N-methyl mesoporphyrin IX, *Nucleic Acids Res. 40*, 5432-5447.

27. Nicoludis, J. M., Miller, S. T., Jeffrey, P. D., Barrett, S. P., Rablen, P. R., Lawton, T. J., and Yatsunyk, L. A. (2012) Optimized end-stacking provides specificity of N-methyl mesoporphyrin IX for human telomeric G-quadruplex DNA, *J. Am. Chem. Soc. 134*, 20446-20456.

42. Tataurov, A. V., You, Y., and Owczarzy, R. (2008) Predicting ultraviolet spectrum of single stranded and double stranded deoxyribonucleic acids, *Biophys. Chem. 133*, 66-70.